



# Stability in Waves Committee

## Final Report and Recommendations to the 27th ITTC

### 1. INTRODUCTION

contributions on uncertainty and extreme waves, respectively.

#### 1.1. Membership and Meetings

Membership. The Committee appointed by the 26th ITTC consisted of the following members:

- Dr. A. M. Reed (Chairman)  
Carderock Division, Naval Surface Warfare Centre (NSWCCD), USA
- Mr. A. Peters (Secretary)  
QinetiQ, Haslar, UK
- Professor W. Y. Duan  
Harbin Engineering University, China
- Assoc. Professor P. Gualeni  
University of Genoa, Italy
- Assoc. Professor T. Katayama  
Osaka Prefecture University, Japan
- Dr. G. J. Lee  
Korea Research Institute of Ships & Ocean Engineering (KRISO), S. Korea
- Dr. F. van Walree  
Maritime Research Institute Netherlands (MARIN), the Netherlands

The committee would like to acknowledge the valuable contributions of wave data to the reviews from MARIN; and the work from Joel Park and John Telste from NSWCCD for their

Meetings. Four Committee meetings were held as follows:

- Osaka, Japan - February 2012
- Athens, Greece - September 2012
- Washington, D.C, USA - June 2013
- Daejeon, Korea - March 2014

#### 1.2. Tasks from the 26th ITTC

• Update the state-of-the-art for predicting ship stability in waves, emphasizing developments since the 2011 International Towing Tank Conference (ITTC). The committee report should include sections on:

- a. Definition of loss and survival of a ship (particularly damaged ships);
- b. The amount of detail required for modelling the internal geometry of a ship;
- c. Leak and collapse pressures for water tight doors and bulkheads; and
- d. Importance of taking air pressure into account (how open or closed compartments are in ships ties into item b above)



- e. Modelling of extreme wave conditions.
  - Review ITTC Recommended Procedures relevant to stability and
    - a. Identify any requirements for changes in the light of current practice, and, if approved by the Advisory Council, update them.
    - b. Identify the need for new procedures and outline the purpose and content of these.
  - Investigate uncertainty analysis for intact and damaged model tests to complement current procedures (Uncertainty in making measurements, and technical means that are used).
  - Investigate the criteria for modelling wave spectra in the determination of dynamic instability of intact vessels [Stability failures in the International Maritime Organization (IMO) sense: pure loss of stability, parametric roll, broaching, dead ship condition (resonant roll in beam seas)], *i.e.*, wave steepness, non-linearity, frequency contents of the spectrum, statistical distribution of wave and crest height and spatial behaviour of the waves and non-linear wave kinematics.
  - Develop better understanding of uncertainties associated with the results from experiments and simulations of extreme motions of intact vessels in realistic irregular seaways and develop quantitative techniques which reflect the nature and magnitude of the phenomena.
  - Review vulnerability criteria (including long term probability of loss of the ship) for intact and damaged ships, and outline further developments that are required. [Directly tied to on-going IMO Sub-committee on Stability, Load Lines & Fishing Vessel Safety (SLF) actions]
  - Update ITTC Recommended Procedure 7.5-02-07-04.2, Model Tests on Damage Stability in Waves, paying specific attention to:
    - a. Investigate the significance of scale effects in air pressure on flooding-model tests under atmospheric conditions. Comment on the need to perform flooding-model tests under scaled air pressure conditions.
    - b. Investigate how to deal with inertia due to the floodwater mass.
  - Investigate roll damping for large-amplitude roll motions in irregular seas. Review suitable data for future benchmarking of time-domain computer codes.
    - a. Time-domain roll damping in irregular waves'
    - b. Modelling of hydrodynamics of large-amplitude roll motion (regular and irregular seas)
  - Cooperate with the IMO SLF subcommittee correspondence group and the ITTC Sea-keeping Committee.
- ## 2. STATE-OF-THE-ART REVIEW
- ### 2.1. Review
- During the past few years major efforts have been on-going in ship stability research. The most well known references in this area are the International Stability Conference and Workshops. The last Stability Conference occurred in Athens, Greece in 2012 (STAB, 2012) and the last two stability workshops occurred in Washington, D.C, USA, in 2011 (ISSW, 2011) and another in Brest, France in



2013 (ISSW, 2013) The focus of this state-of-the-art review is enumerated in Steps a–e of Section 1.2.

## 2.2. Definition of Loss and Survival of a Ship

In any structured framework or methodology aimed at assessing ship safety, an accurate definition of the boundary between survival and loss is necessary.

The whole assessment methodology is yet to be properly defined and validated (Peters, *et al.* 2012) in order to recognise in a reliable way the possible ship-specific weakness in that term.

The term “ship loss” is commonly used as a statement of an undesired event, but the same expression can be used to describe many different scenarios. The opposite statement “ship survival” is also regularly used, but also suffers from the same problem—lack of a precise definition of the situation.

In current literature, a trend has been observed to mention the concept of “ship loss” when dealing with an intact ship, while “ship survival” is more likely to be used when discussing the safety of a damaged ship.

## 2.3. Relationship between Loss and Survival

Detailed examination is required of the definitions and relationship between “ship loss” and “ship survival” in order to avoid redundancies, overlapping concepts or contradictions.

In terms of probabilistic definition, survivability,  $P_S$ , is the combination of susceptibility,  $P_H$ , the inability to avoid an undesired event or a related initiating event and vulnerability,  $P_{K/H}$ , the inability to withstand the effect of an undesired event (Ball & Calvano, 1994). Therefore, survivability is defined as :

$$P_S = 1 - P_H \cdot P_{K/H}.$$

If susceptibility and vulnerability are the inability to avoid or withstand, respectively, the effect of a certain situation, their combination is defined as the mathematical complement to survivability, *i.e.*, the ability to survive.

Susceptibility in and of itself is a complex concept to fully understand and model. In the case of a damaged ship, for example, it might correspond to the probability that a ship will be hit by another ship. For an intact ship, this might correspond to the probability that a ship is caught in a severe storm.

Vulnerability represents the probability of severe consequences or even total loss of a vessel when an undesired initiating event has occurred.

We can assume that “loss” is an extreme negative consequence given a certain undesired initiating event. In this perspective it can be considered the mathematical complement to survivability.

## 2.4. Definition of Loss

The loss of a ship is an expression that, in addition to an explicit negative connotation, can be used to indicate many different levels of severity of a situation. One approach would be to decide to focus only on sinking



and/or capsizing, the latter defined as the transition to another stable equilibrium, other than upright, which is intrinsically unsafe. It is evident that from a safety point of view, some other intermediate levels of undesired severe situations should be taken into account.

During the recent IMO activities regarding the development of second-generation intact-stability criteria, a new terminology was identified, *i.e.*, “intact-stability failure” (IMO, 2008). This is defined as “a state of inability of a ship to remain within design limits of roll (heel, list) angle and a combination of rigid body accelerations”. A “total stability failure” and a “partial stability failure” are defined below:

- Total Stability Failure — Capsizing, being the total loss of a ship’s operability with likely loss of lives.
- Partial Stability Failure — The occurrence of very large roll (heel, list) angles and/or excessive rigid body accelerations, which will not result in loss of the ship, but which would impair normal operation of the ship and could be dangerous to crew, passengers, cargo or ship equipment.

It is immediately evident that besides the well-known concept of ship loss coinciding with ship capsize, it is important to discuss scenarios where the roll angles exceed a prescribed limit; and where the combinations of lateral and vertical accelerations exceed prescribed limits.

The so-called prescribed limits of roll angles can be fixed in absolute terms (*e.g.*, 45 degrees, 30 degrees) or other less precise terms (*e.g.*, deck-edge immersion or immersion of some defined critical point like the down-flooding openings) (Bačkalov, 2012).

The adoption of a fixed absolute roll-angle value as a limit to define a capsizing event is very common in literature, even if it is well recognised that this, in principle, might change from ship to ship due to the different dynamics of each ship. Beaupuy, *et al.* (2012) suggest that this aspect should be investigated by assuming that the critical threshold is a percentage of the angle of vanishing stability of each ship. Another possible event of partial failure, cargo shift, is mentioned in Kubo, *et al.* (2012).

In Kobyliński (2006), the concept of a loss-of-stability accident (LOSA) was introduced as a better description of the situation that occurs in reality, instead of talking about just a capsizing event. Kobyliński referred to a prolonged discussion on the definition of capsizing during the second International Conference on Stability of Ships & Ocean Vehicles (STAB) conference in 1982. He proposed that capsizing be defined as a situation where amplitudes of rolling motion or heel exceed a limit that makes operation or handling a ship impossible for various reasons (loss of power, loss of manoeuvrability, necessity to abandon the ship). Kobyliński’s proposed definition of capsizing did not necessarily assume the ship taking the inverted position. Therefore, capsizing might be better defined as LOSA and the definition might also be suitable for use in assessing the risk of capsizing.

LOSA can be divided into subcategories to cover the different types and severity of loss, *i.e.*, sudden capsizing, large heel with loss of power and manoeuvrability, large heel with progressive flooding and eventually capsizing or foundering.

In the case of a damaged-ship scenario, a reference is often made to a critical limiting-heel angle to define loss of a vessel. A 45-



degree mean angle was used by Spanos & Papanikolaou (2012). Alternatively, for Roll On-Roll Off (RO-RO) passenger ships, the procedure derived from the Directive 2003/25/EC is used where a ship is regarded as capsized if the roll angle exceeds 30 degrees instantaneously or if the steady (mean) heel angle is greater than 20 degrees for a period longer than three minutes (Kwon, *et al.*, 2012). In the same paper, the importance of the ship structures condition for a damaged ship is discussed as well: the rapid deterioration and degradation of the structural integrity might become important as much as stability deficiency for some types of ships.

The concept of critical limiting heel angle was also discussed by Montewka, *et al.* (2013) where the loss of the Roll On Passenger (ROPAX) is expected if two consecutive limiting states are exceeded, namely crashworthiness and stability. In application, ship capsizing is assumed to occur when 60 degrees of roll angle is exceeded.

It should be recognised that intact and damaged ships have some basic analogies when defining ship loss.

When considering the dynamic behaviour of a damaged ship in a seaway, the threshold definition should be treated in line with the intact-ship approach, *i.e.*, recognising the concepts of total loss or partial loss dealing with roll angles, accelerations, and immersion of critical points. These concepts need to be discussed within specific restrictions in relation to the residual operational capability required for a ship.

As regards the sinking phenomenon, this is generally applicable to a ship with damage to her hull, leading to a significant ingress of water and a consequent reduction of the reserve of buoyancy. For an intact ship, water

might enter from unprotected openings, which could be just as critical.

In line with the treatment of stability failure, it might be possible in principle to consider a “total loss of buoyancy” and a “partial loss of buoyancy”. Partial loss of buoyancy can be defined as a situation that will jeopardize the normal operations of a ship and its crew, or present a possibly critical situation for passengers, cargo or ship equipment.

Therefore, a situation other than the total sinking of a ship should be read in terms of residual buoyancy and equilibrium waterline characteristics.

A possible combination of different measures of various safety elements synthesised in a Relative Damage Loss Index (RDLI) is applied by Peters & Wing (2009) allowing a more comprehensive evaluation of a ship’s damage performance.

## 2.5. Loss of Functional Capability

The rule-making framework for ship safety is currently focused towards goal-based standards. With goal-based standards, functional requirements must be complied with in order to meet the overall goal. IMO has already agreed in principle with the following goal, valid for all kinds of new ships: “Ships are to be designed and constructed for a specified design life to be safe and environmentally friendly.” (IMO, 2005).

This implies that a ship must have characteristics adequate to minimise the risk of loss of the ship.

This new approach tends to avoid prescriptive standards in favour of rules referring



to safety goals, with an identified level of performance, but without specifying the means of achieving that level (Kobyliński, 2012).

It is, therefore, important to focus on the functional capabilities that are vital for a ship so that the “loss of ship” definition can coincide with the loss of such functional capabilities.

For a ship in the intact condition, it is reasonable to define the main list of functional capabilities as:

- Buoyancy
- Watertight integrity
- Stability
- Navigation
- Some specific operational and systems activity

Traditionally, for a ship in a damaged condition, reserve buoyancy and stability are the key desirable functions while possibly accepting a degraded level of performance. The most important issue is the ability to perform the evacuation and the emergency procedures, but some other key activities might also be required, for example returning to port under your own power.

IMO has recently introduced the regulatory concept of safe return to port (Spanos & Papanikolaou, 2012) through the International Convention for the Safety of Life at Sea (SOLAS) Regulation II-1/8-1, where a passenger ship shall be designed so that key specified systems remain operational when a ship is subject to flooding of any single watertight compartment.

A passenger ship is deemed capable of returning to port, when key functions and systems such as propulsion, navigation, and essential hotel services remain operational.

The orderly evacuation and abandonment of a ship, therefore, becomes a secondary option only to be employed if the casualty threshold is exceeded. In this case the issue of energy production and distribution is another functional capability that should be considered as a key to safe abandonment, when defining the concept of ship loss or survival.

## 2.6. Internal Geometric Modelling

The European Union (EU) Integrated Flooding Control & Standards for Stability & Crisis Management Project (FLOODSTAND) (Naar & Vaher, 2010) was a European research project which set out to derive detailed data on flooding mechanisms to validate numerical simulation tools and to help develop a standard for damaged-ship stability, focussing on the risk of flooding.

The modelling of internal geometry and effects on stability modelling have been studied by Karlberg, *et al.* (2011) as part of the FLOODSTAND project. As described in this report, the routes floodwater takes as it progresses inside a ship and the order in which compartments fill can have a significant effect on the consequent motions and events onboard, and in some cases on the final flooded state of a vessel.

In large passenger ships the internal layout of a vessel is typically characterised by watertight subdivisions such as double bottoms, watertight bulkheads and bulkhead decks. More specifically, it also includes the decks and significant non-watertight subdivisions, which make up the corridors and cabins, etc. This complex internal structure makes it challenging to model the damage stability of a passenger vessel both numerically and physically.



The progress of flooding is typically characterised by the amount of incoming floodwater and how it is distributed in a ship. The distribution of floodwater affects sinkage, heel and trim of a ship, and consequently the stability, which are the most important factors governing the survivability of a vessel. With complex subdivisions and multiple damage openings, very small changes in floodwater flow can result in various possibilities for a flooding sequence. Therefore, it is not always straightforward to predict with certainty what the final flooded state of a vessel will be.

The use of time-domain flooding simulation tools has expanded in recent years with the increase in available computer capability. It is well known that simulation results depend on applied input data for ship openings. The leakage and collapsing of non-watertight structures, such as closed fire doors, can have a very remarkable effect on the time-to-flood calculations.

The main objective of the Work Package 2 in the FLOODSTAND project was to provide data for more accurate and realistic modelling of progressive flooding in time-domain simulations. In the study, both experimental and numerical studies were performed in order to develop guidelines on modelling leaking and collapsing structures for use in flooding simulation. Furthermore, discharge coefficients for water flow through typical openings were evaluated.

It was clear that the exact values for discharge coefficients for leakage through a closed door cannot be evaluated for each opening in a large passenger ship. Therefore the discharge coefficients that are used have to be based on approximations and estimates.

The effect of variations in the input data on the results of a flooding simulation was studied through systematic sensitivity analysis with three different damage scenarios. The results indicate that the effect of these flow coefficients and collapse pressures on transient heeling in the beginning of flooding is minimal. However, the parameters were found to have a notable effect on the time-to-flood. A higher critical collapse pressure was found to significantly slow down the flooding process. The leakage area ratio also was found to have a significant effect on the time-to-flood, especially in a flooding case where closed doors do not reach collapse. In a flooding case where most of the flooding was simulated as leakage through closed doors, the applied leakage area ratios had a dominant effect on time-to-flood. Underestimation of this coefficient by 50% was shown to potentially lead to a 50% overestimation in the time-to-flood according to the FLOODSTAND report.

It was also found during the study that during simulations, variations of critical pressure head for collapse had a significant effect on the way the flooding progressed, and thus had an effect on the overall flooding rate and the time-to-flood. These also affected the resulting vessel-heeling behaviour, and in turn, the flooding rate. In the early flooding phases, leakage modelling was shown to have a clear effect on the time-to-flood.

## **2.7. Leak and Collapse Pressures of Water-tight Doors and Bulkheads**

Part of the FLOODSTAND Project focussed on work to investigate flooding through watertight doors and hatches.

Utilising full-scale testing for the leakage and collapse of watertight doors and bulkheads,



real-time data was collected to help develop simulation tools. Full-scale bending, tensile strength and compressive tests were carried out on individual wall-panel materials. Numerical studies and simulation analyses were carried out using Finite Element Methods and Computational Fluid Dynamics in order to give a comparison between experimental and numerical data.

Through extensive simulations for different damage scenarios, the FLOODSTAND research established some guidelines for modelling these structures during progressive flooding.

During the FLOODSTAND physical tests undertaken by the Centrum Techniki Oretowej (CTO) in Gdansk, Poland, water-pressure head was gradually increased at 0.5 m increments until the test object was damaged, the water-flow-rate value exceeded a critical value of 90 litres/second, or the critical pressure was above 220 kPa. Measurements included leakage-flow rate, deflection of the test object at six points and pressure head at structural failure.

Twenty different types of doors, windows, walls and hatch configurations were tested, including;

- Class A-60 double leaf-hinged-marine fire door,
- Class B joiner door — hinged,
- Steel frames for Class B wall and cabin wall,
- Steel frames for cabin wall,
- Cool Room sliding door,
- Semi Watertight Door--sliding steel frames,
- Cross flooding hatch,
- Sliding door and Hinged door.

The point of collapse or maximum flow rate was found to be dependent on the type, material and construction of a door and frame. Due to the fact that pressure was at its highest at the bottom of a door panel, structural deformation and structural leakage to the lower door hinges and sills occurred.

A key finding from these experiments was that for many doors, the leakage-area ratio increased almost linearly as a function of the pressure head. For example, the results obtained for a light watertight door showed that the leakage through the test door started at a water height of about 2 m and had leakage of less than 1.0 litre/second until structural damage occurred at a pressure head of about 8.0 m. Even after significant structural failure, the leakage through the door was approximately 40 litres/seconds, which corresponded to a leakage-area ratio of 0.017.

A Class A60 double leaf-hinged door, a Class A60 sliding door and a cabin wall were also modelled. The panel bending tests showed a good correlation with the Finite Element Method (FEM) analysis. Generally, the ability to compare FEM results with physical tests was limited. The doors tested had a leakage rate too high to be comparable with FEM results. It was found in the study that the use of analytical methods is not always justified, as door failure often depends on the strength of the hinges as opposed to the strength of the main body of the door.

For many doors it was found that the assumption that the leakage area is evenly distributed vertically is not valid as there is often a gap between the bottom of the door and the sill.

The FLOODSTAND study concluded that different categories of doors behave very differently under flooding conditions and even



the same door within the same category can behave very differently as the gap between the sill and the door can vary considerably. General guidelines were presented for both Class A and B doors, but it was noted that significant further work is needed, including further physical testing. With Class A structures, sensitivity analysis was recommended to consider the variability in the results, while Class B structures were found to fail at water levels lower than expected.

### **3. UNCERTAINTY ANALYSIS FOR INTACT AND DAMAGED MODELS USED IN SEAKEEPING AND EXTREME MOTION TESTS<sup>1</sup>**

The results of seakeeping and extreme motions testing are the characteristics of stochastic processes in random seas. As such, there is no uncertainty to be reported in the results, but rather confidence bands on the statistics characterizing the results of the experiment. The statistical uncertainty of seakeeping and extreme motions in a seaway will be discussed in Chapter 5, which follows.

In seakeeping and extreme-motions experiments, the area where traditional deterministic uncertainty analysis applies is in determining the mass properties of the model being tested. Documentation of surface-ship-model tests usually includes tables of the results but does not explicitly include the equations in the ballasting process or the instrumentation.

Given the uncertainty range on the mass properties of a seakeeping or extreme-motions test, the ideal approach would be to repeat the experiment with the model ballasted to the

extremes of uncertainty of the mass properties to determine the impact of this uncertainty on the experimental results. Technically the above approach is impossible as there would again be uncertainties associated with the mass properties for these new tests. The only feasible approach to determining the impact of the uncertainties in mass properties on the uncertainties of experimental results appears to be computational, although there is no established procedure.

From a practical perspective, the use of a validated linear seakeeping code is the most realistic approach to solving the above problem, as it will allow rapid assessment of the impact of the various mass-properties uncertainties in various combinations on the measured motions. Although a linear code will have its own accuracy issues, it will provide a consistent metric against which the impact of mass-properties uncertainties can be judged. Also, as a linear code provides a lowest common denominator, it will allow realistic comparisons between various experimental facilities and organizations without introducing many computational tool variables into the assessment.

The material that follows outlines the equations typically used to determine the mass properties of a model for seakeeping and extreme-motions testing, and derives the uncertainty equations for ballasting based on ISO GUM (JCGM, 2008) and ITTC (2008).

#### **3.1. Model Weight and Mass**

The formulation is from the Archimedes principle; that is, a ship's weight is equal to its buoyancy force. In that case, the equation for a ship or model weight is given by:

---

<sup>1</sup> This section is based largely on unpublished notes by Dr. Joel Park of DTMB (NSWCCD).



$$W = \rho g \nabla \quad (1)$$

where  $\rho$  is water density,  $g$  is local acceleration due to gravity, and  $\nabla$  is the displaced volume. From (1), the model weight is then computed as:

$$W_m = m_s \rho_m g_m \nabla_m / (\rho_s \nabla_s) \quad (2)$$

where  $m$  is mass and the subscripts  $m$  and  $s$  are for the model and ship, respectively. However, the displaced volume is related to the scale ratio by:

$$\nabla_s / \nabla_m = \lambda^3 \quad (3)$$

The scale ratio is defined as the ratio of the ship length to the model length:

$$\lambda = L_s / L_m$$

From (2) and (3), the model weight is then

$$W_m = m_s \rho_m g_m / (\rho_s \lambda^3) \quad (4)$$

In mass units, (4) becomes

$$m_m = m_s \rho_m / (\rho_s \lambda^3) \quad (5)$$

The calculation of the model weight and mass from (4) and (5) should be computed on the basis of the standard values for  $\rho_s$  (1026.021 kg/m<sup>3</sup> for salt water at 15° C) and  $g_c$  (9.80665 m/s<sup>2</sup>) for full scale, and the values of  $\rho_m$  (generally fresh water) and  $g_m$  appropriate for the experimental facility. Standard gravity is fixed at an internationally accepted value of 9.80665 m/s<sup>2</sup> from Thompson & Taylor (2008).

The values for freshwater and seawater for standard field and laboratory conditions can be

found in international standards. The seawater values are in TEOS-10 (IOC, SCOR & IAPSO, 2010), and freshwater values are in Harvey, *et al.* (2008) and IAPWS (2008). The uncertainty in density may be computed from the measured temperature and salinity.

From (4) and (5), the expanded relative uncertainty in weight and mass is as follows:

$$U_{W_m} / W_m = \left\{ (U_{\rho_m} / \rho_m)^2 + (3U_{L_m} / L_m)^2 + (U_{g_m} / g_m)^2 \right\}^{1/2} \quad (6)$$

$$U_{m_m} / m_m = \sqrt{(U_{\rho_m} / \rho_m)^2 + (3U_{L_m} / L_m)^2} \quad (7)$$

After the model weight and mass are adjusted to the values from (4) and (5), the model must be weighed. After the model is weighed, the combined uncertainty in model mass includes the result of the measured weight and the computed weight. The combined uncertainty is then:

$$U_c = \sqrt{U_{meas}^2 + U_{mm}^2} \quad (8)$$

The final measured weight and mass as computed from (4) and (5) should be within the uncertainty of (8). The uncertainty estimate in density for (6) and (7) should be the maximum difference between the value applied during ballasting and value measured during testing. The uncertainty in the model length should be obtained from direct measurements of the model dimensions while the uncertainty in  $g$  is from an internationally recognized standards organization.

### 3.2. Longitudinal Centre of Gravity

The remaining procedures described here require suspension of the model from a struc-



turally rigid frame. The process includes a beam to which the model is attached.<sup>2</sup> The beam is attached to the frame by a pivot point. The determination of the longitudinal centre of gravity (LCG) is a two-step measurement process:

- The CG of the beam is measured.
- The CG of the beam and model is measured.
- The CG of the model is then computed from the previous two steps.

One method in the determination of the CG is simply to move the beam, or the beam and model combination until the beam is level. In this case, the CG is directly below the pivot. However, the uncertainty in the CG location by levelling may be unreliable. A more direct method is suspension of the model at two points: one near the bow and the second near the stern. The location of the CG is then computed from the moments and the uncertainty is easily established. The load at the bow and stern is measured with electronic load cells attached to the suspension cables.

### 3.2.1. Levelling Method

The simplest method for locating the LCG may be by moving the beam alone under the pivot until it is level, and then moving the model on the beam until the model on the beam is level. When the model is level, the LCG is located directly below the pivot point. Any deviation of the LCG is given by:

$$\tan \theta = x/z.$$

where  $\theta$  is the pitch angle,  $x$  is deviation from the true LCG, and  $z$  is the vertical distance

from the pivot point to the CG. For a pitch angle near zero, the result is

$$\theta = x/z \quad (9)$$

Calculation of the location of the vertical CG is described in the following section.

From (9), uncertainty in the displacement from the true LCG is:

$$U_x = \sqrt{(\theta U_z)^2 + (z U_\theta)^2} \quad (10).$$

For a pitch angle near zero, (10) becomes:

$$U_x = z U_\theta.$$

The combined uncertainty relative to the model reference point for the LCG is then

$$U_c = \sqrt{(z U_\theta)^2 + U_{xm}^2}.$$

If the instrument for measurement of level is removed from the fixture, an equivalent weight should be located at the measurement point.

### 3.2.2. Two-point Suspension Method

The LCG location can be measured by supporting the beam at two points (1, near the stern, and 2, near the bow), suitably far apart with the LCG somewhere in-between (the beam is not necessary for this). At both points there should be a load cell measuring the weight at that point. The model should also be levelled. The weights from the load cells are as follows:

For the beam

$$W_b = F_1 + F_2 \quad (11).$$

<sup>2</sup> The beam is not required for all procedures, but is required for some, those for which the beam is not necessarily required will be noted.



For the beam and model

$$W_{bh} = F_3 + F_4 \quad (12).$$

From (11) and (12), the weight of the hull is

$$W_h = (F_3 - F_1) + (F_4 - F_2) \quad (13)$$

where  $F_1$  and  $F_3$  are the load cell readings at the stern and  $F_2$  and  $F_4$  are at the bow.

Similarly, the moments are as follows:

For the beam

$$x_b W_b = x_1 F_1 + x_2 F_2 \quad (14).$$

and  $x_l$  is the distance from the reference location (say amidships) to the aft suspension cable (negative aft) and  $x_2$  is the distance from the reference location to the forward suspension cable (positive forward). For the beam and hull

$$x_{bh} W_{bh} = x_1 F_3 + x_2 F_4 \quad (15).$$

From (13)–(15), the CG of the model relative to the reference location is

$$\begin{aligned} x_h &= (x_1 F_{31} + x_2 F_{42}) / (F_{31} + F_{42}) \\ &= (x_1 F_{31} + x_2 F_{42}) / W_h \end{aligned} \quad (16)$$

where

$$\begin{aligned} F_{31} &= F_3 - F_1 \\ F_{42} &= F_4 - F_2 \end{aligned}$$

For the uncertainty estimates, the sensitivity coefficients from (16) are as follows:

$$\begin{aligned} c_1 &= \partial x_h / \partial x_1 = F_{31} / (F_{31} + F_{42}) = F_{31} / W_h \\ c_2 &= \partial x_h / \partial x_2 = F_{42} / (F_{31} + F_{42}) = F_{42} / W_h \end{aligned}$$

$$c_3 = \partial x_h / \partial F_{31} = F_{42} (x_1 - x_2) / W_h^2$$

$$c_4 = \partial x_h / \partial F_{42} = -F_{31} (x_1 - x_2) / W_h^2.$$

The distances  $x_1$  and  $x_2$  are likely measured with the same device, and the uncertainty in the distance will be the same and correlated. Similarly, the load cells for the measurement of the aft and forward locations may have the same uncertainty. If they are calibrated at the same time with the same equipment, then the load measurements are also correlated. The uncertainty in the location of the LCG is as follows:

$$U_{x_m} = \sqrt{(c_1 + c_2)^2 U_x^2 + (c_3 + c_4)^2 U_F^2}.$$

In tests where equipment will be added to the model later, the LCG of the model hull is determined by either of the previous methods, and components are added. Mass properties of the smaller components are measured with a mass properties instrument. The total weight of the model then is

$$W_m = \sum_{i=1}^n W_i \quad (17),$$

where  $n$  is the number of components. The LCG is given by

$$x_m = \sum_{i=1}^n (x_i W_i / W_m) \quad (18).$$

The uncertainty in the weight is

$$U_{W_m}^2 = \sum_{i=1}^n U_{W_i}^2 \quad (19),$$

and the uncertainty in the LCG is



$$U_{\text{xn}}^2 = \sum_{i=1}^n (W_i U_{x_i} / W_m)^2 + \sum_{i=1}^n (x_i U_{W_i} / W_m)^2 + \sum_{i=1}^n (x_i W_i U_{W_m} / W_m^2)^2 \quad (20)$$

The previous formulation assumes the measurements are independent; however, some of the measurements are correlated. The hull weight and LCG are independent of the measurements by the mass-properties instrument, although the measurements of the components by the mass-properties-instrument are correlated. In any case, the uncertainty from the hull measurements will be the dominant term in the estimate.

If both the levelling and two-point suspension methods are applied in the determination of LCG, the result should be within the uncertainty estimates of both methods. Estimates using both methods indicate a discrepancy in LCG location by the levelling method in comparison to the two-point load method. The difference is larger than the uncertainty estimates on the location of the LCG. This illustrates the difficulty in getting accurate results using the levelling method.

### 3.3. Vertical Centre of Gravity

The vertical centre of gravity (VCG) is determined by the added weight or inclining method in air. In added weight or inclining method, a weight is added or moved transversely, respectively, resulting in a heeling moment. The added weight or inclining method is as follows:

$$z = (w / W_m)(y_w / \tan \phi - z_w) \quad (21)$$

where  $w$  is the added or shifted weight,  $y_w$  is the lateral location,  $z_w$  the vertical location be-

low the pivot point on the frame, and  $\phi$  the heel angle. The instrument for measuring the heel angle should be located on the model where the instrument replaces a mass of equal weight. A fixture may be added that is included in the added weight so that weight may be moved to multiple locations. Then the  $(y_w / \tan \phi)$  term can be computed as the slope from  $y_w$  versus  $\tan \phi$  by regression analysis as a better estimate.

From (21), the sensitivity coefficients are as follows:

$$\begin{aligned} c_1 &= \partial z / \partial w = (1 / W_m)(y_w / \tan \phi - z_w) \\ c_2 &= \partial z / \partial W_m = (w / W_m^2)(y_w / \tan \phi - z_w) \\ c_3 &= \partial z / \partial y_w = w / (W_m \tan \phi) \\ c_4 &= \partial z / \partial \phi = w y_w / (W_m \sin^2 \phi) \\ c_5 &= \partial z / \partial z_w = -w / W_m \end{aligned}$$

The uncertainty in the VCG is then

$$U_z = \left\{ (c_1 U_w)^2 + (c_2 U_{W_m})^2 + (c_3 U_{y_w})^2 + (c_4 U_\phi)^2 + (c_5 U_{z_w})^2 \right\}^{1/2} \quad (22)$$

If the slope method for  $(y_w / \tan \phi)$  is applied, the uncertainty in the slope must be added to (22). The sensitivity coefficient for the slope is from (21)

$$c_6 = w / W_m$$

For the uncertainty with the slope, (22) becomes

$$U_z = \left\{ (c_1 U_w)^2 + (c_2 U_{W_m})^2 + (c_3 U_{y_w})^2 + (c_4 U_\phi)^2 + (c_5 U_{z_w})^2 + (2c_6 U_b)^2 \right\}^{1/2} \quad (23)$$



where  $u_b$  is the standard uncertainty in the slope  $b$  from linear regression analysis.

The VCG of the hull is computed from the hull-beam combination from the following:

$$z_h = (W_{bh}z_{bh} - W_bz_b) / W_h$$

The sensitivity coefficients from (23) are as follows:

$$c_1 = \partial z_h / \partial W_{bh} = z_{bh} / W_h$$

$$c_2 = \partial z_h / \partial z_{bh} = W_{bh} / W_h$$

$$c_3 = \partial z_h / \partial W_b = z_b / W_h$$

$$c_4 = \partial z_h / \partial z_b = W_b / W_h$$

$$c_5 = \partial z_h / \partial W_h = (W_{bh}z_{bh} - W_bz_b) / W_h^2$$

The uncertainty of the VCG for the hull is then

$$U_{z_h} = \left\{ (c_1 U_{W_{bh}})^2 + (c_2 U_{z_{bh}})^2 + (c_3 U_{W_b})^2 + (c_4 U_{z_b})^2 + (c_5 U_{W_h})^2 \right\}^{1/2}$$

For a model assembled from several parts, the VCG is

$$z_m = \sum_{i=1}^n z_i W_i / W_m$$

where the assembled model weight is given by (17) and  $x$  is replaced with  $z$  in (18). The uncertainty in model weight is given in (19).

From (20) the uncertainty in the VCG is:

$$U_{z_m}^2 = \sum_{i=1}^n (W_i U_{z_i} / W_m)^2 + \sum_{i=1}^n (z_i U_{W_i} / W_m)^2 + \sum_{i=1}^n (z_i W_i U_{W_m} / W_m^2)^2$$

### 3.4. Moment of Inertia

The moment of inertia of a model is computed from the oscillation of the model about the pivot point on the frame. The moment of inertia (MOI) in pitch is:

$$I_\theta = mgd(T_\theta / 2\pi)^2 \quad (24)$$

where  $d$  is the distance from the pivot point to the CG, and  $T_\theta$  is the period of oscillation. The period of oscillation is determined by attaching a precision electronic inclinometer to the model and collecting a time series of its signal with a digital-data-collection system. The sensitivity coefficients from (24) are as follows:

$$c_1 = \partial I_\theta / \partial m = gd(T_\theta / 2\pi)^2$$

$$c_2 = \partial I_\theta / \partial d = mg(T_\theta / 2\pi)^2$$

$$c_3 = \partial I_\theta / \partial g = md(T_\theta / 2\pi)^2$$

$$c_4 = \partial I_\theta / \partial T_\theta = mgd(T_\theta / 2\pi)^2 / (2\pi^2)$$

The uncertainty in the MOI is

$$U_{I_\theta} = \left\{ (c_1 U_m)^2 + (c_2 U_d)^2 + (c_3 U_g)^2 + (c_4 U_{T_\theta})^2 \right\}^{1/2}$$

The period in (24) is obtained by linear regression analysis of the time series with a damped sine wave of the following form:

$$y = a \exp(-bt) \sin(2\pi t / c + d) + e \quad (25)$$

where  $a$ ,  $b$ ,  $c$ ,  $d$ , and  $e$  are constants that are computed from linear regression analysis. In this equation,  $c$  is the period,  $T_\theta$ . Regression analysis also provides the standard deviation. The combined uncertainty in the period is computed from:



$$U_{T\theta} = \sqrt{(2u_c)^2 + U_t^2} \qquad k_\theta = \sqrt{I_{\theta cg} / m_m} \qquad (27)$$

where  $u_c$  is the standard deviation or standard uncertainty of the period from linear regression analysis and  $U_t$  is the uncertainty in the time traceable to an internationally recognized standards organization for the electronic device.

In some cases, damping may be low, and the damping term in (25) may be dropped. That is, a sine wave curve fit may work better. Then, (25) becomes

$$y = a \sin(2\pi t / c + d) + e$$

Calculations for the MOI indicate that a time standard traceable to an internationally recognized standards organization is critical in the measurement of the oscillation period.

The hull MOI is separated from the beam and hull MOI by the following:

$$I_{\theta h} = I_{\theta hb} - I_{\theta b} \qquad (26)$$

The uncertainty in the hull alone from (26) is

$$U_{\theta h} = \sqrt{U_{\theta hb}^2 + U_{\theta b}^2}$$

where  $I_{\theta hb}$  is the MOI of the beam and hull assembly and  $I_{\theta b}$  is the MOI of the beam only.

The MOI about the CG and its uncertainty are given by

$$I_{\theta cg} = I_{\theta m} - m_m d_m^2$$

$$U_{I_{\theta cg}} = \sqrt{U_{I_{\theta m}}^2 + d_m^4 U_m^2 + 4(m d_m U_{d_m})^2}$$

The radius of gyration is defined as

From (27), the sensitivity coefficients are as follows:

$$c_1 = \partial k_\theta / \partial I_{\theta cg} = \frac{1}{2\sqrt{m_m I_{\theta cg}}}$$

$$c_2 = \partial k_\theta / \partial m_m = -\frac{1}{2}\sqrt{I_{\theta cg} / m_m^3}$$

The uncertainty in the radius of gyration in roll is

$$U_{k_\theta} = \sqrt{(c_1 U_{I_{\theta cg}})^2 + (c_2 U_{m_m})^2}$$

The previous equations in this section for the MOI of pitch are also applicable to roll where the subscript  $\theta$  is replaced with  $\phi$ .

### 3.4.1. Composite Pitch MOI

For a model assembled from a number of pieces, the MOI and its uncertainty for an assembled model are as follows in pitch:

$$I_{\theta m} = \sum_{i=1}^n [(x_{ci}^2 + z_{ci}^2)m_i + I_{\theta i}]$$

where  $x_{ci}$ ,  $y_{ci}$ , and  $z_{ci}$  are the Cartesian coordinates relative to the model CG. The sensitivity coefficients are as follows:

$$c_{1i} = \partial I_{\theta m} / \partial m_i = x_{ci}^2 + z_{ci}^2$$

$$c_{2i} = \partial I_{\theta m} / \partial x_{ci} = 2x_{ci}m_i$$

$$c_{3i} = \partial I_{\theta m} / \partial z_{ci} = 2z_{ci}m_i$$

$$c_{4i} = \partial I_{\theta m} / \partial I_{\theta i} = 1$$

The composite uncertainty for the model in pitch is then



$$U_{I\theta m}^2 = \sum_{i=1}^n \left[ (c_{1i} U_{mi})^2 + (c_{2i} U_{xci})^2 + (c_{3i} U_{zci})^2 + U_{I\theta i}^2 \right]$$

For the MOI of components measured on the same mass-properties instrument, the uncertainties may be considered correlated. In that case, the uncertainties may be summed for those parts.

### 3.4.2. Composite Roll MOI

For a model assembled from a number of pieces, the MOI and its uncertainty for an assembled model are as follows in roll where  $x$  is replaced by  $y$  in the pitch equation,

$$I_{\phi m} = \sum_{i=1}^n [(y_{ci}^2 + z_{ci}^2) m_i + I_{\phi i}].$$

The sensitivity coefficients are as follows:

$$\begin{aligned} c_{1i} &= \partial I_{\phi m} / \partial m_i = y_{ci}^2 + z_{ci}^2 \\ c_{2i} &= \partial I_{\phi m} / \partial y_{ci} = 2y_{ci} m_i \\ c_{3i} &= \partial I_{\phi m} / \partial z_{ci} = 2z_{ci} m_i \\ c_{4i} &= \partial I_{\phi m} / \partial I_{\phi i} = 1 \end{aligned}$$

The composite uncertainty for the model in roll is then

$$U_{I\phi m}^2 = \sum_{i=1}^n \left[ (c_{1i} U_{mi})^2 + (c_{2i} U_{y_{ci}})^2 + (c_{3i} U_{z_{ci}})^2 + U_{I\phi i}^2 \right] \quad (28)$$

For a symmetric model where  $y_{ci} = 0$ , (28) becomes

$$U_{I\phi m}^2 = \sum_{i=1}^n [(z_{ci}^2 U_{mi})^2 + (2z_{ci} m_i U_{z_{ci}})^2 + U_{I\phi i}^2].$$

### 3.5. Transverse Metacentric Height

The transverse metacentric height is determined by performing an inclining experiment in water, floating the model in calm water and adding weight to the model in the transverse direction. The method and equations are similar to those for the VCG. The result for the metacentric height is as follows:

$$GM_T = w(y_w / \tan \phi + z_w) / (w + W_m).$$

The sensitivity coefficients are then

$$\begin{aligned} c_1 &= \partial GM_T / \partial w \\ &= W_m (y_w / \tan \phi + z_w) / (w + W_m)^2 \\ c_2 &= \partial GM_T / \partial W_m \\ &= w (y_w / \tan \phi + z_w) / (w + W_m)^2 \\ c_3 &= \partial GM_T / \partial y_w = w / [\tan \phi (w + W_m)] \\ c_4 &= \partial GM_T / \partial \phi = w y_w / [\sin^2 \phi (w + W_m)] \\ c_5 &= \partial GM_T / \partial z_w = w / (w + W_m) \end{aligned}$$

The uncertainty in  $GM_T$  is

$$U_{GM_T} = \left\{ (c_1 U_w)^2 + (c_2 U_{W_m})^2 + (c_3 U_{y_w})^2 + (c_4 U_{\phi})^2 + (c_5 U_{z_w})^2 \right\}^{1/2} \quad (29)$$

A better estimate of  $(y_w / \tan \phi)$  may be computed by linear regression analysis of the slope of the  $y_w$  versus  $\tan \phi$  curve at  $\phi = 0$ . (Linear curve fit requires model inclination that does not exceed 5 degrees.) In that case, the sensitivity coefficient is

$$c_6 = w / (w + W_m)$$

The uncertainty in  $GM_T$  is then from (29) with the addition in the uncertainty of the slope is:



$$U_{GMT} = \left\{ (c_1 U_w)^2 + (c_2 U_{vm})^2 + (c_3 U_{yw})^2 + (c_4 U_\phi)^2 + (c_5 U_{zv})^2 + (2c_6 u_b)^2 \right\}^{1/2}$$

where  $u_b$  is the standard uncertainty of the slope  $b$  from linear regression analysis.

## 4. MODELING OF WAVE SPECTRA

### 4.1. Extreme-wave Modelling Related to Stability Research

When nonlinear or extreme wave modelling is considered with respect to ship-stability research, the following related questions can be raised:

- How often do extreme waves occur and how relevant are they,
- What are their typical shapes and kinematics,
- How can we model extreme waves.

These questions shall be treated in the following, looking both at state-of-the-art methods and at recent research. This section is organized accordingly.

### 4.2. Probability of Occurrence and Relevance of Extreme Waves

From the numerous data sets investigated during the Cooperative Research on Extreme Seas and their Impact Joint Industry Project (CresT JIP), on the effect of extreme-wave impacts on offshore structures, it was concluded that a second-order wave-crest-

distribution function is a good basis for the estimation of a design-wave crest, Buchner, *et al.* (2011). However, depending on parameters such as directional spreading, sea-state steepness and propagation distance, crests may exceed the second-order distribution in some severe seas by around 10%. On the other hand, the very highest crests may be limited by breaking and even fall below a second-order model.

### 4.3. Effect of Directional Spreading

For three different sea states at the same peak period, the effect of spreading is illustrated in Figure 4-1. Three spreading factors are shown, increasing from top to bottom. The three sea states were measured in the MARIN Offshore Basin during the CresT project. The waves were steep, with a nominal significant wave height of 12 m and a peak period of 12 seconds. The model scale was 50. The theory, Provosto & Forristall (2002), shows that the deviation from second-order theory is much less in short-crested waves. The measured crest-height distribution lies above both the Rayleigh distribution and the standard second-order distribution for the long-crested and the low-spreading case. It should be noted that the figures correspond to one phase seed per sea state. In on-going projects, corresponding investigations concern a large number of seeds.

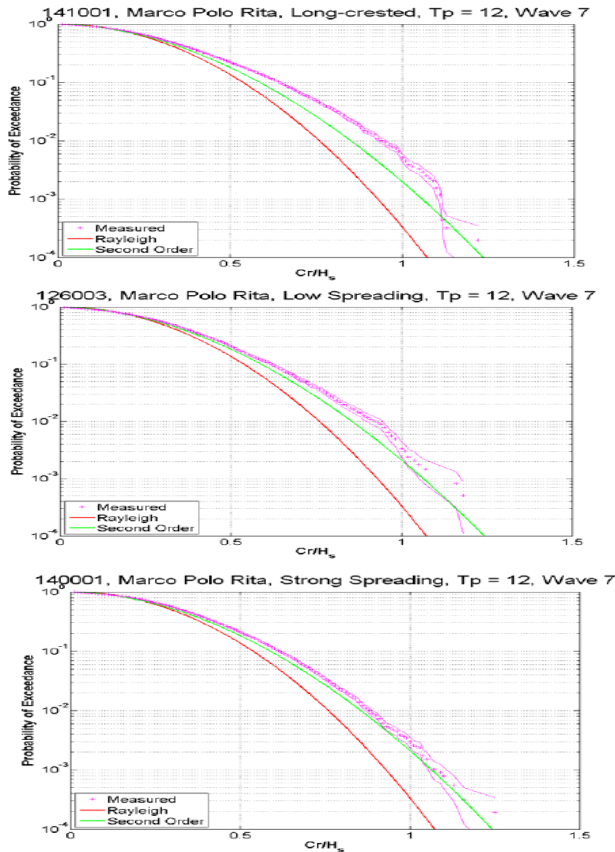


**Figure 4-1 Wave-crest distribution depending on spreading, from top to bottom: Long-crested, low-spreading ( $s=15$ ) and strong-spreading ( $s=4$ ), measurements by MARIN for the Crest JIP.**

#### 4.4. Effect of Sea State Steepness

The effect of sea state steepness is illustrated in Figure 4-2 showing the measured crest distributions for 4000 hours of field data, increasing from top to bottom. The sea state steepness is defined on the basis of the mean spectral period,  $T_1$ :

$$S_1 = \frac{2\pi H_s}{g T_1^2}$$

It can be seen that the wave crests become larger with increasing sea-state steepness,

starting from below the second-order theory and increasing up to a significant deviation beyond second order. For the largest crests, wave breaking as a counteracting effect limits a further increase and the wave-crest distributions fall even below second order. This effect of wave breaking as a limiting process is considered an important observation.

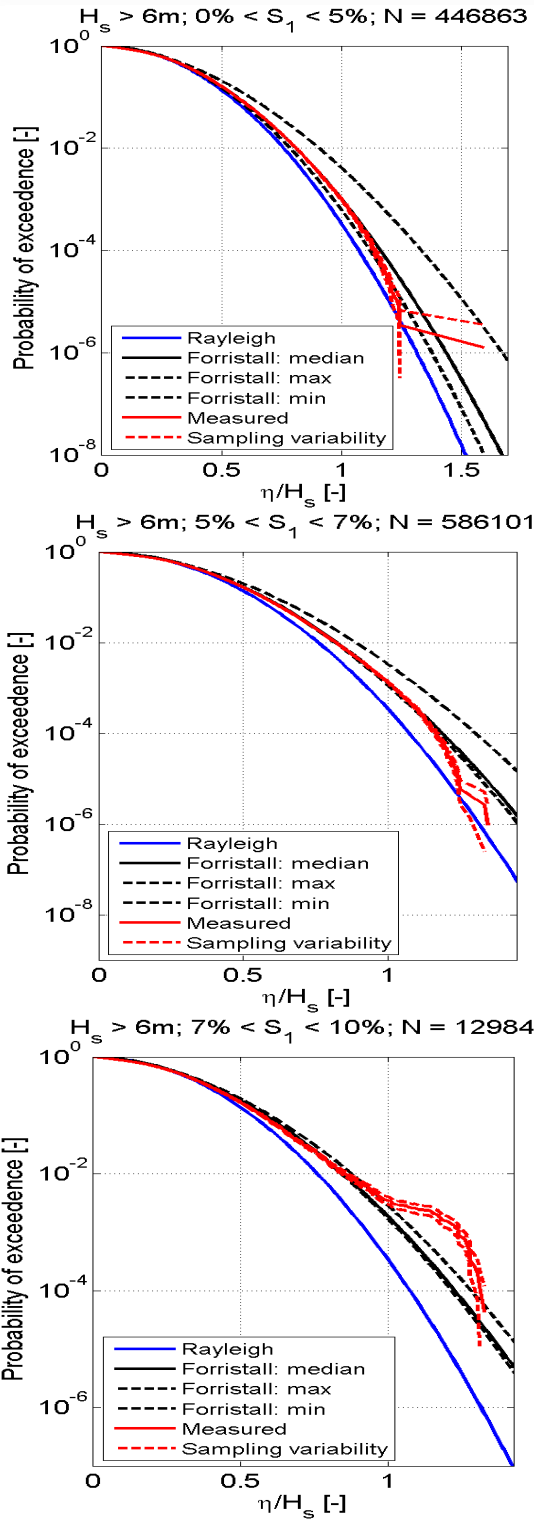


Figure 4-2 Wave-crest distribution depending on sea-state steepness, increasing from top to

bottom: Analysis of 4000 hours of field measurement by Shell for the Crest JIP.

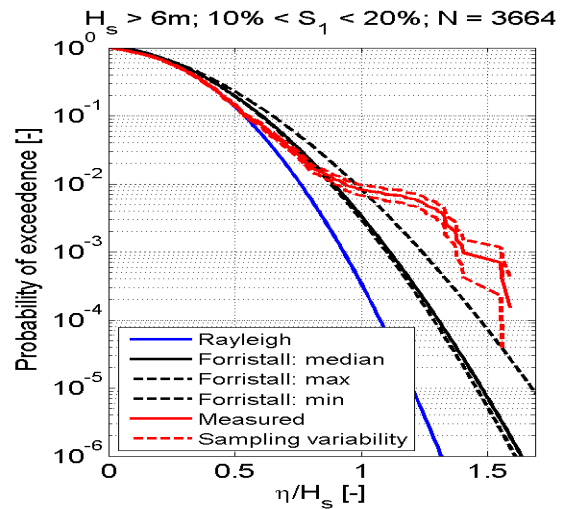


Figure 4-2 (Continued).

#### 4.5. Effect of Distance (from a Wave Maker)

In order to investigate the effect of wave evolution with distance on wave-crest distributions, measurements at several locations along MARIN's Offshore Basin length were carried out. Figure 4-3 shows the distribution of wave probes over the basin length.

Following the evolution of the wave with increasing distance from the wave generator, it can be observed that breaking does not stop the possible further development of extreme crests. Figure 4-4 shows crest-height distributions for the same test, but at greater distances from the wave generator. These measurements show that in long-crested waves, it may take a few wavelengths to modify the crest-height distribution. The observed growth may be due to third-order resonant interactions, or Benjamin-Feir instabilities, accompanied by a shift of spectral energy in the frequency band, and observed growth



seems somewhat faster here than has been reported in some other studies—at scale 1:50, the MARIN Offshore Basin has a length of 5–10 wavelengths.

In summary, for the wave statistics, the following can be concluded from the research undertaken in CrestT:

1. Use the Forristall distribution for the wave height.
2. Use second order distribution as basis for the crest height.

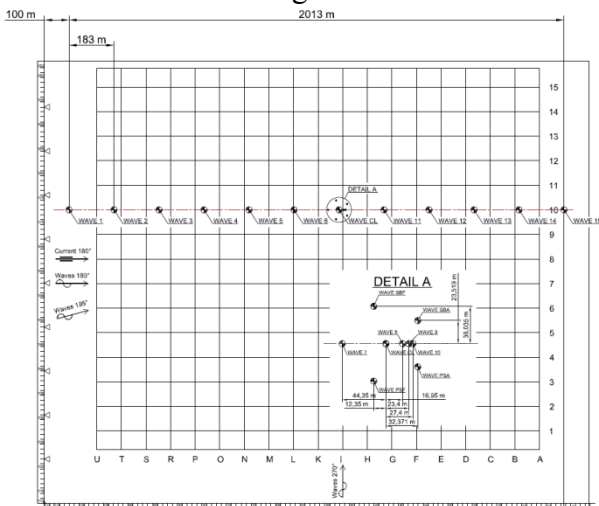


**Figure 4-3 Distribution of wave probes along MARIN's Offshore Basin.**

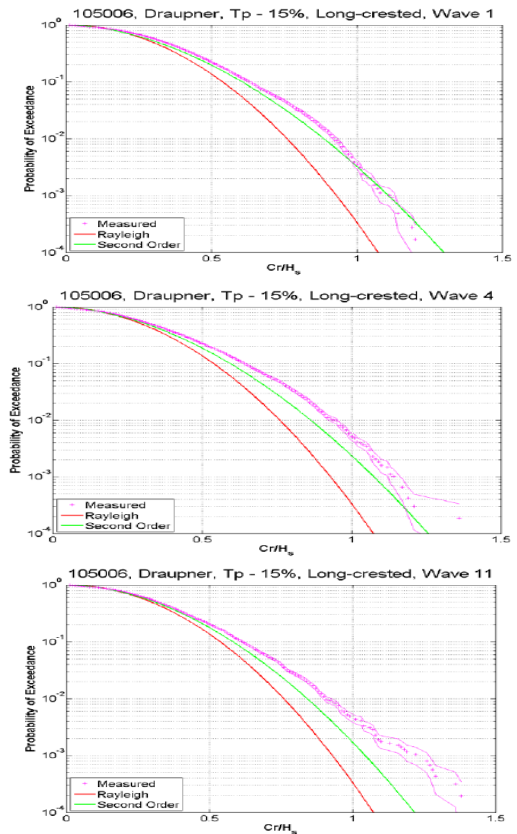


**Figure 4-4 Crest-height distribution observed for long-crested seas in the MARIN Offshore Basin, 100 m from wave flap, approximately 2 wavelengths from the wave generator (649 m) and approximately 5 wavelengths from the wave generator (1930 m), scale 1:50.**

3. Correct for observed deviations from second order. (This is the subject of ongoing research.)

Understanding the processes described previously and giving useful recommendations demands an effort in defining the correct wave spectrum, understanding wave amplification and breaking, and generating fully nonlinear crest statistics in a scheme useful for engineering applications.

#### 4.6. Shape and Kinematics of Extreme Waves

In order to answer this question, the following aspects are considered:

- How to model the most realistic wave directionality
- Wave loading and response in short-crested waves

In case of short-crested waves the directional distribution of the wave energy has to be defined. The directional spectrum,  $S(\omega, \theta)$ , is a combination of a frequency-dependent spectrum,  $S(\omega)$ , and a frequency- and direction-dependent spreading function,  $D(\omega, \theta)$ :

$$S(\omega, \theta) = S(\omega) \cdot D(\omega, \theta) / G(\omega, \theta)$$

$$G(\omega, \theta) = \int_0^{2\pi} D(\omega, \theta) d\theta$$

The frequency dependent,  $S(\omega)$ , can be described using a JONSWAP formulation, for example. For the spreading function,  $D(\theta)$ , a number of formulations that do not depend on  $\omega$  are commonly used, amongst others:

$$D(\theta) = \cos^{2s} \left( \frac{\theta - \theta_m}{2} \right) \Big| \theta \in [0, 360]$$

An illustration of this type of spreading function is given in Figure 4-5.

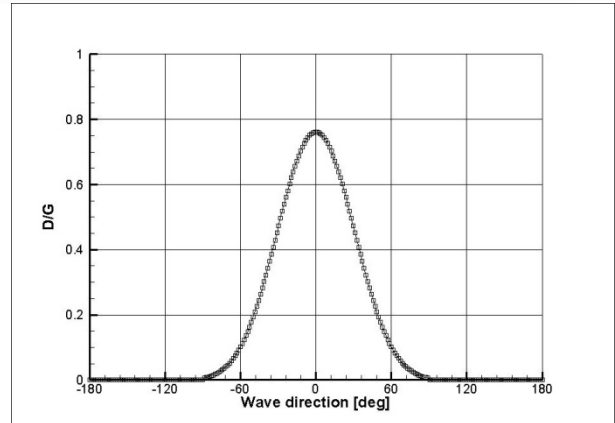


**Figure 4-5 Formulation of the spreading function  $D(\theta)/G(\theta)$  with  $s = 7$ .**

By using an  $s$ -parameter that is frequency-dependent, each of these formulations can be used to describe a  $D(\omega, \theta)$  function. For example, in the Park, *et al.* (2001) spreading function, the exponent in the  $\cos^{2s}$  formulation is frequency dependent:

$$s(\omega) = \begin{cases} s_{\max} \left( \frac{\omega}{\omega_p} \right)^5, & \text{for } \frac{\omega}{\omega_p} < 1 \\ s_{\max} \left( \frac{\omega}{\omega_p} \right)^{-2.5}, & \text{for } \frac{\omega}{\omega_p} \geq 1 \end{cases}$$

where  $\omega_p$  denotes the peak frequency of the  $S(\omega)$  spectrum.

An example of a frequency-dependent spreading is given in Figure 4-6.

#### 4.7. Calibration of Directional Waves

To improve the quality of waves in a model basin, a calibration loop can be used. For a target wave spectrum the wave-maker- control

software determines the theoretical flap motions, leading to a wave realization in the basin. Depending on the quality of the wave-maker theory used, the resulting wave in the basin can differ from the target spectrum. In a typical calibration loop the generated wave is measured and analyzed. The resulting spectrum is compared against the target spectrum. Next, the target spectrum sent to the wave maker can be adjusted in an attempt to obtain a better-quality basin wave.

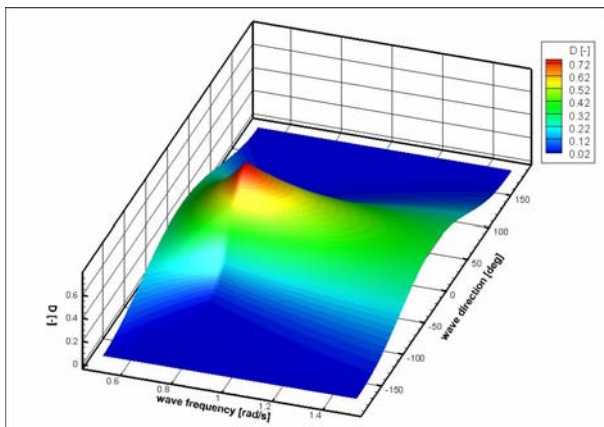


**Figure 4-6 Frequency-dependent directional-spreading function  $D(\omega_p = 0.80 \text{ [rad/s)]}$ .**

For long-crested waves the calibration procedure is well-established and included in common wave-generation software. For short-crested waves a similar approach was implemented and tested at MARIN: First the directional spectrum,  $S(\omega, \theta)$ , was defined as a combination of a frequency-dependent spectrum,  $S(\omega)$ , and a frequency- and direction-dependent spreading function  $D(\omega, \theta)$ ; in the correction procedure,  $S(\omega, \theta)$  and  $D(\omega, \theta)$  are treated separately. In a global overview the calibration worked as follows:

1. A wave was generated in the basin for the theoretical spectrum,  $St(\omega)$ , and the spreading function,  $Dt(\omega, \theta)$ .
2. The results were measured and analysed to determine the measured spec-

trum,  $Sm(\omega)$ , and the measured spreading function,  $Dm(\omega, \theta)$ .

3. The corrections,  $CS(\omega)$  and  $CD(\omega, \theta)$ , were computed.
4. A new wave attempt based on  $CS(\omega)St(\omega)$  and  $CD(\omega, \theta)Dt(\omega, \theta)$  was generated.
5. The calibration process was repeated from point 2 until satisfactory results were obtained.

To measure the waves, resistance-type, wave-elevation probes were used. The probe layout consisted of a number of small footprint arrays distributed over a larger area of the basin. To determine the wave spectral density, a combination of two methods was used: Extended Maximum Likelihood Method (EMLM), Waals, *et al.* (2002) and Maximum Entropy Method (MEM), Briggs (1982)] which were both implemented and tested for typical probe arrays. For frequencies above 2.5 rad/s (18 s prototype), a slope-based MEM method was used on each of the small footprint arrays to obtain local information on the  $Dm(\omega, \theta)$ . At lower frequencies, *i.e.*, longer waves, the slope fell within the resolution/measurement accuracy of the wave probes within a small footprint array. As an alternative, a phase-difference-based EMLM method was used, based on single-wave probes distributed over a larger area in the basin. Combining the two methods gave a reliable analysis for a wide range of frequencies. The correction factor,  $CD(\omega, \theta)$ , was computed using:  $CD(\omega, \theta) = Dm(\omega, \theta)/Dt(\omega, \theta)$ . The correction was only computed for the range of  $\omega$  and  $\theta$  with sufficient spectral energy.

#### 4.8. Extreme Wave Modeling in Model Basins

To model extreme waves accurately in both in test basins and in numerical simulations,



different approaches are required which are addressed briefly in the following sections. Numerical wave tanks are addressed elsewhere.

Deterministic-wave generation means to reproduce a predefined target wave train at a given position in a basin. For the generation of deterministic-wave sequences in a model basin, different types of wave makers are available. The wave generation process, as illustrated in Figure 4-7 (an example of a double-flap wave maker), can be divided into four steps:

1. Definition of the target wave train: the target position in time and space is selected—for example, the position where a ship encounters the wave train at a given time. At this location, the target wave train is designed—based on defined parameters or a wave record.
2. Upstream transformation: the target wave train is transformed upstream to the position of the wave maker, *e.g.*, by means of a nonlinear wave propagation model.
3. Calculation of control signals: the corresponding control signals are calculated using adequate transfer functions of the wave generator.
4. Performing the model tests: the control signals are used to generate the specified wave train, which is measured at selected positions in the tank.

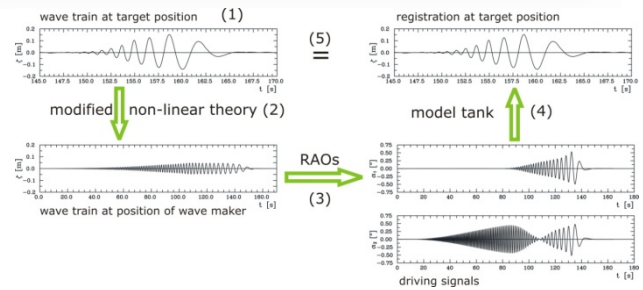


**Figure 4-7 Process of deterministic-wave generation: Calculation starts from the desired target wave train, defined by particular parameters (1). Modelling wave propagation properly, the wave train at the position of the wave maker (2) as well as the corresponding wave-maker-control signals (3) are calculated. The resulting wave train can be measured at the target position (4) and compared to the given target wave (5).**

#### 4.9. Optimization of Wave Realisations

Furthermore, the target wave can be achieved by optimization applied both to a numerical and a physical wave tank. In the figure below, (an example of the well-known “New-Year Wave” as an extreme directional wave), this optimization process is illustrated. The “New-Year Wave” was measured on 01/01/95 in the Norwegian sector of the North Sea (Draupner) by a down-looking radar, Haver & Anderson (2000). It is a 20-min wave record, with  $T_p = 10.8$  s,  $H_S = 11.92$  m,  $H_{MAX} = 25.6$  m  $\Rightarrow H_{MAX}/H_S = 2.15$ , Crest height 18.5 m, water depth = 70 m. The directional-wave generation based on optimization works as follows:

- Combining target wave train (time domain) and directional spectrum (frequency domain) to “fronts” as a unique parameter set of wave frequency, heading, amplitude and phase



- Transferring wave fronts upstream using linear theory
- Calculating the motion of the first-wave board, and then of neighboring boards
- Generating, measuring and analyzing waves
- Optimizing wave-board motions, based on comparisons with the target wave

Figure 4-8 shows the result of the optimized-basin realization of the short-crested New-Year Wave.

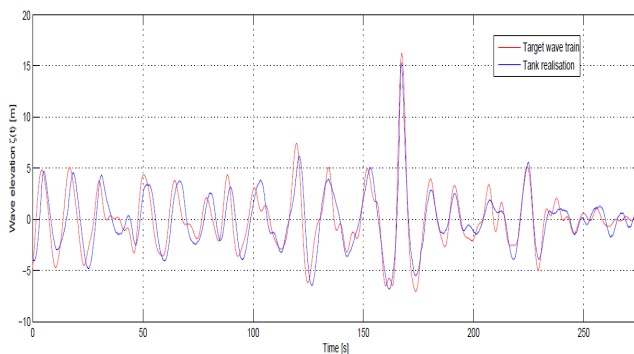


**Figure 4-8 “New-Year Wave” modelled in the basin by using an optimization method.**

#### 4.10. Focused Waves

Focused wave techniques (Claus, 2008) can be used to deterministically generate extreme waves in model tests such as capsizing tests and is based on the in-phase superposition of component waves at a target location (or at a focusing point), at a given target time. Another input can be the spectral shape of a single wave and/or the underlying sea state. Focused-wave techniques can be applied to the determination of response amplitude operators (RAOs) (linear focusing waves), the simulation of extreme events and embedding extreme waves in sea states. The advantages of these techniques are a short test duration, smooth transfer functions and extreme waves controllable in space and time. Figure 4-9 gives an example of a focused-wave generated in a model basin.

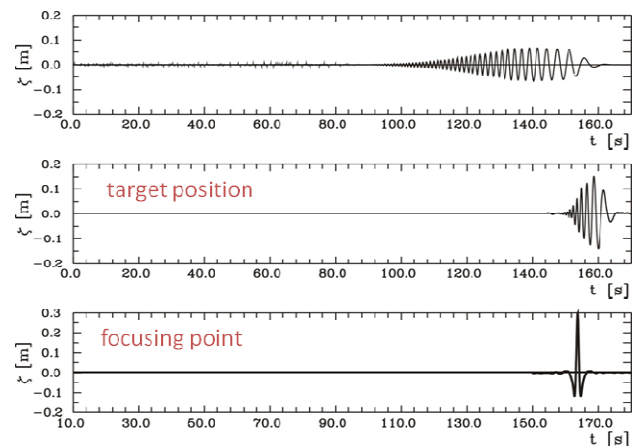


**Figure 4-9 Focused waves generated for model tests.**

#### 4.11. Numerical Methods

Modelling of extreme waves requires a nonlinear wave-propagation model for both physical and numerical wave generation. Numerical wave tanks can be based on potential (e.g., WAVETUB) or viscous-flow solvers,



which can be coupled with motion- simulation tools. Also a coupling between potential and viscous flow solvers is a good approach to limit the calculation domain and save simulation time. Wave-structure interaction can be simulated in a wave field introduced via a pressure distribution (requires coupling with a wave model) or wave-velocity inlet (requires a wave-maker model in CFD).

Such advanced methods are required to model extreme-wave properties such as: wave-propagation speed increasing with wave steepness; vertical asymmetry of wave crest and trough; mass transport; interaction between wave frequencies; and Benjamin-Feir instabilities (*cf.* Green & Naghdi, 1986, 1987; Dommermuth & Yue, 1987; Webster, 2009).

For use in simulation methods for stability investigations, advanced CFD-based methods are still too “central processing unit (CPU)-intensive” for practical use. Higher order theories based on potential flow can be used for such purposes as described in the next sections.

#### 4.12. Pressure Modelling

For a nonlinear environmental representation, the selection of the proper hydrodynamic pressure model is an important issue. The model must be able to represent the pressure in directional sea states, account for the increased steepness of wave crests, allow for the accurate representation of the wave kinematics in both the surf zone and the fluid domain, contain a statistical structure consistent with that observed in nature, and allow fast simulations of ambient sea-state pressures for use in the prediction of vessel and platform responses. Second-order theory meets most of these requirements.

For a single monochromatic wave, exact second-order theory gives very close to zero total (hydrostatic plus hydrodynamic) pressure on the free surface up to wave steepness’s approaching 1/7. However, in a steep sea state composed of many waves of different frequencies, the sum- and the difference-frequency exponential terms can contribute unrealistically large terms that result in free-surface pressures that are far from zero. Therefore, we shall adopt an approximation that uses a two-term Taylor series expansion of the first-order term, which the literature suggests is one of the best compromises for dealing with these issues. This can be thought of as a two-term expansion of the exponential term that gets very large in the exact second-order solution.

##### 4.12.1. Coordinate System

An earth-fixed Cartesian  $X, Y, Z$  coordinate system is used where  $Z$  points upward and the plane,  $Z=0$ , lies in the mean free-surface level. The horizontal  $X$  and  $Y$  axes are such that the coordinate system is right-handed; otherwise, the orientations of the horizontal axes are arbitrary.

##### 4.12.2. Determining Linear-Wave Amplitudes

Given a two-sided linear spectrum,  $\mathfrak{S}(\omega)$ , such that the quadratic spectrum

$$\mathfrak{S}_2(\omega) = \mathfrak{S}(\omega) + 2 \int_{-\infty}^{\infty} d\sigma \mathfrak{S}(\sigma) \mathfrak{S}(\omega - \sigma) \mathcal{Z}^2(\sigma, \omega - \sigma)$$

is a good approximation to some desired two-sided target spectrum,  $\mathfrak{S}_r(\omega)$ , linear-wave amplitudes are determined from the equation



$$a_j \equiv \mathbf{a}(\omega_j) = 2\sqrt{\mathfrak{S}(\omega_j)\Delta\omega}.$$

It is assumed that  $\mathfrak{S}(0)=0$  and  $\mathbf{a}_0=0$ , but it is not assumed that  $\Delta\omega$  is uniform. Therefore, the user may provide wave periods  $T_j=2\pi/\omega_j$  in decreasing order for  $j=1, 2, \dots, N$ . The frequencies,  $\omega_j$ , might also be determined so that  $\mathfrak{S}(\omega_j)(\omega_{j+1}-\omega_{j-1})$  is approximately constant. In either case, the increments  $\Delta\omega$  are defined from the  $\omega_j$  as follows:

$$\Delta\omega = \begin{cases} (\omega_{j+1} - \omega_{j-1})/2 & \text{if } j=1, \dots, N-1 \\ (\omega_N - \omega_{N-1}) & \text{if } j=N \end{cases}$$

For all  $j$  between 1 and  $N$ ,  $\mathbf{a}_{-j} = \mathbf{a}_j$ .

For positive  $j$ , phase angles,  $\varepsilon_j$ , are chosen so that they are random numbers uniformly distributed between 0 and  $2\pi$ . For negative  $j$ , the phase angles satisfy the equation  $\varepsilon_j = -\varepsilon_{-j}$ . The phase angle for  $j=0$  is irrelevant since the magnitude,  $\mathbf{a}_0$ , vanishes and thus may be defined as 0.

#### 4.12.3. Perturbation Series

The velocity potential, wave elevation, and pressure are written as a perturbation series

$$\begin{aligned} \phi_I &= \phi_I^{(1)} + \phi_I^{(2)} + \dots \\ \zeta_I &= \zeta_I^{(1)} + \zeta_I^{(2)} + \dots \\ p_I &= p_I^{(0)} + p_I^{(1)} + p_I^{(2)} + \dots \end{aligned}$$

where  $\phi_I^{(\ell)}$ ,  $\zeta_I^{(\ell)}$ , and  $p_I^{(\ell)}$  are  $O(\varepsilon^\ell)$ . The perturbation parameter,  $\varepsilon$ , is often taken to be the wave steepness or the wave amplitude.

#### 4.12.4. Equations to Obtain First- and Second-Order Pressures

The perturbation series are substituted into the Bernoulli equation to obtain the equation

$$\begin{aligned} 0 &= \frac{p_I}{\rho} + gZ + \frac{1}{2}\nabla\phi_I \cdot \nabla\phi_I + \frac{\partial\phi_I}{\partial t} \\ &= \frac{1}{\rho}(p_I^{(0)} + p_I^{(1)} + p_I^{(2)} + \dots) + gZ \\ &\quad + \frac{1}{2}\nabla(\phi_I^{(1)} + \phi_I^{(2)} + \dots) \cdot \nabla(\phi_I^{(1)} + \phi_I^{(2)} + \dots) \\ &\quad + \frac{\partial}{\partial t}(\phi_I^{(1)} + \phi_I^{(2)} + \dots) \\ &= \left[ \frac{p_I^{(0)}}{\rho} + gZ \right] + \left[ \frac{p_I^{(1)}}{\rho} + \frac{\partial\phi_I^{(1)}}{\partial t} \right] \\ &\quad + \left[ \frac{p_I^{(2)}}{\rho} + \frac{1}{2}(\nabla\phi_I^{(1)} \cdot \nabla\phi_I^{(1)}) + \frac{\partial\phi_I^{(2)}}{\partial t} \right] + \dots \end{aligned}$$

The sum of all terms of order,  $\ell$ , on the left side of the equation must equal the sum of all terms of order,  $\ell$ , on the right side of the equation for all  $\ell$ . Therefore, the following equations are obtained:

$$\begin{aligned} p_I^{(0)} &= -\rho gZ, \\ p_I^{(1)} &= -\rho \frac{\partial\phi_I^{(1)}}{\partial t}, \\ p_I^{(2)} &= -\rho \left( \frac{\partial\phi_I^{(2)}}{\partial t} + \frac{1}{2}\nabla\phi_I^{(1)} \cdot \nabla\phi_I^{(1)} \right). \end{aligned}$$

#### 4.12.5. Zeroth-Order Pressure

The zeroth-order velocity potential and the zeroth-order wave height vanish, but the



zeroth-order pressure is nonzero and equals the linear hydrostatic pressure:

$$p_i^{(0)} = -\rho g Z.$$

#### 4.12.6. First-Order Pressure

There are  $N$  linear wave components with associated positive frequencies,  $\omega_j$ , and positive wave numbers,  $k_j = \omega_j^2 / g$ , for  $j = 1, 2, \dots, N$ . The  $j$ -th wave component propagates in the direction that makes the angle,  $\beta_j$ , with respect to the positive  $X$ -axis where  $\beta_j$  is measured counter-clockwise about the  $Z$ -axis as seen from a point on the positive  $Z$ -axis. It has amplitude,  $a_j$ , and a phase angle,  $\varepsilon_j$ . The phase angles are random numbers uniformly distributed between 0 and  $2\pi$ . To compute the first-order pressure, additional  $N$  wave components,  $j = -N, \dots, -1$ , are defined with negative frequencies and wave numbers as:

$$\begin{aligned}\omega_{-j} &= -\omega_j \\ k_{-j} &= -k_j \\ k_j &= \omega_j |\omega_j| / g \\ a_{-j} &= a_j \\ \varepsilon_{-j} &= -\varepsilon_j \\ \beta_{-j} &= \beta_j\end{aligned}$$

Where it is assumed that  $a_0 = 0$ . Using this notation, the linear pressure is a sum of components

$$\begin{aligned}p_i^{(1)}(X, Y, Z, t) &= \rho g \sum_{j=1}^N a_j e^{|k_j|Z} \\ &\times \cos\left[\omega_j t - k_j (X \cos \beta_j + Y \sin \beta_j) + \varepsilon_j\right]\end{aligned}$$

#### 4.12.7. Second-Order Pressure

To shorten the equation, it is helpful to define the quantity,  $k_{j\ell}^\pm$ , by the equation

$$k_{j\ell}^\pm = \sqrt{k_j^2 + k_\ell^2 \pm 2k_j k_\ell \cos(\beta_j - \beta_\ell)}$$

The second-order pressure,  $p_i^{(2)}$ , can be determined from the equation

$$\begin{aligned}p_i^{(2)}(X, Y, Z, t) &= -\frac{\rho}{2} \sum_{\ell=1}^N a_\ell^2 \omega_\ell^2 e^{2k_\ell Z} \\ &+ \frac{\rho}{2} \sum_{j=1}^N \sum_{\ell=1}^N (1 - \delta_{j\ell}) a_j a_\ell \omega_j \omega_\ell \left[1 - \cos(\beta_j - \beta_\ell)\right] \\ &\times \left[ \frac{(\omega_j + \omega_\ell)^2 e^{k_{j\ell}^+ Z}}{g k_{j\ell}^+ - (\omega_j + \omega_\ell)^2} + \frac{e^{(k_j + k_\ell)Z}}{2} \right] \cos \Theta_{j\ell}^+ \\ &- \frac{\rho}{2} \sum_{j=1}^N \sum_{\ell=1}^N (1 - \delta_{j\ell}) a_j a_\ell \omega_j \omega_\ell \left[1 + \cos(\beta_j - \beta_\ell)\right] \\ &\times \left[ \frac{(\omega_j - \omega_\ell)^2 e^{k_{j\ell}^- Z}}{g k_{j\ell}^- - (\omega_j - \omega_\ell)^2} + \frac{e^{(k_j + k_\ell)Z}}{2} \right] \cos \Theta_{j\ell}^+\end{aligned}$$

where  $\delta_{j\ell}$  is the Kronecker delta and  $\Theta_{j\ell}^\pm$  is defined as

$$\begin{aligned}\Theta_{j\ell}^\pm &= (\omega_j \pm \omega_\ell) t - X(k_j \cos \beta_j \pm k_\ell \cos \beta_\ell) \\ &- Y(k_j \sin \beta_j \pm k_\ell \sin \beta_\ell) + (\varepsilon_j \pm \varepsilon_\ell)\end{aligned}$$

The single sum and the first double sum are the contributions due to sum frequencies. The second double sum is the contribution from difference frequencies.



#### 4.12.8. Pressure Above the Mean Free-Surface Level

One could evaluate the pressure above the mean free-surface level just as given in the equations for  $Z \leq 0$ . However, as is pointed out by Gudmestad (1993), this leads to unrealistic results as terms involving  $e^{k_j Z}$  become very large near the crests of waves. Therefore, the approach of Stansberg, *et al.* (2006) is used here. Of the various methods considered by them, their second-order model has provided computed data closest to measured data. The pressure given by this second-order wave model for  $0 < Z < \zeta_i^{(1)}(X, Y, t) + \zeta_i^{(2)}(X, Y, t)$  is

$$p_i(X, Y, Z, t) = p_i^{(1)}(X, Y, 0, t) + p_i^{(2)}(X, Y, 0, t) + Z \left[ \frac{\partial}{\partial Z} p_i^{(1)}(X, Y, Z, t) \right]_{Z=0}$$

#### 4.12.9. Computational Methods

Unidirectional- and multidirectional-wave systems are treated separately since the computational methods for the two cases are significantly different.

##### Unidirectional Waves

If waves travel in the direction that makes the angle  $\beta$ , measured counter clockwise from the positive earth-fixed  $X$ -axis as viewed from above, then one can change to a primed coordinate system with coordinates  $X', Y', Z'$  such that

$$\begin{aligned} X' &= X \cos \beta + Y \sin \beta \\ Y' &= -X \sin \beta + Y \cos \beta \\ Z' &= Z \end{aligned}$$

The direction of wave propagation then coincides with the positive  $X'$ -axis.

*First-Order Sums.* The first-order pressure is given by the equations

$$p_i^{(1)}(X, Y, Z, t) = \rho g \sum_{j=1}^N a_j e^{k_j Z} \times \cos(\omega_j t - k_j X' + \varepsilon_j)$$

where it is assumed that  $a_0 = 0$  holds.

*Second-Order Sums.* The second-order correction to the pressure for unidirectional-wave systems is entirely due to difference frequencies:

$$p_i^{(2)}(X, Y, Z, t) = p_i^{(2-)}(X, Y, Z, t) = \frac{\rho}{4} \sum_{j=-N}^N \sum_{\ell=-N}^N a_j a_\ell Z_{j\ell}^{p-} e^{i[(\omega_j + \omega_\ell)t - (k_j + k_\ell)X' + (\varepsilon_j + \varepsilon_\ell)]}$$

where  $Z_{j\ell}^{(p-)}$  is defined by the equation

$$Z_{j\ell}^{(p-)}(k_j, k_\ell) = \begin{cases} 0 & \text{if } k_j k_\ell > 0 \\ \left| \omega_j \omega_\ell \right| e^{(|k_j| + |k_\ell|)Z} + \left| \omega_j + \omega_\ell \right| \max(|\omega_j|, |\omega_\ell|) \times e^{|k_j + k_\ell|Z} & \text{if } k_j k_\ell < 0 \end{cases}$$

##### Multidirectional Waves

An efficient method for calculating first- and second-order pressures is not known for situations in which wave directions and wave frequencies are irregular. Therefore, it is assumed that wave amplitude is supplied on a topologically rectangular grid of points in the  $(\omega, \beta)$ -plane so that

$$a_{p\ell} = a(\omega_p, \beta_\ell)$$



for  $p = -N_\pi, \dots, N_\pi$  and  $\ell = 1, \dots, N_\beta$  where  $\mathbf{a} = \mathbf{a}(\omega, \beta)$  is a real-valued function whose domain is a subset of  $\{(\omega, \beta) : -\infty < \omega < \infty \text{ and } 0 \leq \beta < 2\pi\}$ . The frequencies,  $\omega_p$ , satisfy the equation,  $\omega_p = -\omega_{-p}$ , and the discrete amplitudes,  $\mathbf{a}_{p\ell}$ , satisfy the equation,  $\mathbf{a}_{-p\ell} = \mathbf{a}_{p\ell}$ . For each  $p$  and  $\ell$  there is a phase angle,  $\varepsilon_{p\ell}$ . For positive  $p$ , the phase angles are uniformly distributed random numbers between 0 and  $2\pi$  radians. For negative  $p$ , the phase angles are chosen so that  $\varepsilon_{-p\ell} = -\varepsilon_{p\ell}$ . It is assumed that the wave numbers are equally spaced so that  $k_p = p\Delta k$  for some  $\Delta k$ . The discrete wave numbers and angular frequencies are related by the equation  $k_p = \omega_p / \omega_p / g$ .

The first-order pressure is given by the equation

$$p_1^{(1)}(X, Y, Z, t) = \rho g \sum_{\ell=1}^{N_\beta} \left\{ \sum_{p=0}^{N_\pi} \mathfrak{R} \left\{ \mathbf{a}_{p\ell} e^{i\varepsilon_{p\ell}} e^{i\omega_p t} \right\} e^{k_p Z} \right. \\ \times \cos \left[ k_p (X \cos \beta_\ell + Y \sin \beta_\ell) \right] \\ \left. + \sum_{p=0}^{N_\pi} \mathfrak{I} \left\{ \mathbf{a}_{p\ell} e^{i\varepsilon_{p\ell}} e^{i\omega_p t} \right\} e^{k_p Z} \right. \\ \left. \times \sin \left[ k_p (X \cos \beta_\ell + Y \sin \beta_\ell) \right] \right\}$$

The primed summation symbol indicates that the first term in the summation should be halved. The inner sums can be evaluated with the aid of Clenshaw's algorithm (Goertzel, 1960; Luke, 1976; Newman, 1987; Press, *et al.*, 1986) if the wave numbers are equally spaced.

The second-order correction to the pressure is given by the equation

$$p_1^{(2)}(X, Y, Z, t) = \frac{\rho}{4} \sum_{\ell=1}^{N_\beta} \sum_{m=1}^{N_\beta} \left\{ \sum_{p=-N_\pi}^{N_\pi} \mathbf{a}_{p\ell} e^{i\varepsilon_{p\ell}} e^{i\omega_p t} \right. \\ \times e^{-ik_p(X \cos \beta_\ell + Y \sin \beta_\ell)} \\ \times \sum_{q=-N_\pi}^{N_\pi} \mathbf{a}_{qm} e^{i\varepsilon_{qm}} e^{i\omega_q t} Z_{p\ell qm}^{(p)} \\ \left. \times e^{-ik_q(X \cos \beta_m + Y \sin \beta_m)} \right\}.$$

The function  $Z_{p\ell qm}^{(p)} = Z^{(p)}(\omega_p, \beta_\ell; \omega_q, \beta_m)$  is defined by the equation

$$Z_{p\ell qm}^{(p)} = \begin{cases} \omega_p \omega_q \left[ 1 - \cos(\beta_\ell - \beta_m) \right] \\ \times \left[ \frac{(\omega_p + \omega_q)^2}{gk_{p\ell qm} - (\omega_p + \omega_q)^2} e^{k_{p\ell qm} Z} \right. \\ \left. + \frac{1}{2} e^{(|k_{p\ell}| + |k_q|)Z} \right] & \text{if } pq < 0 \\ \omega_p \omega_q \left[ 1 + \cos(\beta_\ell - \beta_m) \right] \\ \times \left[ \frac{(\omega_p + \omega_q)^2}{gk_{p\ell qm} - (\omega_p + \omega_q)^2} e^{k_{p\ell qm} Z} \right. \\ \left. + \frac{1}{2} e^{(|k_{p\ell}| + |k_q|)Z} \right] & \text{if } pq > 0 \end{cases}$$

If  $p = -q$  and  $\ell = m$ , there is a removable singularity. In this case, the transfer function equals  $-\omega_p^2 e^{2|k_p|Z}$ . The sum over  $q$  can be obtained with the aid of Clenshaw's algorithm after which the sum over  $p$  can be obtained with the same algorithm.

If the second-order pressure due to the sum frequencies is desired, then the definition of

$Z_{p\ell qm}^{(p)}$  should be modified so that it is 0 if



$pq < 0$ . Similarly, if the second-order pressure due to the difference frequencies is desired, then the definition of  $Z_{pqm}^{(p)}$  should be modified so that it is 0 if  $pq > 0$ .

#### 4.13. Linear Spectrum from a Nonlinear Spectrum

In extreme nonlinear seas, one cannot directly use the measured spectra,  $S_r(\omega)$ , from these seas in an analysis, or to derive a sea-keeping prediction, but rather one must derive the underlying linear spectrum to describe the waves that should be simulated. This is because nonlinear interactions between the linear waves will provide second-order, nonlinear contributions through the physics capturing wave-wave interactions.

At extreme wave heights theoretical spectra such as the Joint North Sea Wave Observation Project (JONSWAP) spectrum have nonlinear tails that are unrealizable in an experimental facility due to the breaking of high frequency waves. The underlying realizable spectrum may be derived as the corresponding linear spectrum by the techniques to be described.

The derivation of the linear spectrum underlying the nonlinear spectrum requires the solution of an integral equation describing the measured spectrum by either direct or indirect methods. This section will introduce two possible methods of solving this problem, with the assumption that the process involves only first- and second-order processes, a reasonable assumption in most circumstances.

##### 4.13.1. Determining a Linear Spectrum

Only the case of unidirectional waves is considered here since an integral equation similar to the one that exists for unidirectional waves is not known for the case of multidirectional waves. A two-sided target spectrum,  $S_r(\omega)$ , is assumed to have been provided by the user. A two-sided linear spectrum  $S_l(\omega)$ , is sought which approximately satisfies the equation

$$S_r(\omega) = S_l(\omega) + 2 \int_{-\infty}^{\infty} d\sigma S_l(\sigma) S_l(\omega - \sigma) Z^2(\sigma, \omega - \sigma) \quad (30)$$

for real  $\omega$  where

$$Z(\sigma, \omega) = \begin{cases} (\sigma^2 + \omega^2) / (2g) & \text{if } \omega\sigma > 0 \\ -|\sigma^2 - \omega^2| / (2g) & \text{if } \omega\sigma < 0 \end{cases} \quad (31)$$

The details of the derivation are presented in Sclavounos (1992). The spectral density,  $S_l(\omega)$ , is that of the linear model and is defined as follows:

$$\frac{1}{8} a_j^2 = S_l(\omega_j) \Delta\omega$$

Therefore, the statistical inference of a second-order model reduces to the determination of the wave amplitudes,  $a_j$ , so that the second-order spectral density best matches the measured spectrum,  $S_r(\omega)$ . The linear spectral density,  $S_l(\omega)$ , may be selected from any of the standard families with parameters such that the equality (30) is satisfied in a least squares sense.



For example, the ITTC spectrum may be used for the representation<sup>3</sup>,  $\mathfrak{S}_1(\omega)$ :

$$S_1(\omega) = \frac{0.110}{4\pi} H_{1/3}^2 T_1^2 \lambda^{-5} e^{-0.440\lambda^4}, \quad (32)$$

$$\lambda = \frac{\omega T_1}{2\pi}$$

In (32) an accurate estimate of the modal period,  $T_1$ , may be available from full-scale measurements. Significant wave height on the other hand must be selected so that (30) is satisfied as accurately as possible, given  $\mathfrak{S}_r(\omega)$ . The amplitudes of the regular wave components then follow from (31) and are used in equations for the representation of the linear- and second-order velocity potentials which then yield all desired quantities in the second-order wave-kinematics model.

An alternative numerical approach such as the following might be considered. Using the definition of  $Z$  (31) and assuming that the spectra,  $\mathfrak{S}_1(\omega)$  and  $\mathfrak{S}_r(\omega)$ , are even functions of  $\omega$ , the integral equation can be rewritten as

$$S_T(\omega) = S_1(\omega) + 2 \int_{-\infty}^{\infty} d\sigma S_1(\sigma) \left[ S_1(\omega + \sigma) Z^2(-\sigma, \omega + \sigma) + S_1(\omega - \sigma) Z^2(\sigma, \omega - \sigma) \right]$$

The integral equation has no solution if the target spectrum has content of higher than the second order in the wave amplitude. This subsection describes how a least-squares approximation to the desired linear spectrum,

$\mathfrak{S}_1(\omega)$ , may be obtained and thus avoids the issue of whether a solution exists or not.

The numerical scheme that follows requires that discrete frequencies be equally spaced. If this is not the case, then  $\omega - \sigma$  in the discretized integral equation will not be one of the discrete frequencies,  $\omega_j$ , and any numerical scheme becomes complicated. The discrete frequencies in this subsection are therefore not necessarily those for which linear wave amplitudes,  $a_j$ , are chosen in the next subsection, and the  $N$  used in the description of the numerical scheme is not necessarily the number of positive wave frequencies used in the next subsection. It is assumed that  $\omega_j$  are given by the equation

$$\omega_j = j\Delta\omega$$

for  $j = 0, \pm 1, \pm 2, \dots$  and some increment of frequency  $\Delta\omega$ .

If  $\mathfrak{S}_{1,0} = 0$ , the integral equation can be discretized as

$$\mathfrak{S}_{r,\ell} \approx \mathfrak{S}_{1,\ell} + 2\Delta\omega \sum_{n=1}^{\infty} \mathfrak{S}_{1,n} \left[ \mathfrak{S}_{1,\ell+n} Z_{-n,\ell+n}^2 + \mathfrak{S}_{1,\ell-n} Z_{\ell-n}^2 \right]$$

Where  $Z_{pq} = Z(p\Delta\omega, q\Delta\omega)$ . Here  $\mathfrak{S}_{1,p} = \mathfrak{S}_1(p\Delta\omega)$  and  $\mathfrak{S}_{r,p} = \mathfrak{S}_r(p\Delta\omega)$ . The series is truncated and the equations are written as

<sup>3</sup> This representation can be obtained from equations on page 38 of Beck, *et al.* (1989) if three significant digits are retained.



$$f_\ell = S_{1,\ell} - S_{T,\ell} + 2\Delta\omega \cdot \left[ \sum_{n=1}^{\ell-1} S_{1,n} S_{1,\ell-n} Z_{n,\ell-n}^2 + \sum_{n=\ell+1}^N S_{1,n} S_{1,n-\ell} Z_{n,\ell-n}^2 + \sum_{n=1}^{N-\ell} S_{1,n} S_{1,n+\ell} Z_{-n,\ell+n}^2 \right] = 0$$

for  $\ell = 1, 2, \dots, N$ . The frequency,  $\Delta\omega$ , and the number,  $N$  are provided by the user. The objective is to minimize the sum

$$X^2 = \sum_{\ell=1}^N f_\ell^2$$

An initial guess,  $\mathfrak{S}_{1,\ell}^{(0)}$ , for the discrete linear spectrum is provided by the equation

$$\mathfrak{S}_{1,\ell}^{(0)} = \mathfrak{S}_{T,\ell} \text{ for } \ell = 0, 1, \dots, N$$

All iterates for the linear spectrum are assumed to vanish at  $\omega = 0$  rad/sec:

$$\mathfrak{S}_{1,0}^{(p)} = 0 \text{ for } p = 0, 1, \dots$$

It is now assumed that the  $p$ -th iterate, say  $\mathfrak{S}_{1,m}^{(p)}$ , is known. For  $m = 1, 2, \dots, N$ ,  $\mathfrak{S}_{1,m}^{(p+1)}$  is chosen between  $(1 - \alpha)\mathfrak{S}_{1,m}^{(p)}$  and  $(1 + \alpha)\mathfrak{S}_{1,m}^{(p)}$  such that

$$\sum_{\ell=0}^N f_\ell^2 \left( \mathfrak{S}_{1,1}^{(p+1)}, \dots, \mathfrak{S}_{1,m-1}^{(p+1)}, \mathfrak{S}_{1,m}^{(p+1)}, \mathfrak{S}_{1,m+1}^{(p)}, \dots, \mathfrak{S}_{1,N}^{(p)} \right)$$

is approximately minimized. The number  $\alpha$  is somewhat arbitrary and can be provided by the user; it only serves to bound the interval in which a minimum of  $\chi^2$  is sought. Numerical tests for some spectra indicate that  $\alpha = 0.1$  is acceptable for those spectra. To minimize  $\chi^2$ , we can check the sum at

several, say 10, evenly spaced points,  $\mathfrak{S}_{1,m}^{(p+1)}$ , in the interval,  $[(1 - \alpha)\mathfrak{S}_{1,m}^{(p)}, (1 + \alpha)\mathfrak{S}_{1,m}^{(p)}]$ , and make the change based on the 10 evaluations of  $\chi^2$ . The number 10 is arbitrary and can be replaced by another value supplied by the user. Furthermore, the points do not have to be evenly spaced. The whole process is repeated for a specified number of iterations. The sum  $\chi^2$  can be monitored and the iterative process can be truncated when the fractional change in the sum is less than a user-specified tolerance or no longer decreases.

The desired values,  $\mathfrak{S}_{1,\ell}$ , for the discrete linear spectrum are given by  $\mathfrak{S}_{1,m}^{(p)}$  where  $p$  is the number of the most recent iterate. Interpolation is required if the spectral density function is desired at frequencies other than  $\omega_m = m\Delta\omega$ .

## 5. STATISTICAL UNCERTAINTIES ASSOCIATED WITH (EXTREME) SHIP- MOTIONS IN WAVES

### 5.1. Introduction

Measured data of physical phenomena can be classified as either deterministic or random. Often repeated measurements show variations due to the inability to control experimental conditions and/or due to the randomness of the physical phenomena considered. For example, the results from a standard resistance experiment are a deterministic quantity, which can be affected by small flow disturbances created by previous test runs.



A seaway, the loads on a vessel and the responses of a ship are all random processes. The results of scale-model experiments and numerical simulations of ships in waves depend on the duration of the test runs or numerical simulations. This is a key factor in determining the number of test runs for scale-model experiments and numerical simulations. Furthermore, in analysing test or simulation data, it is important to assess the statistical reliability of motions and events.

Quantities such as incident waves and the resulting first-order ship motions can be regarded as “linear” signals for which straightforward formulas are known that describe its probability-distribution function as a function of the standard deviation of the signal. The distribution of individual oscillations (“local” extremes) is known to satisfy distribution functions which depend on the bandwidth of the frequency spectrum of the signal. The “most probable” extreme value of a signal is then characterised by the number of oscillations and the standard deviation.

In the case of “nonlinear” phenomena such as wave-impact pressures, parametric- roll motions, water ingress on open-top container ships, and broaching, an estimate of the most probable extreme value cannot be solely based on the standard deviation and number of oscillations in the signal. In such cases it is customary to sort the peak values and to plot these as a function of the frequency of exceedance. Fitting a distribution function and extrapolating to the required number of events yields the most probable value. The reliability of such a procedure depends heavily on the number of samples, for instance the number of slams encountered during a certain time period. The intention of this chapter is to provide methods for determining the duration of scale-model experiments or numerical simulations such that linear motions can be obtained

with a given uncertainty margin. At the same time, methods are provided to predict the statistical uncertainty related to the occurrence of extreme motions.

## 5.2. Linear Signals

Incident waves and “linear” ship motions satisfy a Gaussian (or Normal) distribution function (Ochi, 1973). This distribution function is characterised by the standard deviation of the signal,  $s_q$ :

$$s_q = \sqrt{\frac{1}{N} \sum_{i=1}^N (q_i - \bar{q})^2}$$

Here  $N$  is the number of samples,  $q_i$  is the sample value and  $\bar{q}$  is the mean value of the signal:

$$\bar{q} = \frac{1}{N} \sum_{i=1}^N q_i$$

The probability density function of a Gaussian distribution is:

$$p(q) = \frac{1}{\sqrt{2\pi}s_q} e^{-\frac{(q-\bar{q})^2}{2s_q^2}}$$

The probability that a value,  $(q - \bar{q})$ , exceeds a certain value,  $q_m$ , is obtained from the integral:

$$P[q_m \leq (q - \bar{q}) < \infty] = \int_{q_m}^{\infty} p(y) dy \quad (33)$$

Based on (33), Table 5.1 shows exceedance probabilities for several values of  $q_m$ .



Additionally, the stochastic variable,  $q$ , can be described by the distribution of amplitudes (peak values) of  $q$ . When  $q$  has a Gaussian distribution, its amplitudes follow a Rayleigh or Rice distribution, depending on the bandwidth of the frequency spectrum (see Section 5.1). Amplitudes are often the most interesting quantities in ship-motion analysis.

$q_m$	$P[q_m \leq q < \infty]$	$P[-\infty < q \leq q_m]$
$\bar{q} - 3s_q$	99.9	0.13
$\bar{q} - 2s_q$	97.7	2.28
$\bar{q} - s_q$	84.1	15.9
$\bar{q} + s_q$	15.9	84.1
$\bar{q} + 2s_q$	2.28	97.7
$\bar{q} + 3s_q$	0.13	99.9

**Table 5.1 Exceedance probabilities.**

When  $q_a = (q - \bar{q})$  is the amplitude of a Gaussian process then the mean of the highest one-third of the maximum to minimum values of  $q_a$  is known as the significant double amplitude of  $q$ .

The most probable maximum value,  $2q_{a,max}$ , of the variable,  $q$ , depends on the number of oscillations,  $n$ , as shown by Longuet-Higgins (1957):

$$2q_{a,max} = 2s_q \sqrt{2\theta}$$

With

$$\theta = \ln(n) - \ln\left(1 - \frac{1}{2\theta}(1 - e^{-\theta})\right)$$

For large values of  $n$  it can be shown that

$$2q_{a,max} = 2s_q \sqrt{2\ln(n)}.$$

Figure 5-1 shows a schematic view of the main quantities of interest.

### 5.3. Nonlinear Signals

In case of nonlinear quantities like large-amplitude roll motions or wave-impact loads, the estimate of the most probable extreme value cannot be based solely on the standard deviation and number of oscillations of the signal. In this case it is customary to sort the peak values and to plot these as a function of the frequency of exceedance, *i.e.*, the fraction of the amplitudes exceeding a certain value. Fitting a distribution function and extrapolating to the required number of events yields the most probable value. In this procedure the highest value with zero “frequency” is actually not accounted for.

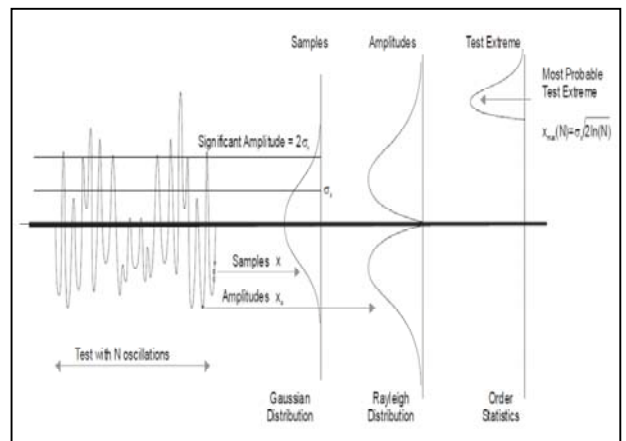


**Figure 5-1 Schematic view of a test signal; sigma represents the standard deviation.**

The cumulative, 3-parameter, Weibull-probability-density function is often used to fit the data. The governing parameters in this distribution function are the scale parameter,  $\alpha$ , shape parameter,  $\beta$  and offset,  $\theta$ :



$$P[q > q_m] = e^{-\left(\frac{q_m - \theta}{\alpha}\right)^\beta}$$

If the fit yields a shape parameter of  $\beta \approx 2$ , the results resemble a Rayleigh distribution. For processes which are governed by quadratic values of the underlying motions (like the relative velocity which governs a wave impact pressure),  $\beta \approx 1$ , which corresponds to a negative exponential distribution.

The most probable maximum value is defined by:

$$2q_{a,\max} = \theta + \alpha^\beta \sqrt{-\ln\left(\frac{1}{n}\right)}$$

Ochi (1990) describes several other types of distribution functions and how to derive extreme values with a certain adopted exceedance risk level. The frequency of exceedance is the number of exceedances of a certain amplitude divided by the total number of amplitudes. Figure 5-2 shows a typical frequency of exceedance plot.

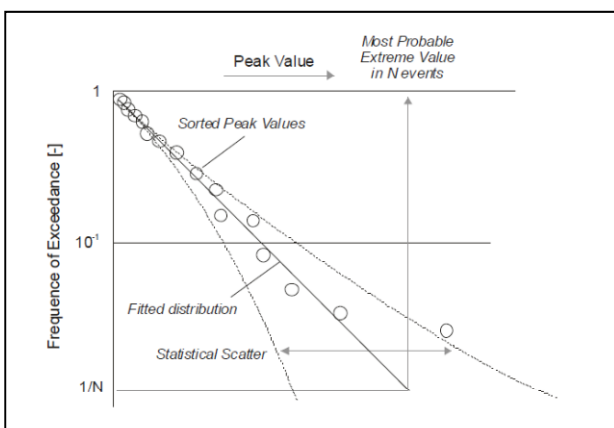


**Figure 5-2 Frequency of an exceedance plot.**

Highly nonlinear and rare processes like capsizing are difficult to fit by means of a distribution function, and prediction of the

capsize probability requires special techniques. Naess & Moan (2012) and Wang & Moan (2004) describe and compare methods for extreme-value estimation such as the Peak over Threshold (POT) method. This method is based on peak values that exceed a certain threshold level; sample values that are below the threshold are not considered. Using the POT method gives allows better modelling of the tail of the peak-value distribution.

The opposite approach is to use only the less nonlinear part of the distribution function to make predictions of a threshold value. In the case of capsizing for instance, the threshold heel angle would be one where the righting moment arm (GZ) curve is at a maximum. A variation on this approach is by Belenky, *et al.*, (2012a) which describes a split-time method with separate approaches for the linear and nonlinear parts.

#### 5.4. Statistical Reliability

Seakeeping tests are generally designed to obtain a fair estimate of the standard deviation of linear quantities. As a rule of thumb, the standard deviation of linear signals obtained from realisations with a typical duration of 180 wave encounters will show scatter (*i.e.*, a standard deviation of the standard deviations of multiple runs of about 5%).

For the analysis below it is assumed that the observed processes are stationary and ergodic. For stationary processes the true mean value of a quantity is time independent and the auto-covariance function is a function of time only. A stochastic process is said to be ergodic if its statistical properties (such as its mean and variance) can be deduced from a single, sufficiently long sample (realisation) of the process.



For a given system under evaluation, the question is what is a sufficiently long measurement duration? In general this depends on two properties of the spectral density function of a signal: the frequency where the spectrum has its peak value,  $\omega_P$ , and the bandwidth of the spectrum,  $b$ . This is illustrated in Figure 5.3.

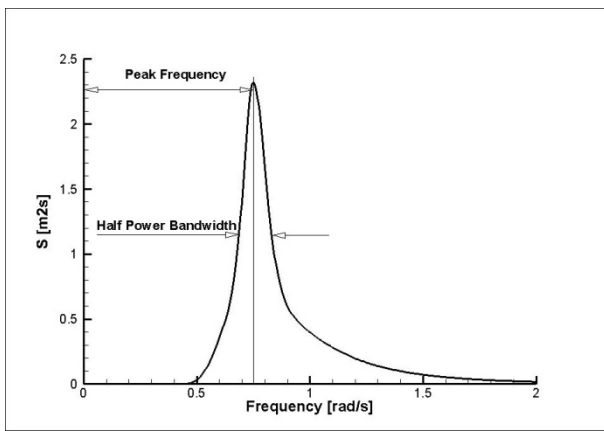


**Figure 5-3 Plot of spectral density vs frequency.**

Peak frequency is usually easily recognised (note that more than one peak may exist). The response bandwidth is small (narrow-banded) for lightly damped resonant-roll motions. A more broad-banded response is observed for heave and pitch motions in head seas. Low frequency responses due to wave- drift forces and course keeping enlarge the bandwidth of the frequency spectrum and have a profound influence on the statistical error as shown below.

An estimate of the statistical error in the mean value is given by Pierce (1992) as:

$$\varepsilon_{\bar{q}} = \sqrt{\frac{A_{lf}}{10} + 4 \frac{1 - A_{lf}}{T^2 \omega_P^2}} \quad (34)$$

where  $T$  is the run duration in seconds and  $A_{lf}$  is the low-frequency-area ratio in the spectrum. This ratio is defined as:

$$A_{lf} = \frac{\int_0^{10\pi/T} S(\omega) d\omega}{\int_0^\infty S(\omega) d\omega} \quad (35)$$

For large durations (10) reduces to:

$$\varepsilon_{\bar{q}} = \frac{2}{T\omega_P} \quad (36)$$

Multiplication of  $\varepsilon_{\bar{q}}$  with the standard deviation of the sample yields the error in physical quantities.

Equation (12) can be used to determine the required duration given a certain error:

$$T = \frac{2}{\omega_P \varepsilon_{\bar{q}}} \quad (37)$$

For a Gaussian process, an estimate for the statistical error of the standard deviation is given by Pierce (1992):

$$\varepsilon_{s_q} = \sqrt{\frac{3\pi}{5\sqrt{2}bT}} \quad (38)$$

where the bandwidth,  $b$ , is defined at half the peak spectral density. Vice versa, the required duration given a certain error follows from:

$$T = \frac{3\pi}{5\sqrt{2}b\varepsilon_{s_q}^2} \quad (39)$$

In summary, the variability of the standard deviation decreases when the bandwidth of the response spectrum increases and reduces with one over the square root of the duration. The variability of the mean value depends on the low-frequency content and the peak frequency



of the spectrum and is independent of the bandwidth of the signal. It reduces with one over the duration, provided the low-frequency content is very low.

It should be noted that for forward-speed cases, peak frequency and bandwidth of the encounter spectrum should be used in (34)–(39).

### 5.5. Nonlinear Signals and Extreme Events

The number of extreme events is generally much smaller than the number of wave encounters. Due to this and the statistical scatter of nonlinear phenomena, the statistical reliability of this information may be quite limited. Extrapolation of the probability of exceedance of measured extreme values to larger extreme values further increases the scatter; a reliable assessment of extreme and/or rare values requires a long test or a numerical simulation procedure.

To illustrate the above problem, Figure 5.4 shows the results of a numerical experiment in which a large number of time series (batches) were generated. Each time series contained  $N$  peaks. The function values followed a prescribed Weibull distribution.

For 180 events (wave encounters or oscillations) and  $\beta = 2$ , a Rayleigh Distribution, the standard deviation of the batch mean amplitude is around 4%. For  $N=180$  the standard deviation of the *most probable extreme* is about 8%. When extrapolating smaller batches with  $N=20$  to the 1/180 probability level, the uncertainty in the most probable extreme increases to between 10 and 20%.

Considering the results for a nonlinear process ( $\beta=1$ ) and a batch size of 20, the standard deviation of the most probable extreme is about 30%; the standard deviation of the extrapolated most-probable extreme value with a 1% exceedance probability is some 40%.

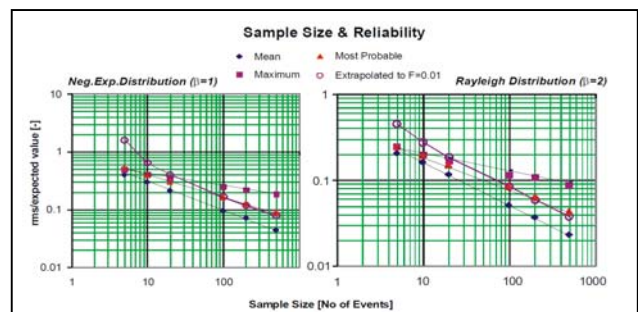


Figure 5-4 Sample size and reliability.

### 5.6. Confidence Intervals for Mean and Standard Deviation

When performing scale-model tests or numerical simulations, one may use the number of wave encounters to determine the required duration of a time series of linear motions and loads such that the results are accurate within an adopted confidence interval. For nonlinear motions and rare and/or extreme events, the number of encounters is usually unknown *a priori*, and statistical accuracy can only be determined *after* a certain test or numerical-simulation duration has been obtained. Statistical accuracy can be assessed when uncertainty estimators are derived from the time signals. The procedure below outlines derivation of such uncertainty estimators for single- and multiple-time records.



## 5.7. Multiple Uncorrelated Time Records

Multiple uncorrelated time records are obtained when a number of test runs or simulations are obtained under identical conditions but with a different wave sequence for each run or simulation.

The mean value can be estimated using an averaged quantity of a single realisation over a time interval. If the time series,  $q_j(t)$ , is the  $j^{\text{th}}$  realisation of a stationary random process with time average,  $\bar{q}_j$ , and  $N$  samples per realisation,

$$\bar{q}_j = \frac{1}{N} \sum_{i=1}^N q_{ji}(t)$$

An ensemble average,  $\bar{q}_n$ , is an average quantity of a set of  $n$  realisations:

$$\bar{q}_n = \frac{1}{n} \sum_{j=1}^n \bar{q}_j$$

The time-average,  $\bar{q}_j$ , and the ensemble average,  $\bar{q}_n$ , are estimators of the true mean,  $\bar{q}$ . Due to practical restrictions, the signal length,  $T$ , is often limited causing a difference between estimated averages and the true mean. When a finite set of  $n$  repeated time series,  $q_j(t)$ , is available, the variance,  $V_n = s_n^2$ , and the standard deviation,  $s_n$ , of the mean values are defined as:

$$s_n^2 = \frac{1}{n-1} \sum_{j=1}^n (\bar{q}_j - \bar{q}_n)^2 \quad (40)$$

For uncorrelated sample mean values, the first-order estimate of the random uncertainty,  $u_{1,est}$ , follows from:

$$u_{1,est} = \frac{s_n}{\sqrt{n}}$$

The 95% confidence interval for the mean value is then obtained from:

$$\bar{q}_{U95} = \bar{q}_n \pm 1.96u_{1,est}$$

The factor 1.96 stems from a normal distribution for a 5% probability of exceedance.

The variance of a single time trace is given by:

$$s_j^2 = \frac{1}{N} \sum_{i=1}^N (q_i - \bar{q}_j)^2$$

The mean variance,  $\bar{s}^2$ , is given by

$$\bar{s}^2 = \frac{1}{n} \sum_{j=1}^n s_j^2$$

The variance of the variance for the ensemble of time records is

$$s_v^2 = \frac{1}{n-1} \sum_{j=1}^n (s_j^2 - \bar{s}^2)^2 \quad (41)$$

The random uncertainty,  $u_{1,est}$ , follows from

$$u_{1,est}^+ = s_v \sqrt{\frac{n-1}{\chi_{\alpha/2}^2}} \quad \text{and} \quad u_{1,est}^- = s_v \sqrt{\frac{n-1}{\chi_{1-\alpha/2}^2}}$$

where  $\chi^2$  is the asymmetrical Chi-squared distribution-function value. The 95% confidence interval for the standard deviation is then obtained from

$$s_{U95} = s_v \pm u_{1,est}^\pm$$



In its report to the 26th ITTC, the Specialist Committee on Stability provides an example of the application of the methodology for calculating variance of the mean and variance of the variance (ITTC, 2011a, Sect. 5).

If there is only a single time record available,  $n = 1$ , this procedure does not work due to the factor,  $n-1$ , in the denominator of (40) and (41). For single-time records a different procedure can be adopted as outlined in the next section.

### 5.8. Single-time Records

As explained by Bendat & Piersol (2010), the auto-covariance function of a signal enables the computation of the expected variance of the mean and variance of the variance. The auto-covariance function shows the dependence between current (at time,  $t$ ) and previous (time shift,  $\tau$ ) values of quantities in a stochastic process. For stationary processes the true mean value of a quantity,  $\mu_x$ , is time independent and the auto-covariance function is a function of time only. The mean value and the auto-covariance function can be calculated using temporal averages for an ergodic, stationary random process:

$$xx^C(\tau) = \lim_{T \rightarrow \infty} \frac{1}{T} \int_0^T (q(t) - \bar{q}) \times (q(t-\tau) - \bar{q}) dt \quad (42)$$

where  $\tau$  is the time shift and  $T$  is the duration of the time series. The mean value is defined as:

$$\bar{q} = \lim_{T \rightarrow \infty} \frac{1}{T} \int_0^T q(t) dt$$

When  $\tau = 0$ , the auto-covariance value,  $xx^C(0)$ , is equal to the variance of the signal. It is noted that the auto-covariance function,  $xx^C(\tau)$ , is related to the auto-correlation function,  $xx^R(\tau)$ , by

$$xx^C(\tau) = xx^R(\tau) - \bar{q}^2$$

with

$$xx^R(\tau) = \frac{1}{T} \int_0^T q(t)q(t-\tau) dt$$

The variance of the mean value is given by Bendat & Piersol (2010):

$$\bar{s}^2 = \frac{2}{T} \int_0^T \left(1 - \frac{\tau}{T}\right) xx^C(\tau) d\tau$$

while the first-order estimate of the random uncertainty,  $u_{1,est}$ , now equals the standard deviation,  $\bar{s} = \sqrt{\bar{s}^2}$ .

The variance of the variance is given by Bendat & Piersol (2010) as

$$s_v^2 = \frac{2}{T} \int_0^T \left(1 - \frac{\tau}{T}\right) (xx^C(\tau))^2 d\tau.$$

The first-order estimate of the random uncertainty,  $u_{1,est}$ , is the standard deviation.

The uncertainty of the signal variance,  $s_v^2$ , is presented by the confidence interval

$$\left[ s_v^2 - \alpha_- u_{1,est}, s_v^2 + \alpha_+ u_{1,est} \right]$$



Here  $\alpha_-$  and  $\alpha_+$  are the confidence factors to be obtained from a Chi-square distribution,  $\chi_v^2$ , where  $v$  equals the degrees of freedom. It is noted that this is an asymmetrical distribution with  $\alpha_- \neq \alpha_+$ . For more information see Bendat & Piersol (2010) or other statistical handbooks like Ochi (1973).

Several methods can be found in literature for the computation of the auto-covariance function (Brouwer, *et al.*, 2013). The direct calculation according to (42) is a time-consuming process. A more efficient approach is to use Fourier transforms. The Fourier transform of the auto-covariance function,  $xx^C(\tau)$ , equals the spectral density function,  $q(f)$ :  $S_{xx}(f)$ . The inverse transform yields

$$xx^C(\tau) = \int_{-\infty}^{\infty} S_{xx}(f) e^{2\pi i f \tau} df$$

where  $f$  denotes the frequency,  $f = 2\pi\omega$ .

This computation is not without numerical problems; repetition and noise amplification can occur. Belenky, *et al.* (2007) proposed to smooth the spectrum to prevent numerical problems. Brouwer, *et al.* (2013) proposed to use a biased auto-covariance function to prevent such problems. Brouwer, *et al.* (2013) also proposed an alternative method to determine the uncertainty of the mean and variance by using the covariance of *correlated* segments. These segments are consecutive parts of a single, sufficiently long time record. Sufficiently long is defined here as

$$T_s \gg \frac{n}{f_L} \quad \text{and} \quad T_s \gg \frac{n}{b}$$

where  $T_s$  is the length of a segment,  $f_L$  is the lowest frequency component present in the signal,  $b$  is the bandwidth of the spectrum and

$n$  is the number of segments. They show that the estimator for random uncertainty for the mean value in the segment method is

$$u_{1,est} = \frac{s_n}{n}$$

Apparently, splitting a single measurement into several segments shows a much faster decrease of uncertainty than taking several uncorrelated measurements with the same total length. A similar estimator for the variance is under development.

## 6. REVIEW OF VULNERABILITY CRITERIA

The review of vulnerability criteria, including long-term probability of loss of a ship, is carried out both for intact and damaged ships. Further development of vulnerability criteria that are required is outlined in Section 6.4.

### 6.1. What is a Vulnerability Criterion?

The concept of a vulnerability criterion has a very clear definition when dealing with an intact ship. In IMO documents, vulnerability criteria are intended as tools to assess whether a ship is susceptible to different modes of stability failures. If a ship is susceptible to a stability failure that is neither explicitly or properly covered by the existing intact-stability regulations, the ship is regarded as an “unconventional ship” for that particular stability-failure mode.

An intact-stability failure occurs when a ship cannot remain within the design limits of the roll (heel, list) angle and a combination of rigid-body accelerations (IMO, 2008).



The phenomena in waves which may cause large roll angles and/or accelerations have been identified in the 2008 Intact Stability (IS) Code, Section 1.2, Part A as follows:

1. Restoring-arm-variation events such as parametric excitation and pure loss of stability;
2. Critical behaviour under dead-ship conditions (*i.e.*, loss of steering ability or propulsion, and possible endangerment by resonant roll while drifting freely.
3. Manoeuvring-related problems in waves (*e.g.*, broaching-to in following and quartering seas when a ship may not be able to maintain a constant course, which in turn may lead to extreme angles of heel).

Therefore, under the specific agenda item devoted to “second-generation intact-stability criteria,” the activity at the IMO is focussed on the development of specific vulnerability criteria for parametric roll, pure loss of stability, dead-ship conditions, and broaching. Recently, attention has also been given to the issue of excessive accelerations.

“Second-generation intact-stability criteria” are based on a multi-tiered assessment approach: for a given ship design, each stability-failure mode is evaluated using two levels of vulnerability assessment. The two levels of vulnerability assessment criteria at the different tiers are characterized by different levels of accuracy and computational effort.

A ship which fails to comply with the first level is assessed by the second-level criteria. In a case of unacceptable results, the vessel must then be examined by means of a direct assessment procedure based on tools and methodologies corresponding to the best

state-of-the-art prediction methods in the field of ship-capsizing prediction. This third-level criteria should be as close to the physics of capsizing as practically possible.

Direct assessment procedures for stability failure are intended to employ the most advanced technology available, yet be sufficiently practical so as to be uniformly applied, verified, validated, and approved using currently available infrastructure. Ship motions in waves, used for assessment on stability performance, can be reproduced by means of numerical simulations or model tests (IMO, 2013a).

At present, a great deal of attention is paid to specifying the characteristics of numerical simulations that adequately replicate ship motions. This field will attract the interest and efforts of researchers and the rule-making community for the next several years (IMO, 2014).

In recent years the activity at the IMO has focussed on the development of first- and second-level criteria. The first level of criteria is designed to be a simple procedure based on geometry/hydrostatics, load conditions, and basic operational parameters, thus having low complexity but a higher safety margin. The second level of criteria relies on simplified physics-based calculations with reasonable computational efforts and straight-forward applications following suitable guidelines. This second level is characterised by a moderate level of complexity coupled with the appropriate safety margin. It is important to point out that this second level vulnerability criterion should be able to eliminate any suspicion of vulnerability and if this is not the case it should confirm vulnerability and justify the application of direct stability assessment for this mode (IMO, 2010).



For a damaged ship, it is uncommon to find explicit reference to the term “vulnerability criteria” in the literature. There currently appears to be no structured reference framework for damaged ships as there is for intact ships with functions and purposes.

In the warship context, the word vulnerability may be defined as an antonym of the term survivability (see Paragraph 2.3) since vulnerability is the conditional probability of being ‘lost’ given a certain scenario. In a situation where susceptibility (probability of being damaged) is equal to 1, survivability and vulnerability can be considered mathematical “opposites” for the purpose of this review.

## **6.2. Second-generation Intact-stability Vulnerability Criteria**

There is a need to properly balance the assessment of the probability of capsizing between a specific sea state and an average of sea conditions. This need is well illustrated by Reed (2009) where the criticalities due to predictions based on linear superposition of a phenomenon claimed universally as nonlinear are discussed.

### **6.2.1. Review of Vulnerability Criteria**

As already discussed, vulnerability criteria for specific stability failures are under development at the IMO. In the last ten years research communities have been very active in this subject area. At STAB conferences and ISSW workshops there have been dedicated sessions on related in the area of vulnerability criteria.

Two levels of vulnerability criteria and standards for parametric-roll resonance, for pure loss of stability, and for broaching are

going to be finalised very soon. Further development is needed in relation to dead-ship conditions and excessive accelerations (IMO, 2014).

For the pure loss-of-stability failure mode, the vulnerability criteria are expressed in IMO (2013a). The first vulnerability level is focussed on the transverse metacentric height, GM, which is calculated when a longitudinal wave passes a ship. In this calculation the moment of inertia of the water plane is considered at a draft corresponding to the level of the wave trough. The wave height that is used in this calculation is described in this method. The criterion is very simple and straightforward and is based on the traditional hydrostatics of a vessel.

As an alternative at the first level, the metacentric height (GM) can be determined as the minimum value calculated for a ship balanced on a wave crest. The wavelength is selected equal to the ship length and with a specific wave height. The wave crest is then centred at different longitudinal positions along the vessel and the hydrostatics are calculated.

The second level of vulnerability criteria takes into account characteristics of the righting arm, GZ, in longitudinal waves and then weighted averages of these stability parameters are calculated. As in the level one method, the calculations are conducted with the vessel balanced on a wave with the wave crest at different longitudinal positions along the vessel.

The selection of wave heights and wavelengths used in the calculations are still under discussion, with two main options. The first option is based on sixteen representative wave cases. The second option is based on Grim’s (1961) effective wave height calculated for all possible



significant wave heights and zero-crossing wave periods in the wave scattering diagram of the North Atlantic, but with the wavelength equal to the ship length (Umeda, 2013).

In the case of parametric-roll-stability failure mode, reference is made to IMO (2013a, 2013b). The first level vulnerability criteria is based on the ratio between variations of amplitude of the GM when a longitudinal wave passes a ship, and, the GM of loading conditions in calm water. Variations of the GM amplitude are evaluated by considering half the difference between the moment of inertia of the water plane calculated at the draughts corresponding to the height of the wave crest and the wave trough. Wave height is again described in the methodology.

Another alternative in determining the variation of GM may be calculated as half the difference between the maximum and minimum values of the GM calculated, assuming a ship to be balanced on a series of waves with the wavelength equal to ship length and prescribed wave height, with the wave crest centred at the longitudinal centre of gravity and at each  $0.1L$  forward and aft from the longitudinal centre of gravity.

Second-level vulnerability criteria consists of two stages. Evaluation of the first stage employs the calculation of the ratio of GMs from the first level of vulnerability, but uses a statistical average of the results from multiple wavelengths and wave heights in the computations instead of using a single wavelength and single wave height. The ratio in the first stage of second-level vulnerability also assumes the ship to be balanced on a set of waves defined in terms of prescribed wavelengths and wave heights.

In the second stage of the second-level of vulnerability criteria, a weighted average-roll

amplitude in head and following seas is also evaluated. Roll response is calculated using the equation for uncoupled roll motion while accounting for the influence of pitch and heave quasi-statically. A range of speeds is considered and the environment is described by a specified set of waves. Grim's effective wave height is calculated for all possible significant wave heights, and for zero-crossing wave periods appearing in the wave-scatter diagram of the North Atlantic, with wavelength equal to ship length. With this procedure the roll amplitude for all possible short-term sea states in the North Atlantic is obtained. The probability of encountering critical sea states where the roll amplitude is greater than the critical angle can be calculated and compared with the required standard (Umeda, 2013).

For broaching stability failures (IMO 2013a), the first vulnerability level is very simple and only considers the Froude number and ship length.

For the second level of vulnerability, the critical Froude number (*i.e.*, corresponding to the susceptible threshold of surf-riding), is evaluated for a regular wave with a specific steepness and a specific ratio between the wave and ship length. The short-term probability of surf riding can be calculated with Longuet-Higgins's theoretical formula for the joint-probability-density function of local wave height and length. The long-term probability of surf riding needs to be calculated with the wave scatter diagram of the North Atlantic and compared with an acceptable standard (Umeda, 2013).

The issue of dead-ship conditions (IMO, 2013a) at the first vulnerability level is dealt with by the adoption of the IMO weather criteria, and amended in the specific area of wave steepness.



For the second level of vulnerability criteria, a weighted average representing a comprehensive failure index, is evaluated considering different combinations of possible environmental conditions (IMO, 2012). The reference exposure time is one hour. Calculation of a possible critical-roll angle is repeated for several sea states according to the relevant wave-scattering diagram. The necessary calculations can be made using one of two methodologies, both of which are based on the same underlying one degree of freedom (DoF) model, but are slightly different in their calculation details (IMO, 2013c). One method uses the linearization of the GZ curve in the vicinity of the equilibrium heel angle under the action of mean wind, and estimating the failure probability by means of the equivalent-area concept. The second method approximates the original GZ curve with piece-wise linear curves. More details about the two methodologies are available in IMO (2009). Bassler, *et al.* (2009) provides a critique of the two approaches from a theoretical point of view.

For the problem of excessive accelerations, proposals for the first and second vulnerability levels are still under development at the IMO. The most recent version of these criteria is given in IMO (2012).

Based on the work described above, especially for the second-level vulnerability criteria, it is evident that the assessment of a ship is structured in terms of ship-environment interaction. While formulating the criteria, ship characteristics are given as defined by a design team and fixed in terms of geometry and speed. The loading condition is defined as the “loading condition under investigation.”

Attention, therefore, is very much focussed on the issue of including environmental conditions in the methodology of assessing

ship vulnerability. In general, this inclusion is made by means of a weighted average using a large number of wave cases. This approach seems to be sufficiently appropriate to measure, with a certain level of accuracy, the vulnerability of a ship. The adequacy of the assessment tools requires further examination when combined with standard values.

Notwithstanding the robust and efficient theoretical and methodological approaches as the basis of the present vulnerability criteria, consistency with the use of other possible sources of wave statistics (on the discretion of various nations’ Administrations) needs to be taken into consideration.

As an extrapolation, the so-called “direct assessment” can be considered a vulnerability criterion also. In this case the approach consists of two major parts: identification of a tool/methodology that adequately predicts ship motions in waves; and development of a procedure that determines ship safety based on the likelihood or risk of stability failure. IMO (2013a) provides a description of the capabilities of a methodology which is used for direct assessment presented by different stability-failure modes. In the same document measurement of stability-failure likelihood is described as a probabilistic performance-based criteria.

Validated numerical tools are necessary, but not sufficient by themselves to complete a direct stability assessment. There should be a prescribed procedure of applications of the tools, and following such a procedure, multiple applications should reach the same conclusions on a subject vessel. The procedure should also describe how to choose loading and environmental conditions. The measure of likelihood of stability failure is the main result of a direct stability assessment.



When using validated numerical tools, the following issues must be addressed: time of exposure; the problem of rarity (see also IMO, 2011, Annex 1; and IMO, 2007b); statistical uncertainty; a set of loading conditions (reasonably selected from a vessel-stability booklet); and environmental conditions (in terms of the type of wave spectrum and its characteristics).

The proper selection of wave conditions is a key issue (Belenky, *et al.*, 2009a). In order to provide practical and consistent vulnerability criteria, stability failures must be evaluated for reasonable environmental and operational conditions. It is usually possible to find a combination of these conditions which results in a stability failure. While excluding unrealistic operational conditions is relatively obvious, determination of appropriate wave conditions is more difficult, due to their stochastic nature.

For the intact-ship condition the biggest issues of vulnerability assessment, in addition to the environmental context, are the proper prediction of the physical behaviour of an intact ship in her interaction with a seaway, coupled with the statistics of ship conditions (displacement, center of gravity (CG), speed, etc.). All of these factors need to be taken into account in an overall capsize-probability assessment (Ypma & Harmsen, 2012). In this perspective an Insufficient Stability Event Index (ISEI) has been defined and applied to several full-scale capsizing events with appropriate numerical methods and procedures in order to establish appropriate threshold values (Krueger & Kluwe, 2010).

The attention to ship vulnerability is evident also in the field of naval ships (Beaupuy, *et al.*, 2012; Gu, *et al.*, 2012) and is expressed in terms of capsizing probability.

### 6.2.2. The Problem of Rarity

For the treatment of the problem of rarity, several techniques have been investigated: envelope peaks over threshold (EPOT) (Ypma & Harmsen, 2012); critical wave groups (Shigunov, *et al.*, 2012); split time for dead-ship conditions and split time for surf riding (Belenky, *et al.*, 2012b).

The split-time method is proposed as a possible way to simplify the approach for predicting the probability of ships capsizing in irregular waves, and separating the prediction process into a rare problem and a non-rare problem. The non-rare problem is treated through direct statistical processing of the time-domain motion data so the intermediate threshold is expected to be low enough that up-crossing statistics may be evaluated directly. The rare problem is solved by using the roll rate at the instant of up-crossing in order to find the value that leads to the specified stability failure (Belenky, *et al.*, 2013; Belenky, *et al.*, 2009b). A very interesting discussion of potential applications of POT and EPOT approaches is given in Belenky & Campbell (2012).

In Themelis & Spyrou (2006) an interesting alternative use of a short-term or long-term prediction is postulated. Given a particular ship, the methodology can be deployed for short- or long-term assessments, depending on the intended period of exposure to the weather. In the current context, “short-term” is described as an assessment for a single trip, with a time window of a “few hours” forecast of weather parameters. Such an assessment could serve as a decision-making tool in an operational situation. Long-term assessments are performed for a variety of reasons on an annual basis or projected on a ship’s lifespan. The use of a long-term assessment is most common during the design phase of a ship.



### 6.3. Damaged-ship Survivability Criteria

There are several degrees of increased complexity involved in damaged-ship dynamic-stability studies compared with intact-ship dynamic-stability studies (Peters & Wing, 2009).

Additional issues involved in developing survivability criteria for a damaged ship versus an intact one include the damage scenario itself, the flooding process, and the presence of water on-board after damage.

The damage itself introduces further statistical and probability issues into the problem. Flooding, especially in the progressive transient phase is characterised as stochastic in nature, while water on-board enhances the nonlinear implications in the behaviour of a ship.

Because of the uncertainty and stochastic nature of flooding, the identification and discussion of vulnerability criteria are further complicated with regard to the intact-ship problem. Therefore, dealing with a damaged ship will require a more comprehensive tool for the prediction of the physical behavior of the ship, inclusive of the damage scenario and flooding phenomenon (Ruponen, *et al.* 2012; Dankowski, 2012).

Harmsen (2006) presented a study about the impact on stability of progressive flooding through small openings. However, additional studies are required on how to deal with these effects in static-stability calculations.

In damaged-ship scenarios, time is a central issue in vulnerability investigations (Spanos & Papanikolaou, 2014), and often represents the most important factor in many situations: *e.g.*, time-to-flood and time-to-

capsize (Spanos & Papanikolaou 2007; Spanos & Papanikolaou, 2014; Jalonen, *et al.*, 2012); time-to-sink (Van't Veer, *et al.*, 2002; Ruponen, 2007); survival time (Jasionowski, *et al.*, 2004; Pawłowski, 2008). In Ran, *et al.* (2012) the importance of the proper modelling of water ingress is pointed out because of its influence on time-to-capsize.

The strong influence of time on ship survivability is emphasised, especially for Ro-Ro ships, in Spanos & Papanikolaou (2010) where time-dependant survivability is analysed. The time issue for passenger ships is also discussed in Spanos & Papanikolaou (2012) where time-to-capsize for a given ship is assumed as a random variable depending on: random environmental conditions during a flooding casualty; the random shape and location of the hull breach; and the ship's loading and local (*e.g.*, arrangements and permeability) details of the flooded spaces. In the case of passenger ships, the statistical probability distribution (when capsizing is a possible event), can be approached with a basic Monte Carlo simulation. In this method time-to-capsize is sampled from a deterministic time-domain simulation for ship flooding and for a sufficiently large number of damage cases to meet statistical convergence of the results.

A comprehensive approach to possible passenger ship loss must consider both the issue of time-to-sink together with an evacuation model (Skjong, *et al.*, 2006; Spyrou & Roupas, 2006).

Determination of the time required to carry out emergency procedures for a damaged ship is the result of a survivability assessment (Spanos & Papanikolaou, 2012; and Jasionowski, *et al.*, 2010). This problem of the time needed to carry out emergency procedures is implicit in the safe-return-to-port concept (IMO, 2007a). Within a certain



damage threshold, it is assumed that the ship will survive indefinitely, whereas if the threshold is exceeded and abandonment becomes a possible event, then sufficient time is needed to carry out emergency procedures.

In investigations where “time” is a fixed parameter (30 minutes, one hour, etc.), the outcome of the assessment process is given in terms of: capsizing probability (Jasionowski, *et al.*, 2004); probability of survival (Tagg & Tuczu, 2002; van’t Veer, *et al.*, 2004; IMO, 2005); capsizing risk, capsizing index, and capsizing band (Papanikolaou, *et al.* 2010; Tsakalakis, *et al.* 2010). In these investigations with “time” a fixed parameter, attention is paid to environmental conditions, in particular to significant wave height. It is recognized that predicting ship survival is not a well-defined process, but there is a range of conditions within which the transition from “safe” to “unsafe” takes place. By convention this range has been named the “capsizing band.” This band begins at highest wave height where no capsizes are observed and ends at the lowest wave height where all predictions result in loss of ship. In order to better describe the capsizing band, the term, rate-of-capsize, has been introduced.

For example, a capsizing band is created by reporting the rate-of-capsize as a function of different, significant wave heights, creating a sigmoid distribution. The rate-of-capsize is the probability of capsizing (PF) given a particular sea state.

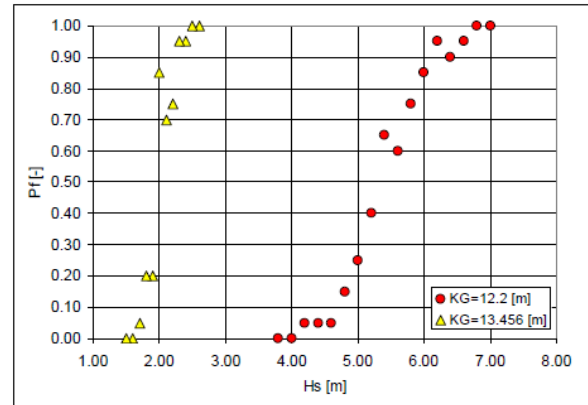


**Figure 6-1 Capsize-rate values for different Hs and different loading conditions (Tsakalakis, *et al.* 2010).**

Therefore PF will be 0 at the lower end of the capsizing band and 1 at the upper end. The point of the capsizing band where PF = 0.5 is the critical wave height and it is this value that is used by convention when referring to ship survivability.

It is also important to analyse the influence of a specific damage/flooding scenario as shown by Tellkamp & Cramer (2002). In Vassalos (2012) and in Vassalos & Jasionowski (2013), a definition of vulnerability is given as “the probability that a ship may capsize within a certain time when subjected to any feasible flooding case.”

The above definition is applied in Jalonen, *et al.*, (2012), where expressions like “vulnerability to flooding” and “vulnerability to open watertight doors” are used in relation to a rapid capsizing.

For the survivability of a ship in a damaged condition, safety rules have recently shifted from a deterministic approach to a probabilistic one (IMO, 2005), where a comprehensive procedure is carried out in order to attain an A Index representative of the



global performance of a ship in case of damage. The term 1-A is the probability of capsizing/sinking and is applied in risk evaluation procedures (Zaraphonitis, *et al.*, 2013). A strong correlation between ship survivability and wave height is presented in Peters & Wing (2009) where a global, relative damage-loss index is formulated and applied.

#### 6.4. Further Developments in a Survivability Definition

In the past decade there has been a trend to create principles for a move from prescriptive-based to performance-based approaches in the field of ship safety and in particular, in the fields of both intact-ship stability and damaged-ship stability (Peters, *et al.*, 2013; Vassalos, *et al.*, 2005; Kobyliński, 2007).

In developing a new approach in terms of risk assessment, it is assumed that the safety rules will be restructured. In general risk assessment relies on a physics-based assessment of ship behaviour, given some physical and environmental conditions, and the proper treatment of the statistics involved in order to get to a strong probability of occurrence (or non occurrence) of an undesired event.

A large number of experimental studies have been carried out in order to support the possible theoretical approaches and the studies have been shown to be of great importance, particularly in the field of damaged-ship stability.

The assessment of ship vulnerability in terms of ship loss is the result of a comprehensive methodology where the following points are identified:

1. Loss mode
2. Loss threshold
3. Ship operational conditions
4. Environmental conditions
5. Time of exposure
6. Methodology for short-term prediction
7. Methodology for long-term prediction (taking into account the problem of rarity for an intact ship).

The extension of the meaning of “loss” is already considered (Peters & Harrison, 2006) when applied to naval ships. For a naval ship, the concept of mission continuity needs to be part of the meaning of “loss.” Instead of only the physical damage to a naval vessel being considered, mission continuity, which is concerned with the ability of a vessel and crew to both defend herself and perform its required mission, must also be considered. Mission interruption is one example of a mission-continuity loss and can be described as an “indirect loss,” contrasted with “direct loss” from damage to ship systems due to structural and flooding damage.

Validation of the individual steps of a methodology and of an assessment framework as a whole is vital to build confidence in the final outcomes (Smith & Campbell, 2013; Montewka, *et al.*, 2013). The importance of defining the relationship between capsize probability and general ship properties is discussed in Ypma & Harmsen (2012).

In Bassler, *et al.* (2009) some fundamental issues are raised in relation to the selection of realistic environmental conditions. This paper highlights the fact that an unrealistic environmental condition may lead to incorrect results, even if the criteria are technically correct. In Bassler, *et al.* (2009) some possible options for using realistic environmental conditions are listed: *e.g.*, an equivalent wave for life-



time risk; a short-term sea state deemed “representative” of a specific ship-operational profile; and a long-term approach using a scatter diagram for a representative part of the World Ocean.

Consideration must be given to the appropriate application of classical methodologies developed for the evaluation of extreme values of structural loads to stability prediction. A typical scheme for the calculation of extreme loads is based on long-term statistics, so a number of sea states needs to be considered. An operational profile is usually assumed based on existing experience. It includes the fraction of time that a ship is expected to spend in each sea state. Short-term probability of exceedance is calculated for each sea state; then the formula for total probability is used to determine the life-time probability of exceedance of the given level. This level is typically associated with significant wave height and a zero-crossing or mean period.

In calculating extreme loads, actual physical failure and the implied possible nonlinearities are not considered. The discussion in Bassler, *et al.* (2009) highlights the relevance of what is discussed above, specifically in the short-term phase of the evaluation. Considering a regular wave as the equivalent of a specific sea state is attractive because of its simplicity. However, the physics of some stability failures may be quite different in regular and irregular waves.

When vulnerability criteria are probabilistic in nature, then the next important parameter to examine is the time scale, whether long-term or short-term. Short-term, as already mentioned earlier in this report, refers to a time interval where quasi-stationary statistics are assumed. A long-term scale covers a

larger time interval such as a season, a year, or the life-time of a vessel.

A short-term description of the environment can be characterised by one sea state or wave spectrum. However, if either of the above are chosen for use in a vulnerability criteria, justification will be required as to why a particular sea state or wave spectrum is used. Justification of the choice is important because sea states which are too severe may make the criteria too conservative and diminish its value. Special research is needed in order to choose a sea state “equivalent” or “representative” for a ship’s operational profile. This may result in a ship-specific sea-state to use for assessment.

An alternative to the selection of a limited set of environmental conditions may be the use of long-term statistics considering all the combinations of weather parameters available from scatter diagrams or appropriate analytical parametric models.

In the traditional literature of naval architecture and ship design, long-term prediction is usually performed with a statistical model composed of a short-term probability distribution of ship responses obtained with the linear superposition principle and a long-term occurrence-probability distribution of sea states provided in an ocean-wave statistics table.

A difficult issue for finding a shared vision is the identification of a representative, if not realistic, environmental and operational context (Perrault, 2013). It has been proven that proper representation of the wave environment is key to correctly evaluating dynamic-stability-related risks (Rosén, *et al.*, 2013).

For an intact-ship assessment, the non-ergodic nature of capsizing is incompatible with the linear hypothesis of the traditional



statistical procedures used to assess the risk of capsizing for an intact ship. Further development of a proper theoretical approach and/or acceptable approximated methodology is needed.

It must be decided in the case of a damaged ship whether the assessment should be posed in terms of probability of survival or in terms of survival time.

The introduction of the human-factor element is beyond the scope of this Committee but it is an important element in the process of assessing ship vulnerability. Evaluation of ship behaviour should remain in the design domain; however; when moving towards an operational context, the human-factor influence cannot be disregarded (Kobylnski, 2012).

Once a satisfactory process is identified for assessing ship vulnerability, additional effort will be required to evaluate the acceptable level (Sheinberg, *et al.*, 2006).

## 7. DAMAGE-STABILITY-IN-WAVES PROCEDURE

Procedure 7.5-02-07-04.2, “Model Tests on Damage Stability in Waves,” provides a test procedure for carrying out model tests on a damaged ship in irregular waves to determine the probability of capsizing, or the significant wave height that will cause a model to capsize in a fixed time period. The Committee investigated the significance of scale effects in air pressure on flooding-model tests under atmospheric conditions, and also how to deal with inertia due to floodwater mass. Based on these investigations, the Committee updated two ITTC recommended procedures: Procedure 7.5-02-07-04.2, “Model Tests on Damage Stability in Waves,” and Procedure

7.5-02-07-04.4, “Simulation of Capsize Behaviour of Damaged Ships in Irregular Beam Seas.”

### 7.1. Scale Effects in Air Pressure

There are some cases in which the flooding of a ship is affected by the air pressure inside the vessel. The main contribution of air pressure takes place in the “trapped-air case” and in the “vented-air case with small vent area.” In a model test of a damaged ship, if the air pressure is maintained at atmospheric pressure, then scale effects in air pressure occur.

Let  $\lambda$  be the ratio of ship length to model length. The model-scale pressure should be scaled by  $1/\lambda$  in order to maintain dynamic similitude. That is, if the model is small, then the pressure of the air should be reduced proportionally. This is possible only in a depressurised tank facility. However, most model basins can only test under atmospheric air conditions, not under scaled-air pressure conditions. Figure 7.1 reveals, conceptually, the difference in pressure head between scaled air-pressure model test and an atmospheric pressure model test.

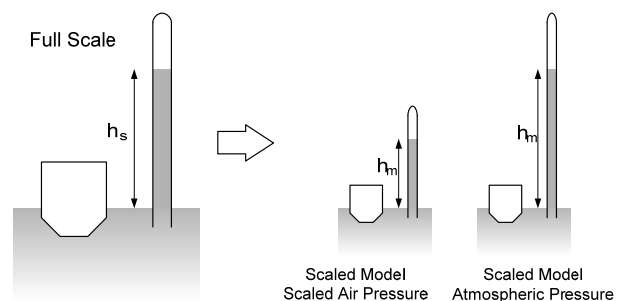


**Figure 7-1 Concept of a scaled-model test.**

For a trapped-air case, the pressure of the model in atmospheric conditions is higher than in scaled pressure. Therefore, flooding to

that compartment is restricted as shown in Figure 7-2.

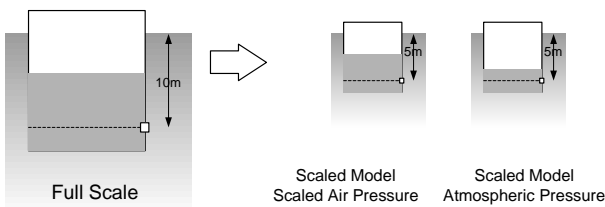


**Figure 7-2 Flooding in a trapped-air case.**

For a vented-air case, air is compressed and the internal pressure increases. The pressure under atmospheric conditions is higher than under scaled-air pressure, so the flooding speed will be slower than under scaled-air pressure, and the following situation will occur, Figure 7-3.

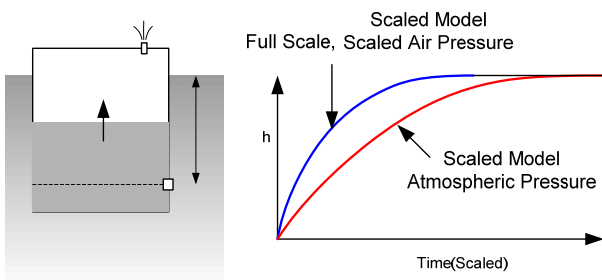


**Figure 7-3 Flooding in a vented-air case.**

The above situation can be simulated by using the state equation of air,

$$PV^\gamma = const.$$

where  $P$  is the absolute pressure of the air,  $V$  is the volume under consideration, and  $\gamma$  is the ratio of specific heats; in the case of air  $\gamma$  is 1.0 for an isothermal process and 1.4 for an adiabatic process. The flow through an opening can be estimated by the orifice equation.

Figures 7-4, 7-5 and 7-6 show the water-height behaviour along with scaled time in the case of a trapped-air case for both small and opening large openings in a compartment bottom.

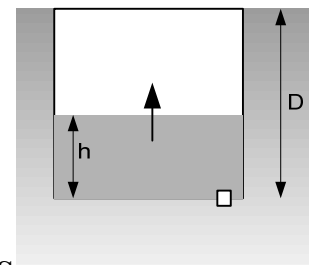


**Figure 7-4 Flooding in a non-vented air case.**

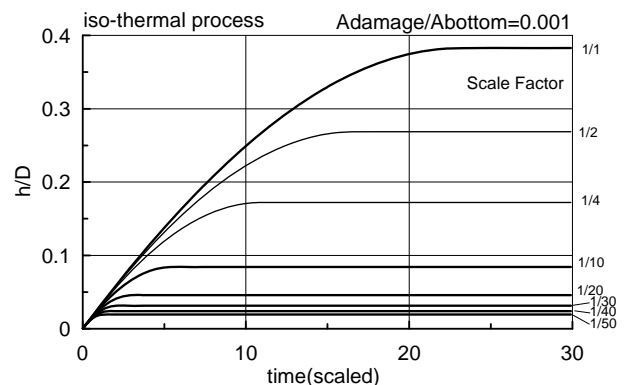


**Figure 7-5 Flooding in a non-vented air case for a small opening.**

The above two figures are exactly the same except for the time scale. This time scale difference comes from the opening-area ratio. As one over the scale ratio becomes small, the final water height is reduced also. In this case, the scale effect of air pressure is significant, regardless of the size of the opening.

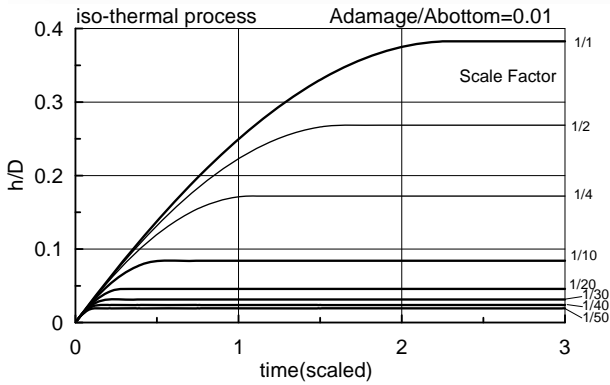


**Figure 7-6 Flooding in a non-vented air-case for a large opening.**

For a vented case, Figures 7-7 to 7-10 show the density ratio of air and water height during the flooding process.

The ratio of vent area to damage area plays an important role in the flooding process. When this ratio is large, *i.e.*, for a large-vent area, the scale effect turns out to be small. For the small-vent area, the scale effect is large during the initial stage, and as time passes the scale effect becomes small.

In order to reflect the damaged-model-test procedure in which a model is initially set in equilibrium condition, the effects of assuming the air-compression process to be isothermal or adiabatic can be simulated after setting the inner air pressure to be equal to the outside water pressure at the position of the damaged opening. For this purpose, the pressure of the compartment is initially set to the outside water pressure for the vented case. Figures 7.11 and 7.12 show the flooding process of the isothermal and adiabatic processes, respectively.

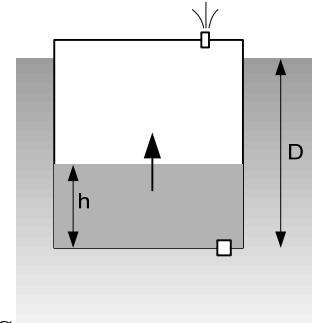


**Figure 7-7 S flooding in a vented-air case.**

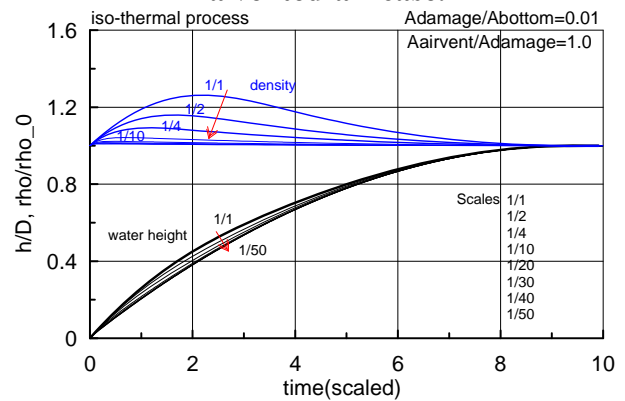


**Figure 7-8 Flooding in a vented-air case for a large air-vent area.**

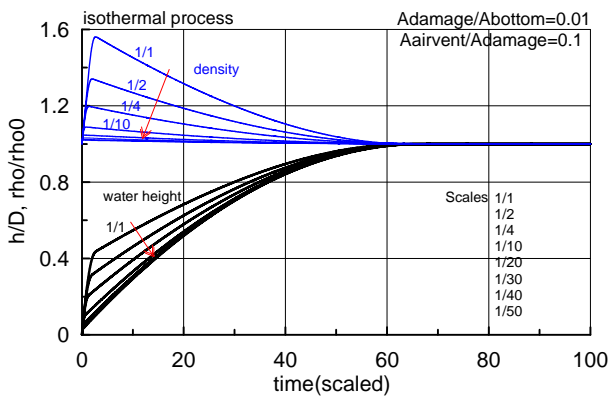


**Figure 7-9 Flooding in a vented-air case for a medium air-vent area.**

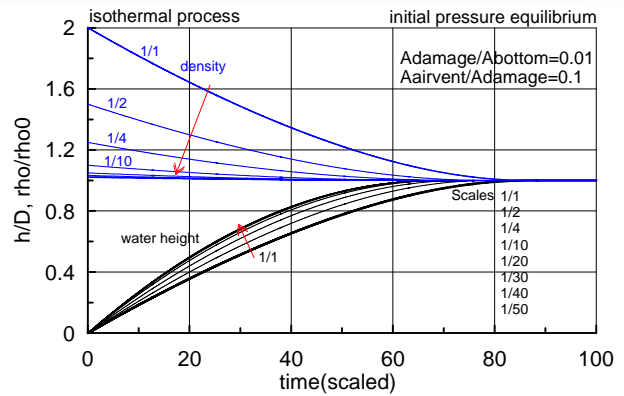


**Figure 7-11 Flooding for the isothermal process when air pressure was initially balanced.**

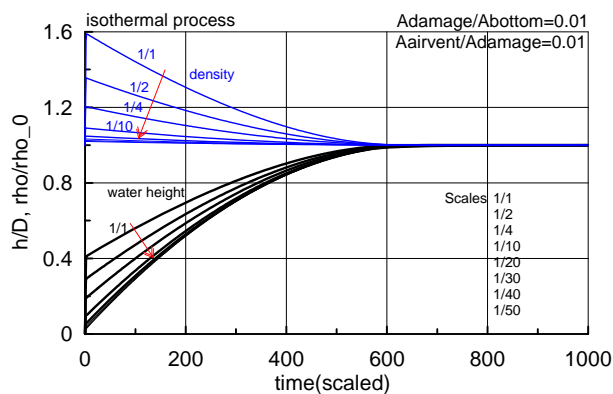


**Figure 7-10 Flooding in a vented-air case for a small air-vent area.**

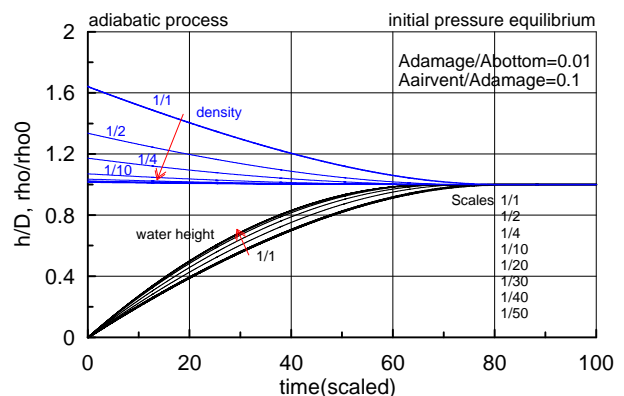


**Figure 7-12 Flooding for the adiabatic process when air pressure was initially balanced.**

If the flooding speed is slow, the air-compression process will be isothermal; if the flooding speed is fast, the air-compression process will be adiabatic. When a damaged ship with a large damage opening floats in waves, the flooding due to wave and ship motion is relatively fast, so an adiabatic process takes place in the air-compression process. Figures 7.11 and 7.12 show that the scale effect is not large.

In line with the above discussion, it can be concluded that the scale effect is large for the trapped air/small-vent area case. For other cases, the scale effect is small and can therefore be ignored in model tests of a damaged ship.

Under atmospheric conditions, it is possible to use alternative methods to reduce the scale effect of air pressure. For the case of a small-vent area, the vent opening can be enlarged to an appropriate size in order to reflect the inflow and outflow of a full-scale situation. For the case of trapped air, a simple solution would be to attach a balloon to the compart-



ment in order to lessen the scale effect of air pressure, and to obtain realistic flooding results in a test condition.

In summary, if a damage opening is large and the compartment is well vented, scale effects due to air pressure will be small, and model tests in atmospheric conditions are suitable. The scale effects will be large in a trapped-air or a small-vent area case. If precise and accurate test results are required, the use of pressure regulation values on compartments to control the internal pressure may be a viable solution in the former situation, or in either case, model tests may be conducted in a depressurised model basin. At a minimum, when model tests are conducted under atmospheric conditions, modifications are recommended to reduce scale effects.

Procedure 7.5-02-07-04.2, “Model Tests on Damage Stability in Waves,” was updated to reflect the above discussion.

## **7.2. Inertia Due to Floodwater Mass**

Floodwater inertia has two main effects on a ship’s behaviour; one is the inflow/outflow effect, and the other effect is the inertia of the flood water itself.

### **7.2.1. Floodwater Domain**

There is a problem of which region of a ship should be treated as floodwater if the damage opening is large enough. First a more reasonable and clear definition of floodwater in the analysis of a damaged ship is needed. If the focus is on the inertial properties of water, floodwater can be determined by looking at whether or not the water is moving together with the ship. If the focus is on the hydrodynamics of floodwater, this may be determined by investigating whether pressure of the floodwater is strongly related to the out-

side water level or not, and whether the hydrodynamic problem of the floodwater can be analysed separately or not. Provided that a boundary condition is given for the matching of inner- and outer-flow domains, the problem can be separated into one of flow in inner- (inside the ship) and outer- (outside the ship) flow domains.

The following questions can be used as criteria to determine how the floodwater should be treated:

- What is the amount of water and is it or is it not moving with the ship?
- What, if any, is the significant pressure jump across the compartment boundary?
- Can the dynamics of the water be solved separately or not?

The above criteria also provide clues as to what to consider as floodwater when examining damaged ships.

### **7.2.2. Partially-flooded Compartments**

The hydrodynamics of floodwater and its force on a compartment partially filled with floodwater can be calculated by theory or by a numerical scheme such as: resonant-mode analysis; potential-flow theory; computational fluid dynamics (CFD) with a free surface; etc. In these methods, the force generated by the floodwater is treated as an external force which affects the motion of a ship. An additional problem to consider is whether the mass of the floodwater should be included in the ship’s mass or not. Since quasi-static analysis considers only the centre of gravity of the floodwater, the mass of floodwater should be included in the ship’s mass for this type of analysis. However, in a fully dynamic analysis, the pressure includes both static and dynamic pressures. The force derived from integrating these pressures on the surface of a compartment includes all the effects of floodwater inertia and flow properties. The force



of the floodwater from a fully dynamic analysis assumes that the body force includes the actual acceleration of the floodwater, *i.e.*, both gravitational acceleration and floodwater acceleration. In this case, the mass of the floodwater should not be included in a ship's mass.

### 7.2.3. Fully-flooded Compartments

Floodwater in a fully filled compartment is often treated as a solid and thus is considered part of the ship. In rectilinear acceleration, floodwater acts like a solid. In rotational acceleration, the moment of inertia of floodwater in a compartment is smaller than that of a solid, because part of the water does not rotate with the ship. Lee (2014) showed the ratio of the moment of inertia of floodwater and that of solids for various shapes of compartments.

$$C_R = I_{Liquid} / I_{Solid}$$

where  $I_{Liquid}$  and  $I_{Solid}$  are the moment of inertias of floodwater when treated as a liquid and a solid, respectively.

Figure 7-13 shows the shapes of compartments treated in his study.

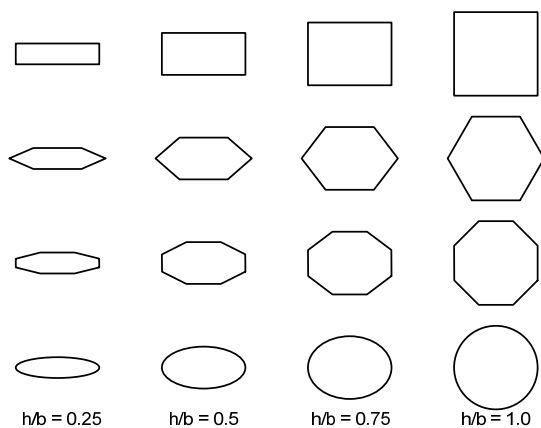


**Figure 7-13 Various shapes of tanks useful for application (Lee, 2014).**

The inertias of fluid in tanks of different aspect ratios and shapes, Figure 7-14, become small as the aspect ratio goes to unity. The solid lines of Figure 7-14 are analytical or numerical results while the dashed lines are from an estimation formula that provides accurate results.

### 7.2.4. Inertia of Floodwater Entering a Ship

Newton's Second Law of Motion states that the force (moment) on a body is equal to its time rate-of-change of momentum (angular momentum). For a body of constant mass (moment of inertia) this translates to  $\vec{F} = m\vec{a}$  ( $\vec{M} = I d\vec{\omega}/dt$ ). However, for a body such as a rocket which is burning fuel and ejecting gas, or a damaged ship in a seaway taking on and possibly discharging water, the  $\vec{F} = m\vec{a}$  analogy is incorrect, because the time-rate-of-change of mass must be taken into account. Since the force of a body must remain independent of the coordinate system, a simple application of the rule for differentiation of the product of two functions does not apply. The contribution from the term for time-rate-of-change of mass belongs on the left-hand side of the equation with the force.

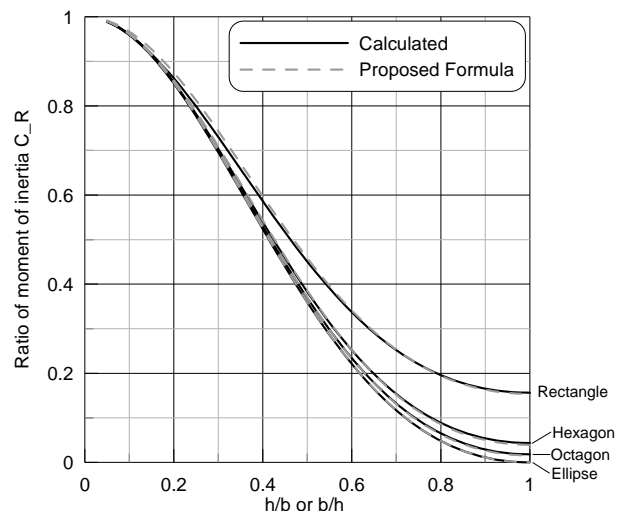




**Figure 7-14 Moments-of-inertia of water in fully filled tanks of various shapes, calculated and estimated from Lee (2014).**

If we represent the momentum of the vessel as  $\vec{p}$  and the angular momentum as  $\vec{L}$ , where  $\vec{p} = m\vec{v}$  and  $\vec{L} = I\vec{\omega}$ , then, with  $m$  the mass of the ship,  $\vec{v}$  the velocity,  $I$  the moment of inertial tensor and  $\vec{\omega}$  the angular velocity, Newton's Second Law of Motion can be written as:

$$\begin{aligned}\vec{F} &= m \frac{d\vec{v}}{dt}, \\ \vec{M} &= I \frac{d\vec{\omega}}{dt}.\end{aligned}\quad (43)$$

When the mass, and hence the moment of inertia are constant, these equations can be reduced to the original  $\vec{F} = m\vec{a}$  equation. However, in the damaged condition, the vessel's mass and moment of inertia vary with time and the equations of motion must be written as in (43). Rewriting (43) to account for the intake and/or discharge of floodwater as for a closed system yields:

$$\begin{aligned}\vec{F} + \vec{v}' \frac{dm}{dt} &= m(t) \frac{d\vec{v}}{dt}, \\ \vec{M} + \vec{\omega}' \frac{dI}{dt} &= I(t) \frac{d\vec{\omega}}{dt},\end{aligned}\quad (44)$$

where  $\vec{v}'$  and  $\vec{\omega}'$  are the velocity and angular velocity of the flooding (discharging) water relative to the vessel, respectively<sup>4</sup>. All of the quantities ( $\vec{v}'$ ,  $dm/dt$ ,  $\vec{\omega}'$ , and  $dI/dt$ ) in (44) can be determined from analysis of the

<sup>4</sup> Note that these velocities are positive in the same direction as that of the ship, which is opposite the convention often used in rocket propulsion, where the positive velocity of the exhaust gases is opposite the positive velocity of the rocket.

flow at the damaged opening. However, if there is flow between flooded compartments, then the force due to the flow of floodwater between compartments must be accounted for in a similar manner. The evaluation of  $dI/dt$  is also somewhat more complex as it involves the actual shape of the compartment.

The above material dealing with the change of inertia due to floodwater was included Procedure 7.5-02-07-04.4.

## 8. IMO LIAISON

ITTC Specialist Committee on Stability in Waves (SiW) has reviewed draft reports of the Intercessional Correspondence Group (ISCG) as well as IMO documents including the SLF54, SLF55 and SDC1 sub-committee reports. The reports discuss methodologies for vulnerability criteria and direct stability assessment for the following stability failures:

- Quasi-steady stability variation in waves in following/stern quartering seas;
- Parametric resonance due to stability variation in waves;
- Dead-ship conditions;
- Broaching, manoeuvrability and course-keeping ability.

As discussed in Chapter 6 of this report, the vulnerability criteria assessment process is broken into three levels. The first level is simple assessment with a relatively large margin of safety. The second level is a more sophisticated assessment using detailed calculations. If a vessel fails the second-level assessment, a direct stability assessment (the third level) is made.

The first and second vulnerability criteria for the stability failures mentioned above are almost finalised. Future work will be focused



on the quality of direct calculation methodologies. The ITTC SiW Committee reiterated the availability of technical specifications for numerical tools for direct assessment of vulnerability criteria that were contained in the Committee's report to the 26th ITTC (ITTC, 2011a).

## 9. PREDICTING ROLL MOTION AND DAMPING

Roll motion is one of the most critical responses of a ship in waves, and the roll response of a ship is an important consideration in its design. Roll motion limits ship operability, affects crew performance and ship habitability, and affects dynamic stability and ship capsizing. The roll motion of a ship can be determined by analysing the various moments acting on the ship: virtual and actual moments of inertia of mass; roll-damping moment; restoring moment; wave excitation; and moments caused by other modes of ship motion. Among them, the roll-damping moment has been considered to be the most important contributor that needs to be correctly predicted. The roll damping moment of a ship needs to be taken into account at the initial stage of ship design to secure the safety of a ship, and also to obtain a better understanding of ship motions in waves.

In order to better understand the roll-damping effects for roll motions in irregular seas, a state-of-the-art review was conducted. This review covered both the validation of numerical results of roll damping, and numerical modelling of hydrodynamics for time-domain computer codes for large-amplitude roll motions.

### 9.1. Validation of Predictions for Roll Damping

Validation is important for numerical calculations, and the selection of adequate validation data is important for accurate stability estimations. The following methods are commonly used to obtain validation data of roll damping:

- Free-decay test. (A)
- Forced-roll test with sinusoidal-roll excitation. (B)
- Forced-roll test around a fixed axis. (C)

Roll-motion data is also used to validate roll-motion simulations. In the following sections, some validation data for numerical results are introduced.

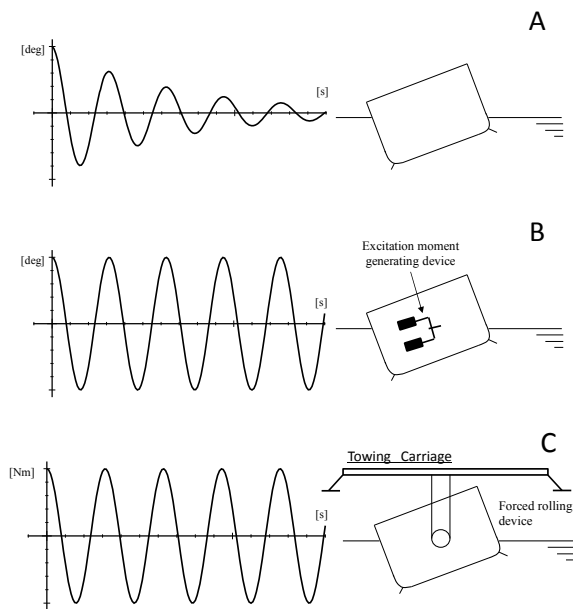


**Figure 9-1 Experiments to obtain validation data of roll damping.**

### 9.1.1. Damping Coefficients from Forced-roll Tests

One of the purposes of using roll damping derived from forced-roll experiments is to calculate the roll amplitude in regular waves. In this case, the frequency-domain roll-damping coefficients are used in equations of motion.

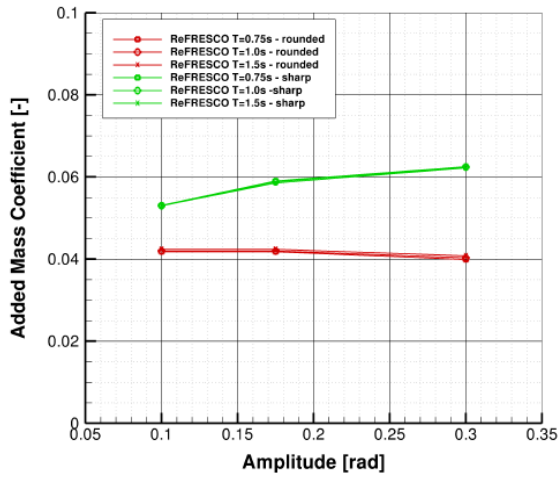
For this purpose, the coefficient of roll damping denotes the equivalent linear damping coefficient. Although the value of the coefficient depends nonlinearly on the roll amplitude and angular velocity for a certain frequency and forward speed, it is assumed that the coefficient is constant during a specific motion for a given roll amplitude.

The equivalent linear damping coefficient is obtained from a forced-roll test. There are two ways to perform a forced-roll test. In one test the model is forced to roll but with

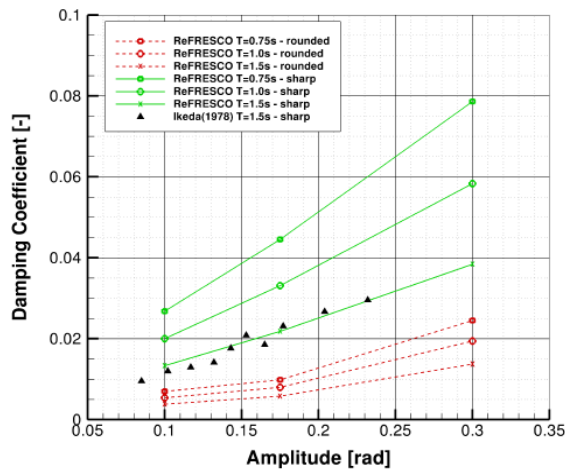
small amplitudes, and is constrained in all other degrees of freedom. For large amplitude forced rolls the model must be allowed to heave and pitch. In both tests the forcing-roll moment and the roll motion are measured starting after four swings from rest in order to remove transient effects (Ikeda, *et al.*, 1988 and Katayama, *et al.*, 2011). The equivalent linear damping can be obtained by frequency analysis of the measured roll moment based on the measured roll at the fundamental frequency component in phase with the roll angular velocity.

In the case of statistical analysis of irregular roll motions, there is another approach to the linearization of the roll-damping expression that can be used. In this linearization, the linear and quadratic damping coefficients from a roll decay or forced roll experiment are added with the quadratic term weighted by the standard deviation of the roll angular velocity in random seas (ITTC, 2011b, Sect. 3.2).

Jaouen, *et al.* (2011) verified and validated MARIN's Unsteady Reynolds Averaged Navier-Stokes (URANS) code ReFRESKO for roll damping of two-dimensional hull sections by comparing the damping coefficients measured by Ikeda, *et al.* (1978), Figure 9-2. Ikeda, *et al.* (1978) showed the measured roll-damping coefficient of Series 60, SR98, SR158, SR108, and also showed the effects of forward speed on the damping coefficient. Ikeda, *et al.* (1978) provided other useful measured data. Ikeda, *et al.* (1976, 1977b, 1979) provided detailed validation data for measured flows around a bilge keel using forced-roll tests. Ikeda, *et al.* (1977b) also showed a number of types of vortices on hulls (Figure 9-3) as well as measured flows around the bilge of a naked hull (Ikeda, *et al.*, 1977a). Figure 9-4 shows the pressure distribution on a two-dimensional model with bilge keels.



(a) Results for  $a_{\phi\phi}$ .



(b) Results for  $b_{\phi\phi}$ .

**Figure 9-2 Coefficients of added mass and damping (Jaouen, *et al.*, 2011).**

Bonfiglio, *et al.* (2011), using FLUENT and CFD-code base on the open source libraries of OpenFOAM, and Henning (2011), evaluated the hydrodynamic damping and added mass coefficients of two-dimensional ship-like hull sections in the case of forced oscillations. The results from Bonfiglio, *et al.* were compared with measured results carried out by the Delft Hydrodynamics Laboratory (Vugts, 1968, 1970). Vugts carried out a forced-roll test for two-dimensional ship sections (Figure 9-5) and showed the measured

added mass, damping and coupling coefficients among roll, heave and pitch. He also carried out a forced-roll test with forward speed for a three-dimensional segmented model and showed the sectional added mass, damping and coupling coefficients among roll, heave and yaw.

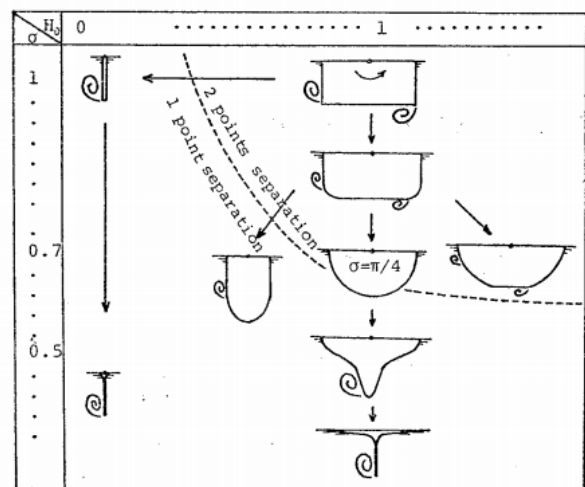


**Figure 9-3 Eddies near a hull (Ikeda, *et al.*, 1977b).**

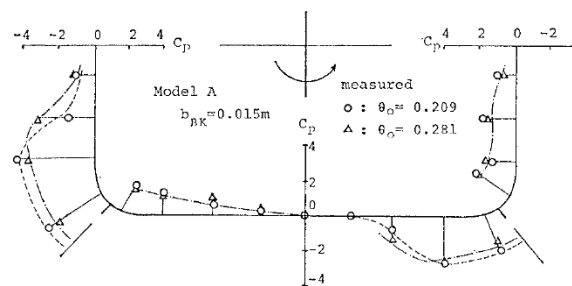


**Figure 9-4 Measured pressure distribution on a hull with bilge keels under forced rolling (Ikeda, *et al.*, 1977a).**

Paap (2005) investigated verification of CFD calculations with forced-roll test results for a circular cylinder with various types of bilge keels and a free surface. The measured data included not only coefficients but also velocity vectors obtained by a particle image velocimetry (PIV) technique (Figure 9-6), *i.e.*,

time histories of bilge-keel force and heights of the radiated wave.

Bangun, *et al.* (2010) calculated the hydrodynamic damping and added mass coefficients of two-dimensional rectangular sections with bilge keels and compared the predictions with measured results by Yago, *et al.* (2008). Yago, *et al.* (2008) showed the measured added mass, the equivalent linear total roll damping, and the wave component of roll damping.

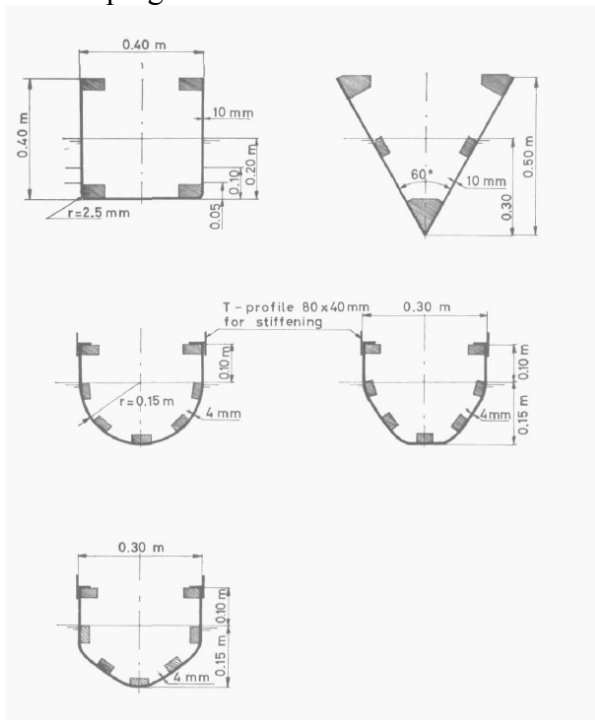


Figure 9-5 Cross sections of cylinders (Vugts, 1970).

### 9.1.2. Free-decay Test Data

Roll damping results obtained from a roll-decay test are not the same as the results obtained from a forced-roll test (Figure 9-7). The difference between the two sets of results occurs particularly during the first few oscillations because roll-decay motion is a transient motion. ITTC (2011, pp 19–20,) shows how to obtain a roll-damping coefficient from a

free-decay test. Some notes on how to carry out a free-decay test are indicated in IMO (2006, pp. 11).

To estimate the onset of large-amplitude roll motions at the roll natural frequency, Sadat-Hosseini, *et al.* (2010) use roll-damping coefficients obtained from a roll-decay test in the equations of motion for a time-domain simulation.

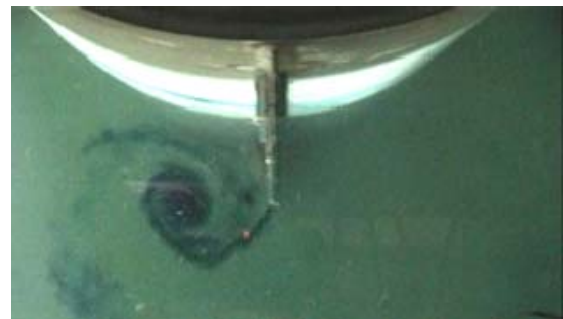
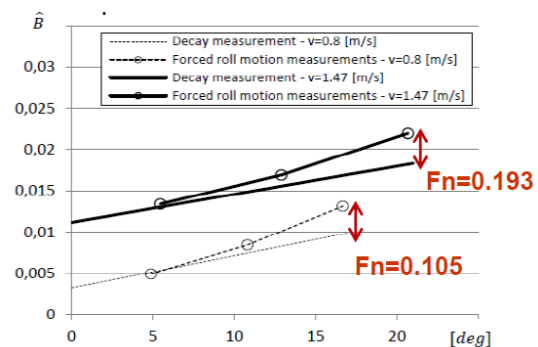


Figure 9-6 Visualized vortex and velocity vectors (Paap, 2005).





**Figure 9-7 Comparison of measured results by free-decay tests and forced-roll tests by sinusoidal harmonic-roll excitation (Handschel, *et al.*, 2012).**

Yang, *et al.* (2012) calculated roll damping of DTMB Model 5512 at different initial roll angles by using the roll-decay simulation in CFD (Figure 9-8). Roll-damping coefficient results were compared with measured results by Irvine (2004). Wilson, *et al.* (2006) used an unsteady Reynolds Averaged Navier-Stokes (RANS) method (CFDShip- Iowa) to compute the motions of DTMB Model 5512, and the resulting flow and wave fields around the models; the calculated results were compared with the measured results obtained by Irvine, *et al.* (2004). Sadat- Hosseini, *et al.* (2010) calculated roll motion with forward speed of the Office of Naval Research (ONR) Tumblehome hull form by CFDShip-Iowa and compared it with the measured roll motion of DTMB Model 5415 (Irvine, 2004). Gao & Vassalos (2011) applied a RANS-based CFD solver to study the roll decay of an intact DTMB Model 5415. The computed roll-decay history and velocity contours were compared with the measured results by Irvine, *et al.* (2004) Figure 9-9. Irvine also provided measured data (roll motion, velocity field, and wave pattern around the hull) for DTMB Model 5512 (<http://www.ihr.uiowa.edu/shiphydro/efd-data5512-roll-decay/>).

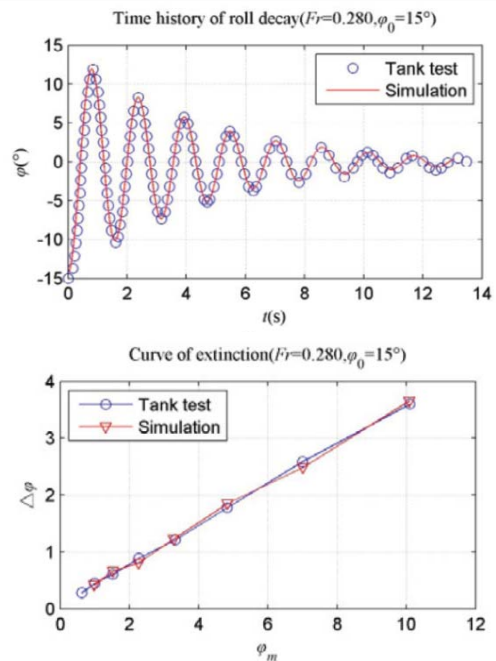


**Figure 9-8 Measured roll motion and curve of extinction (Yang, *et al.*, (2012).**

### 9.1.3. Roll damping in time-domain simulations of large-amplitude motions

For time-domain simulations of irregular motion, roll damping must include the effects of transient motion (Ikeda, *et al.*, 1988; Katayama, *et al.*, 2010, 2013). This means that the validation data must include time histories of the force of moment, the motions and flow around the hull measured under transient and irregular motion conditions. Moreover, if the roll amplitude is large, the validation data must include the effects of nonlinearity caused by the large amplitudes of motion (*e.g.*, Tanaka, *et al.*, 1981; Bassler, 2013). For free motions in extreme waves, the waves which impact the model and the resulting motions are required for validation of the simulation.

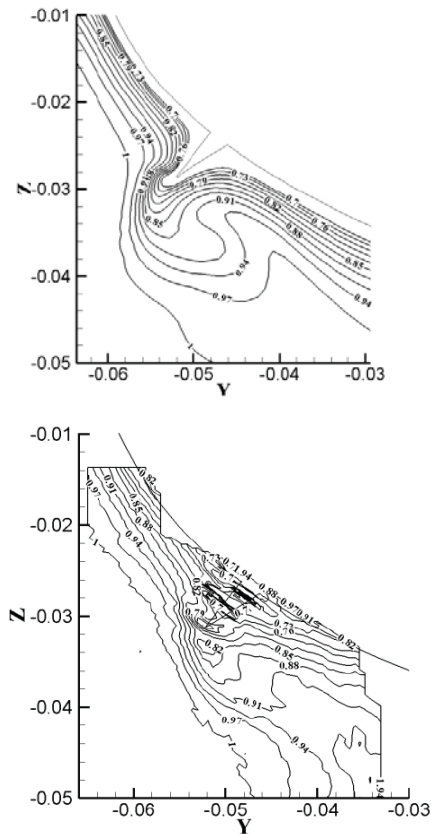


**Figure 9-9 Contours of velocity (Gao & Vassalos., 2011).**

Therefore, the following experimental data may be required for validation of simulations for large-amplitude, irregular-roll motions:

- Irregular- and large-amplitude forced-roll test data
- Irregular- and large-amplitude roll motion data in extreme, irregular waves

However, no studies exist which provide measured data for all the required conditions. In this section, some studies relating to large-amplitude rolls or irregular roll motions are introduced.

The importance of flow-memory effects on roll damping was discussed by Ikeda, *et al.* (1988). Using the Morison Equation instan-

taneous velocity and acceleration are used, for which flow memory is not accounted. The Logarithmic Decrement Method, where an equation without memory is fitted to the motion decay data, has the same deficiency as the Morison Equation Method. Ikeda, *et al.* (1988) showed through experiments that the drag coefficient on plates increased in the first few oscillations when the plate is started rest (Figure 9-10). It takes 3 to 4 oscillations before a steady-state flow field is established and the drag becomes constant. For all Keulegan-Carpenter ( $KC$ ) numbers investigated (defined as  $KC = UT/2h$ , where  $U$  is the maximum flow velocity in the oscillation period,  $T$ , and  $h$  is span of the bilge keel), the drag coefficient in the first oscillation is about half the value for that in a steady condition. This effect is caused by the interaction between previous and present vortices. Only after a few oscillations does a steady, disturbed-flow field exist around the object. An additional valuable observation reported from the experiments by Ikeda, *et al.* (1988) is that the memory effects remain important in irregular motion. When an oscillation has a larger amplitude than the oscillation after it, then the drag coefficient is larger than at a steady oscillation amplitude. When an oscillation is smaller in amplitude than the oscillation after it, the drag coefficient is similar to the drag found in the first oscillation starting from rest.

Katayama, *et al.* (2011) investigated the effects of transient motion on the drag force of a flat plate. In the region of  $KC < 250$ , the drag coefficient for acceleration in one direction is larger than the drag coefficient for acceleration in a uniform flow and smaller than that in a steady oscillatory flow (Figure 9-11). Moreover, in a transient condition under forced oscillation, the drag coefficients from the first to the third oscillation are smaller than that in a steady oscillatory flow. These facts may indicate that the characteristics of transient and

non-periodic rolling affect the drag coefficient. Katayama, *et al.* (2013) proposed an empirical formula for the bilge-keel component of roll damping based on the results of Katayama, *et al.* (2010) that indicate that transient effects on bilge keel drag can affect the onset and amplitude of parametric rolling in a time-domain simulation.

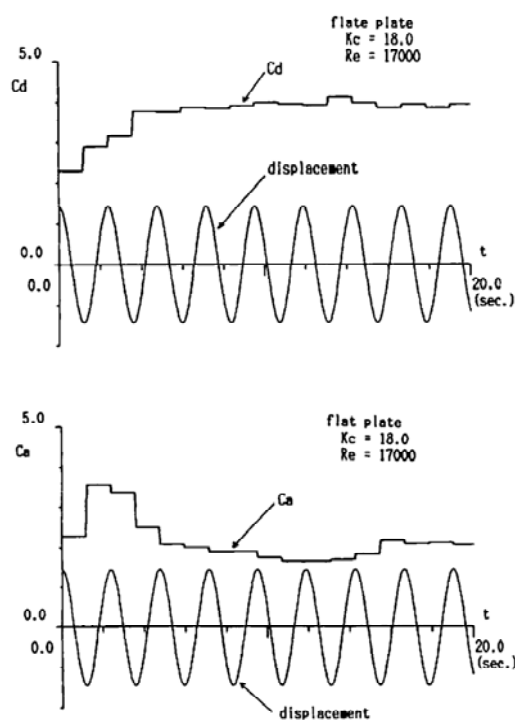


**Figure 9-10 Drag and added-mass coefficients of a sinusoidally oscillating flat plate normal to the motion from rest (Ikeda, *et al.* 1988).**

Tanaka, *et al.* (1981) discussed the effects of shallow draft on roll damping for hulls with bilge keels. Under certain conditions bilge keels add no increase to roll damping for some shallow-draft ships (Figure 9-12). From experimental and theoretical studies, it was shown that the wave-damping component was reduced by the interaction between the waves made by both the hull and bilge keel; the eddy-damping component of bilge-keel damping is

also reduced by deformation of the water surface. These same effects may occur for large-amplitude roll motions for normal-draft ships with bilge keels.

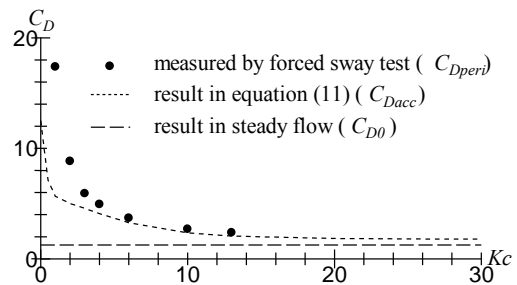


**Figure 9-11 Comparison of drag coefficients of a flat plate from a forced-sway test and a unidirectional accelerating test. Equation (11) is a curve fit to measured data from a unidirectional accelerating test with various accelerations (Katayama, *et al.*, 2011).**

Bassler (2013) analysed the hydrodynamics of large-amplitude ship-roll motions as components of added inertia and damping based on the results of forced-roll tests and CFD. It was shown that the effects of hull geometry, bilge-keel geometry, deck edge, and the free surface all affect the hydrodynamic components during large-amplitude roll motions. Results from the experiments included measurements, observations, and identification of the discrete processes that result in several physical phenomena relevant to large-amplitude roll motions, including bilge-keel interaction with the free surface (emergence and re-entry), vortex shedding, and the effect of vortex shedding on the forces and moments of both hull and the bilge keel. Figure 9-12 shows measured bilge-keel force at various roll amplitudes.



## 9.2. Modelling of large-amplitude roll motions.

Understanding roll motion and its associated damping is essential for the safety of a ship since roll motion, coupled with other motions, may lead to capsizing. Apart from environmental uncertainties, the damping coefficients in equations of motion cannot be derived accurately by theoretical means alone, so experimental studies (e.g., experimental forced-roll and roll-decrement tests) or numerical studies are necessary. Once the decaying curve or forced-moment curve is obtained either from simulations or from model tests, damping coefficients can be obtained by several appropriate techniques.

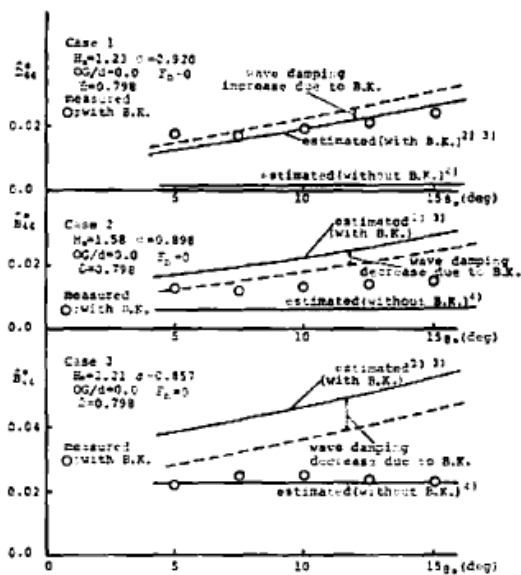


Figure 9-12 Effects of draft and roll amplitude on non-dimensional roll damping of a two-dimensional model. (Tanaka, *et al.*, 1981).

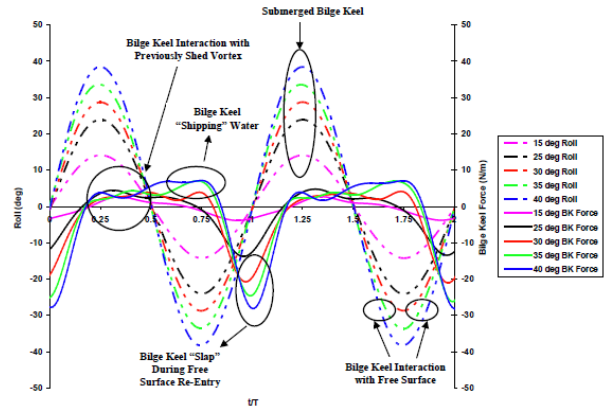


Figure 9-13 Filtered roll-motion measurements and bilge-keel-force measurements for DTMB Model #5699, at various roll amplitudes,  $\phi = 15^\circ$  (purple),  $25^\circ$  (black),  $30^\circ$  (red),  $35^\circ$  (green) and  $40^\circ$  (blue) deg,  $\omega = 2.5$  rad/s, with distinct physical phenomena identified at various stages in the roll cycle. (Bassler, 2013).

Since the pioneering work of Froude, considerable attention has been paid by various researchers to roll damping. Even now roll damping continues to be studied because fluid viscosity and vessel-forward speed create many difficulties in making predictions of ship-roll motions due to roll damping..

### 9.2.1. Current engineering prediction methods.

Current ship-motion-prediction methods rely primarily on potential-flow-based hydrodynamic methods such as:

- Strip theory methods
- Frequency-domain free-surface Green-function panel methods,
- Frequency-domain Rankine-panel methods,
- Time-domain free-surface Green-function panel methods,
- Time-domain Rankine-panel methods.



Except for Strip Theory the panel methods above may include fully three-dimensional effects of flow and free-surface boundary forward-speed effects, which are taken into account in strip theory methods. Local pressures, especially for shorter waves, were much better predicted by panel methods than by strip theory methods.

Frequency-domain methods deal with linear-ship-motion problems based on steady flow. However, these methods may not be applicable to large-amplitude motions for ships with strong flare such as container ships. Therefore, a time-domain-panel method including nonlinearity of hull and free-surface boundary conditions for ship-motion prediction was developed. Generally, time-domain code requires considerable computational time for obtaining a solution. Although hydrodynamic forces, ship motions, and wave pressure are much better predicted using frequency-domain panel methods than by strip theory methods, the calculated accuracy of hydrodynamic forces on lateral motions using frequency-domain panel methods is not satisfactory. This is due to the fact that viscous-flow effects are not accounted for in potential-flow methods and in some situations are introduced into the calculations through empirical corrections.

In fact, predicting roll effects analytically has always been problematic because of significant viscous effects (*i.e.*, the nonlinear nature of roll motions and the strong dependence of roll damping on forward speed). An ideal fluid theory cannot resolve such roll effects. In fact it has a tendency to under predict restoring moments due to the cancellation of the unsteady pressures over the sides and bottom of a ship. Such predictions become progressively worse for round-bottom hulls. Consequently, potential flow methods must be supplemented with empirical information. A

great deal of effort has been directed at developing coefficient-based approaches for roll prediction. The most important contribution to developing such coefficient-based methods was developed by researchers such as Tanaka, Himeno, Ikeda, and Blok. According to them, viscous-damping coefficients can be divided into components related to four effects; friction; lift associated with forward speed; bilge-keel local effects; and vortex-shedding.

Even though numerous sources exist for systematic empirical data, problems remain with limitations in specific ranges of geometry and operating parameters. The standard empirical approach, for example, involves subdividing damping into bare hull, appendage components, etc. These approaches have been used successfully when applied to hull forms for which they were developed. However, these methods require new data when applied to new hull forms.

### **9.2.2. Requirements for large-amplitude Roll motion prediction**

Typical wave-induced ship-motion solution techniques are based on the assumption of using small-amplitude motions and potential flow so that the general 6-DOF nonlinear equations of motions are reduced to two separate sets of linear equations (*i.e.*, vertical plane motions and lateral plane motions) and are solved in the frequency domain. Using those assumptions, predictions show good agreement for vertical-plane motions. For lateral-plane motions, potential-flow-method-based codes simulate viscous effects by incorporating empirically derived roll-damping data. Predictions with these methods are limited to the range of geometry, frequency, and operating parameters for which empirical data are valid. However, these methods are also limited by scale effects.



Even modest damping can significantly affect roll motions. However, our ability to predict roll motions continues to lag behind that of predicting pitch and heave. Unlike other degrees of freedom (that are dictated by potential flow-induced forces), roll is dominated by the turbulent, vortex-driven flows near the bilge of a ship. The hydrodynamics of roll motion of a ship is largely influenced by viscous effects which include drag on the hull form as it rolls and on flow separation from the bilge and keel where subsequent vortex formations account for a large amount of roll damping. Bilge keels significantly increase the damping of roll motions, and at forward speeds, bilge keels generate a lift force which also contributes to damping. At high speeds the lift on a hull can be a significant contributor to roll damping.

As ship roll is typically a lightly damped motion with large wave-driven excitations, significant accelerations can occur near resonance. This raises a practical concern for owners who wish to maximize a ship's range of operability in often marginal conditions. The ability to accurately predict rolling near resonance is therefore a crucial topic, and dictates the need for a better understanding of the viscous and vortical flows that drive damping. The level of understanding required is further reinforced by the fact that viscous flow often exhibits nonlinear (*e.g.*, amplitude-dependent) behavior, and may, therefore affect already extreme motions in a nonlinear manner.

For large-amplitude roll motion, the geometry of a wetted-ship surface may have abrupt geometry changes and bilge keels may become less effective due to emergence and interaction with the free surface. As existing coefficient-based damping models were developed for small- to moderate-roll motions, the amount of energy dissipation for large-amplitude roll motion may be over estimated,

resulting in under-predicted roll motion, *e.g.*, Belenky, *et al.* (2009b).

### 9.2.3. CFD-based Prediction of Roll Damping

Since roll damping is dominated by vorticity, truly robust modeling of the problem requires a technique capable of predicting the creation of vorticity in the boundary layer, the shedding of vorticity upon boundary-layer separation, and the effects of turbulence on pressure in the shed-vortex cores. Thus, there is a critical need for development of methods for predicting both viscous flows and large- amplitude motions for surface ships with appendages. The most common numerical technique for predicting roll damping involves the embedded vortex approach. This approach usually uses a vortex distribution over the body, shed-point vortices in the flow, and a separation model for the flow near the bilge corners. Unfortunately, separation models require some prior knowledge of the boundary-layer separation point, and are therefore difficult to apply for round bilge-hull forms without bilge keels. The techniques are also generally limited to two dimensions (Yeung, *et al.*, 2013).

Steady Reynolds Averaged Navier-Stokes (RANS) methods to calculate resistance and propulsion are the most advanced methods to use when predicting ship resistance. For ship resistance and powering, CFD has become increasingly important and is now an indispensable part of the design process. In comparison, application of unsteady RANS methods to ship motions in waves is less developed due to obstacles from unsteady flows [*i.e.*, ship motions, and complex environments (*e.g.*, incident waves, wave breaking, and bubble flow)]. These obstacles increase required computer resources.



Unsteady RANS methods have the potential to produce superior roll motion predictions compared to other methods since the effects due to viscosity, creation of vorticity in the boundary layer, vortex shedding, and turbulence are naturally included in the calculations. In an effort to develop a physics-based approach to the prediction of ship motions, most studies have focused on two-dimensional oscillating bodies. Yeung & Ananthkrishnan (1992) were perhaps the first to attempt to capture the flow attributes through the application of RANS techniques, and their efforts have set the direction for further studies in this area. RANS-equation methods have been used to study the flow around two-dimensional oscillating cylinders (Korpus & Falzarano, 1997); Yeung, *et al.*, 1998; Sarkar & Vassalos, 2000).

Accurate predictions of forces and moments on a three-dimensional, submerged cylinder fitted with bilge keels and with a prescribed roll motion was demonstrated in Miller, *et al.* (2002). Wilson, *et al.* (2006) demonstrated three-dimensional RANS results for ship-hull forms undergoing roll, but were limited to small-roll amplitudes. Numerical uncertainties for RANS simulations are estimated by using verification and validation (V&V) procedures.

The damping behaviour of a ship model depends on the local effects on the hull and appendages. It also depends on the vortex effects on the pressure distribution on a ship bottom. Wanderley, *et al.* (2007) were able to show the influence of vortex shedding on the roll-damping contribution acting on the bottom pressure of a ship hull. The influence of vortex shedding in roll dynamics depends on the amplitude of motion. For small angles, the vortex quickly vanishes from the hull. For larger angles, however, the vortex increases until linked to the hull bottom, modify-

ing the pressure distribution in that region. The physics of damping behaviour at large angles is still an open question. It is clear that vortex shedding is the dominant aspect of the dynamics of systems with large damping. Oliveira & Fernandes (2009) have proposed a new approach to fit a nonlinear model with a set of data obtained from several roll-decay tests.

Bangun, *et al.* (2010) simulated forced-roll motion from small- to moderate- angular amplitudes for a barge with various bilge-keel orientations. The vorticity contour and roll hydrodynamic coefficients of a rolling barge are calculated from velocity and pressure fields, respectively. In contrast to an inviscid fluid where damping is found to be small at high-wave frequencies, numerical results obtained from a viscous solver show that damping is large even when the wave frequency is high (*i.e.*, when the convective flux dominates the flow over the diffusive flux). It is shown that larger roll-amplitude excitation will cause the vortices generated to interact very near the free surface. It remains a challenge to solve a pressure-correction equation under such a condition.

Yang, *et al.* (2012) used CFD to simulate DTMB Model 5512 roll-damping motions at different initial roll angles and the results showed good agreement with tank test data. It showed that the roll-damping coefficient is unrelated to the initial roll angle and varies linearly rather than nonlinearly if the roll angle is less than 20 degrees.

Stern, *et al.* (2013) summarised the CFD progress on ship hydrodynamics. They showed that CFD studies mainly focus on heave- and pitch-motion simulations by RANS compared with roll simulations. Validation for local flow has not been conducted yet due to the complexity in local flow measurements



for free-running models. For more computer-intensive applications such as seakeeping and route modelling, an extremely long simulation time and a range of operating conditions need to be covered. For these applications, the speed of current CFD solutions is still the limiting factor. Thus, using a faster method such as a system-based method should be considered. However, the mathematical models for these methods could be improved using high-fidelity CFD solutions along with system identification techniques. In addition, innovative numerical methods for easier and faster CFD solutions are required. Finally, taking advantage of faster computers such as the next generation massively parallel multicore machines should be considered.

## 10. CONCLUSIONS AND RECOMMENDATIONS

### 10.1. Technical conclusions

A comprehensive state-of-the-art review on predicting ship stability in waves has been undertaken and has been particularly concerned with the definition of loss and survival of a ship, and modelling the internal geometry of a damaged ship. This review concludes with a discussion of modelling of extreme-wave conditions.

1. This review of modelling of damaged ships has reinforced the importance that methodologies used to model damage must reflect the mechanisms involved with the physics of damaged-ship motions leading to loss of a vessel (i.e., sensitivity to scaling in model tests, nonlinear effects of progressive flooding, and floodwater effects on damping of roll on other degrees of freedom). Leak and collapse pres-

ures of watertight doors and bulkheads is another key area that must be covered for damaged-ship modelling. This review also considers the importance of taking air pressure into account during damage experiments and simulations.

2. A state-of-the-art review has been carried out concerning the definition of loss and survival of a ship. It has been concluded that the two terms, loss and survival, under specific conditions, express complementary concepts. It is possible to identify many analogies but also differences while investigating the concepts of loss and survival for an intact ship versus a damaged one. Nevertheless, the prevalent trend in defining loss and survival is to focus on the capsizing event, but due to inherent practical difficulties in dealing with this phenomenon, attention is often shifted to focus on the definitive representative roll-angle value. However, the critical roll-angle value is a particular characteristic of a specific ship under investigation. From a performance-based assessment perspective, it is recommended that attention also be paid to the loss of functional capabilities, which in some cases the functional capabilities (e.g., ship power production and delivery) are beyond the specific focus of the ITTC.

3. An investigation into uncertainty analysis for use in intact- and damaged-model tests to complement current procedures has been reviewed and an outline guide has been provided. This investigation has focused on the uncertainty involved in making measurements during experiments such as roll, pitch, water height, etc. This investigation concluded that the impact of errors occurring while setting up the model can have a significant impact on the experimental results. However, understanding the source of the errors allows the effects of the errors to be minimised.



4. An investigation on wave modelling spectra in the determination of dynamic instability of intact vessels has looked at nonlinear wave kinematics, statistical distribution of crest and trough height and nonlinear wave propagation. Progress is being made regarding methodologies for stability assessment of both intact and damaged ships, A number of modelling methods are presented to achieve realistic environmental conditions.

5. In order to better understand the uncertainties associated with results from experiments and simulations of extreme motions of intact vessels in realistic irregular seaways, a number of quantitative techniques which reflect the nature and magnitude of the phenomena of extreme motions have been reviewed. These techniques address the statistical reliability of both “linear” and “nonlinear” signals and events. Furthermore, these techniques were reviewed to determine extreme values and confidence intervals for nonlinear signals.

6. A state-of-the-art review has been carried out concerning the definition of vulnerability criteria (including long-term probability of loss of a ship) for intact and damaged ships. An outline of current developments is presented and includes a vision of an harmonized approach for intact and damaged ships, highlighting the different priorities that can be identified in the two states. Common approaches are recommended to identify and discuss the relevance and treatment of the environmental context, ship loading conditions, and time of exposure. These considerations must also be coupled with the current developments of simulation tools for the prediction of nonlinear dynamic ship behaviour. Looking specifically at the case of damaged ship, the stochastic nature of flooding, especially in the transient progressive process, should be addressed in conjunction with the proper stochastic treatment of the entire damage scenario.

A significant difference between an intact and a damaged-ship situation with respect to safety assessments, is the issue of time-to-loss. For an intact ship the time-to-loss interval is so long that the estimation of the rare-event occurrence implies the need to further develop methodologies for statistical extrapolation. For a damaged ship, the critical point to determine is if the time-to-loss is sufficient to perform emergency procedures or to evacuate the ship. The outcome from these investigations is extremely diverse which suggests a review is required for the identification of an efficient, final assessment index.

7. An investigation of model tests on damage stability in waves has examined air compressibility, scale effects on air pressure, and current test procedures. This investigation covered the scale effects on air pressure on flooding-model tests under atmospheric conditions and how to deal with the inertia due to floodwater mass. The investigation concluded that the scale effects on air pressure are not significant in most cases, except for the case of trapped air and for a large-damage opening with a small-vent area. In line with these investigations, Procedure 7.5-02-07-04.2 has been updated. The inertia due to floodwater mass was investigated with regard to computational modelling. This included the momentum change description of floodwater, potential criteria for determining the amount of floodwater and a review of research related to floodwater dynamic properties; this has resulted in a revision to Procedure 7.5-02-0704.4.

8. In order to better understand the roll-damping effects for large-amplitude roll motions in irregular seas, a state-of-the-art review was conducted. This covered both validation data for numerical results of time-domain computer codes of roll damping and numerical modelling of hydrodynamics for time-domain computer codes of roll damping. The review



of validation data focused not only on large-amplitude irregular motion but also on small-amplitude regular motion. Some existing and useful model-scale experimental data has been identified for validation. These data are presented separately as a total hydrodynamic moment, and roll damping with its components.

9. The committee has:

- a. Updated Procedure 7.5-02-07-04.2 for Model Tests on Damage Stability in Waves.
- b. Updated Procedure 7.5-02-07-04.4 for Simulation of Capsize Behaviour of Damaged Ships in Irregular Beam Seas.

## 10.2. Recommendations to the Conference

- Adopt the revised Procedure 7.5-02-07-04.2, Model Tests on Damage Stability in Waves.
- Adopt the revised Procedure 7.5-02-07-04.4, Numerical Simulation of Capsize Behaviour of Damaged Ships in Irregular Beam Seas.

## 11. REFERENCES AND NOMENCLATURE

### 11.1. References

Bačkalov, I. (2012) “A probabilistic analysis of stability regulations for river-sea ships.” *Proc. 11th Int’l. Conf. Stability of Ships and Ocean Vehicles*, Athens, Greece.

Ball, R. E. & C. N. Calvano (1994) “Establishing the fundamentals of a surface ship Survivability Design Discipline.” *Naval Engineers J.*, 106(1):71–74.

Bangun, E. P., C. M. Wang & T. Utsunomiya (2010) “Hydrodynamic forces on a rolling barge with bilge keels.” *Applied Ocean Research*, 32:219–232.

Bassler, C. C. (2013) “Analysis and modeling of hydrodynamic components for ship roll motion in heavy weather.” Ph.D. Thesis, Virginia Polytechnic Institute and State University, Blacksburg, VA, xxiv+253 p.

Bassler, C. C., V. Belenky, G. Bulian, A. Francescutto, K. Spyrou & N. Umeda, (2009) “A review of available methods for application to second level vulnerability criteria.” *Proc. 10th Int’l. Conf. Stability of Ships and Ocean Vehicles*, St. Petersburg, Russia.

Beaupuy, B., N. Stachelhausen, J.-Y. Billard, E. Mogenicato, P. Vonier & J.-F. Leguen (2012) “Operability of French naval ships over 50 years.” *Proc. 13th Int’l. Conf. Stability of Ships and Ocean Vehicles*, Athens, Greece, pp. 575–582.

Beck, R. F., W. E. Cummins, J. F. Dalzell, P. Mandel & W. C. Webster (1989) “Motions in waves.” *Principles of Naval Architecture*, Vol. III, ed. by E. V. Lewis, Jersey City, NJ, Society of Naval Architects & Marine Engineers, pp. 1–190.

Belenky, V., C. C. Bassler, K. Spyrou (2009a) “Dynamic stability assessment in early-stage ship design.” *Proc. 10th Int’l. Conf. Stability of Ships and Ocean Vehicles*, St. Petersburg, Russia.



- Belenky, V. & B. Campbell (2012) "Statistical extrapolation for direct stability assessment." *Proc. 13th Int'l. Conf. Stability of Ships and Ocean Vehicles*, Athens, Greece, pp. 243–256.
- Belenky, V., A. M. Reed & K. M. Weems (2009b) "Probability of capsizing in beam seas with piecewise linear stochastic GZ curve." *Proc. 10th Int'l. Conf. Stability of Ships and Ocean Vehicles*, St. Petersburg, Russia, pp. 637–650.
- Belenky, V., K. M. Weems, C. C. Bassler, M. J. Dipper, B. Campbell & K. J. Spyrou (2012a) "Approaches to rare events in stochastic dynamics of ships." *Probabilistic Engineering Mechanics*, 28:30–38.
- Belenky, V., K. J. Spyrou & K. M. Weems (2012b) "Evaluation of the probability of surf-riding in irregular waves with the time-split method." *Proc. 11th Int'l Conf. Stability of Ships and Ocean Vehicles*, Athens, Greece.
- Belenky, V., K. M. Weems & W-M. Lin (2007) "A probabilistic procedure for evaluating the dynamic stability and capsizing of naval vessels, phase 1: technology demonstration." SAIC Report ASTD 08-017, 211 p.
- Belenky, V., K. M. Weems, & V. Pipiras (2013) "Split-time method for calculation of probability of capsizing due to pure loss of stability." *Proc. 13th Int'l. Ship Stability Workshop*, Brest, France, pp. 70–78.
- Bendat, J. S. & A. G. Piersol (2010) *Random Data, Analysis and Measurement Procedures*. 4th edition, John Wiley & Sons. Inc., New Jersey, USA.
- Bonfiglio, L., S. Brizzolara & C. Chryssostomidis (2011) "Added mass and damping of oscillating bodies: a fully viscous numerical approach." *Recent Advances in Fluid Mechanics, Heat & Mass Transfer and Biology*, pp. 210–215
- Briggs, M. J. (1982) "Multichannel maximum entropy method of spectral analysis applied to offshore platforms." *Proc. 14th Offshore Tech. Conf. OTC*, Houston, TX.
- Brouwer, J., J. Tukker & M. van Rijsbergen (2013) "Uncertainty analysis of finite length measurement signals." *Proc. 3rd Int'l. Conf. Advanced Model Measurement Technology for the EU Maritime Industry*, Gdansk, Poland.
- Buchner B., G. Forristall, K. Ewans, M. Christou & J. Henning (2011) "New insights in extreme crest height distributions (A Summary of the Crest JIP)." *Proc. ASME 30th Int'l. Conf. Offshore Mech. & Arctic Engin.*, Rotterdam, the Netherlands.
- Clauss, G. F. (2008) "The taming of the shrew: tailoring freak wave sequences for sea-keeping tests," *J. Ship Research*, 52(3):194–226.
- Dankowski, H. (2012) "An explicit progressive flooding simulation method." *Proc. 11th Int'l. Conf. Stability of Ships and Ocean Vehicles*, Athens, Greece.



- Dommermuth, D. G. & D. K. P. Yue (1987) "A high-order spectral method for the study of nonlinear gravity waves." *J. Fluid Mechanics*, 184:267–288. (1988) Corrigendum, *J. Fluid Mech.*, 189:589.
- Gao, Q. & D. Vassalos (2011) "Numerical study of the roll decay of intact and damaged ships." *Proc. 12th Int'l. Ship Stability Workshop*, Washington, D.C. pp. 277–282.
- Goertzel, G. (1960) "Fourier analysis." *Mathematical Methods for Digital Computers*, Ed. by A. Ralston & H. S. Wilf, John Wiley & Sons, pp. 258–262.
- Green, A. E. & P. M. Naghdi (1986) "A nonlinear theory of water waves for finite and infinite depths." *Philos. Trans. Royal Soc. London, Series. A*, 320(1552):37–70.
- Green, A. E. & P. M. Naghdi (1987) "Further developments in a nonlinear theory of water waves for finite and infinite Depths." *Philos. Trans. Royal Soc. London, Series A*, 324(1577):47–72.
- Grim, O. (1961) "Beitrag zu dem Problem der Sicherheit des Schiffes im Seegang." *Schiff und Hafen*, 6:490–497.
- Gu, M., J. Lu & T. Wang (2012) "An investigation on stability under dead ship condition of a tumblehome hull." *Proc. 13th Int'l. Conf. Stability of Ships and Ocean Vehicles*, Athens, Greece, pp. 593–598.
- Gudmestad, O. T. (1993) "Measured and predicted deep water wave kinematics in regular and irregular seas." *Marine Structures*, 6:1–73.
- Handschele, S., N. Köllisch, J. P. Soproni, M. Abdel-Maksoud (2012) "A numerical method for estimation of ship roll damping for large amplitudes." *Proc. 29th Symp. Naval Hydrodynamics*, Gothenburg, Sweden, pp. 1–13.
- Harmsen, E. (2006) "Development of probability based quasi-static damage stability criteria for naval ships." *Proc. 9th Int'l. Conf. Stability of Ships and Ocean Vehicles*, Rio de Janeiro, Brasil.
- Harvey, A. H., A. P. Peskin & S. A. Klein (2008) "NIST/ASME Steam Properties Version 2.22: Users' Guide." National Institute for Standards and Technology, Gaithersburg, MD.
- Haver, S. & O. J. Andersen (2000) "Freak Waves: Rare Realizations of a Typical Population or Typical Realizations of a Rare Population?" *Proc. 10th Int'l. Offshore and Polar Engineering Conf.*, Seattle, WA, pp. 123–132.
- Henning, H. L. (2011) "Investigation of the heave, sway and roll motions of typical ship like hull sections using RANS numerical methods." Masters Thesis, University of Stellenbosch, South Africa.
- IAPWS (2008) "Supplementary release on properties of liquid water at 0.1 Mpa." The Int'l Assn. for the Properties of Water & Steam, Berlin, Germany.
- Ikeda, Y., Y. Himeno, N. Tanaka (1976) "On roll damping force of ship: effects of friction of hull and normal force of bilge keels." *J. Soc. Naval Arch. Japan*, 161:41–49. (in Japanese).



- Ikeda, Y., Y. Himeno & N. Tanaka (1977a) "One eddy making component of roll damping force on naked hull." *J. Soc. Naval Arch. Japan*, 142:54–64.
- Ikeda, Y., Y. Himeno & M. Tanaka (1978) "Components of roll damping of ship at forward speed." *J. Soc. Naval Arch. Japan*, 143:121–133.
- Ikeda, Y., K. Komatsu, Y. Himeno & N. Tanaka (1977b) "On roll damping force of ship effects of hull surface pressure created by bilge keels." *J. Soc. Naval Arch. Japan*, 165:31–40. (in Japanese).
- Ikeda, Y., K. Komatsu, Y. Himeno & N. Tanaka (1979) "On roll damping force of ship—effects of hull surface pressure created by bilge keels." Report of Dept. of Naval Arch., Univ. Osaka Prefecture, No. 00402.
- Ikeda, Y., K. Osa & N. Tanaka (1988) "Viscous forces acting on irregular oscillating circular cylinders and flat plates." *J. Offshore Mech. and Arctic Engin.*, ASME, 110(2):140–147.
- IMO (2005) MSC 80/24/Add. 1 "Report of the Maritime Safety Committee on its Eightieth Session." London, UK.
- IMO (2006) MSC.1/Circ 1200 Annex. "Interim guidelines for alternative assessment of the weather criterion." London, UK, 17 p.
- IMO (2007a) MSC 82/24/Add.1 "Adoption of Amendments to the Int'l. Convention for the Safety of Life at Sea, 1974, as Amended." London, UK.
- IMO (2007b) SLF 50/4/4 "Framework for the development of new generation criteria for intact stability." submitted by Japan, the Netherlands, and the United States. London, UK, 6 p.
- IMO (2008) SLF 51 WP2 "Revision of the intact stability code." Report of the Working Group (Part 1), London, UK, 21 p.
- IMO (2009) SLF 52/INF.2 "Information Collected by the Intercessional Correspondence Group on Intact Stability." Submitted by Japan. London, UK, 138 p.
- IMO (2010) SLF 52/WP1 "Development of new generation intact stability criteria." Report of the Working Group (Part 1), London, UK, 15 p.
- IMO (2011) SLF 54/3/1, Annex 1 "Framework for the second generation intact stability criteria, in development of second generation intact stability criteria." Report of the Working Group at SLF 53 (Part 2), Submitted by the Chairman of the Working Group, London, UK, 5 p.
- IMO (2012) SLF 54/WP.3 "Development of second generation intact stability criteria, any other business." Report of the Working Group (Part 1). London, UK, 24 p.
- IMO (2013a) SLF 55/3/11 "Development of second generation intact stability criteria, comparison study of draft level 2 vulnerability criteria for stability under dead ship condition." Submitted by Italy and Japan. London, UK, 4 p.



- IMO (2013b) SLF 55/WP.3 “Development of second generation intact stability criteria; development of amendments to Part B of the 2008 IS Code on Towing, and Anchor Handling Operations; Development of amendments to the Criterion For Maximum Angle of Heel in Turns of the 2008 IS Code; Development of a mandatory code for ships operating in polar waters.” Report of the Working Group (Part 1). London, UK, 540 p.
- IMO (2013c) SDC 1/INF.8 “Development of second generation intact stability criteria.” Information collected by the Correspondence Group on Intact Stability regarding second generation intact stability criteria development, Submitted by Japan. London, UK, 132 p.
- IMO (2014) SDC 1/WP5 “Development of second generation intact stability criteria.” Report of the Working Group. London, UK, 5 p.
- IOC, SCOR & IAPSO (2010) “The international thermodynamic equations of seawater—2010: calculation and use of thermodynamic properties.” Intergovernmental Oceanographic Commission, Manuals and Guides No. 56, UNESCO, 196 pp.
- Irvine, M., Jr. (2004) “Towing tank tests for surface combatant for coupled pitch and heave and free roll decay motions.” Doctorial thesis, University of Iowa, Iowa City, IA.
- Irvine M., Jr., J. Longo & F. Stern (2004) “Towing tank tests for surface combatant for free roll decay and coupled pitch and Heave motions.” *Proc. 25th Symp. Naval Hydrodynamics*.
- ISSW (2011) *Proceedings of the 12th International Ship Stability Workshop*. V. Belenky. Ed., Washington, DC, iv+420 p.
- ISSW (2013) *Proceedings of the 13th International Ship Stability Workshop*. Brest, France.
- ITTC (2008) “Guide in the expression of uncertainty in experimental hydrodynamics.” ITTC Recommended Procedures and Guidelines, 7.5-02-01-01, Revision 01, 25th Int’l. Towing Tank Conf., 17 p.
- ITTC (2011a) “The Specialist Committee on Stability in Waves: Final Report and Recommendations to the 26th ITTC.” *Proc. 26th ITTC*, Rio de Janeiro, Brazil, 35 p..
- ITTC (2011b) “Numerical estimation of roll damping.” ITTC Recommended Procedures 7.5-02-07-04.5, 26th Int’l. Towing Tank Conf., 33 p.
- Jalonen, R., P. Ruponen, A. Jasionowski, P. Maurier, M. Kajosaari & A. Papanikolaou (2012) “FLOODSTAND overview of achievements.” *Proc. 11th Int’l. Conf. Stability of Ships and Ocean Vehicles (STAB’12)*, Athens, Greece, pp. 819–830.



- Jaouen, F., A. Koop & G. Vaz (2011) "Predicting roll added mass and damping of a ship hull section using CFD." *Proc. ASME 30th Int'l Conf. Offshore Mech. & Arctic Engin.*, Rotterdam, Netherlands, 11 p.
- Jasionowski, A., D. Vassalos & L. Guarin (2004) "Theoretical developments on survival time post-damage." *Proc. 7th Int'l. Ship Stability Workshop*, Shanghai, China.
- Jasionowski, A., D. Vassalos & L. Guarin (2010) "Time-based survival criteria for passenger Ro-Ro vessels." *Proc. 11th Int'l. Ship Stability Workshop*, Wageningen, Netherlands.
- JCGM (2008) "Evaluation of measurement data—guide to the expression of uncertainty in measurement." JCGM 100:2008 GUM 1995 with minor corrections, Joint Committee for Guides in Metrology, Bureau Int'l. des Poids Mesures (BIPM), Sèvres, France.
- Karlberg, D., R. Jalonen & P. Ruponen (2011) "Sensitivity analysis for the input data in flooding simulation." FLOODSTAND Report D2.6
- Katayama, T., J. Umeda, H. Hashimoto & B. Yildiz (2013) "A study on roll damping estimation for non periodic motion." *Proc. 13rd Int'l. Ship Stability Workshop*, Brest, France, pp. 44–49.
- Katayama T., Y. Yoshioka, T. Kakinoki & Y. Ikeda (2010) "Some Topics for Estimation of Bilge-keel Component of Roll Damping." *Proc. 11th Int'l. Ship Stability Workshop*, Wageningen, the Netherlands, pp. 225–230.
- Katayama, T., Y. Yoshioka, T. Kakinoki & S. Miyamoto (2011) "A study on estimation method of bilge-keel component of roll damping for time domain simulation." *Proc. 12th Int'l. Ship Stability Workshop*, Washington, DC, pp. 309–316.
- Kobyliński, L. (2006) "Alternative stability requirements based on system and risk approach." *Proc. 9th Int'l. Conf. Stability of Ships and Ocean Vehicles*, Rio de Janeiro, Brazil.
- Kobyliński, L. (2007) "Goal-based stability standards." *Proc. 9th Int'l. Ship Stability Workshop*, Hamburg, Germany.
- Kobyliński, L. (2012) "Stability criteria—50 years of experience and future prospects." *Proc. 13th Int'l. Conf. Stability of Ships and Ocean Vehicles*, Athens, Greece, pp. 91–100.
- Korpus, R. & J. Falzarano (1997) "Prediction of viscous roll damping by unsteady Navier–Stokes techniques." *J. Offshore Mech. and Arctic Engin.*, 119:108–113.



- Krueger, S. & F. Kluwe (2010) "Development of threshold values for a minimum stability criterion based on full scale accidents." Technische Universität Hamburg-Harburg, Institut für Entwerfen von Schiffen und Schiffssicherheit, Final Report BMWi Project LaSSE—Loads on Ships at Sea, 03 SX 128 D, 167 p. (English Translation from the German original.)
- Kubo, T., N. Umeda, S. Izawa & A. Matsuda, (2012) "Total stability failure probability of a ship in irregular beam wind and waves: model experiment and numerical simulation." *Proc. 11th Int'l. Conf. Stability of Ships and Ocean Vehicles*, Athens, Greece.
- Kwon, S., Q. Chen, G. Mermiris, & D. Vassalos, (2012) "Coupling of progressive structural failure and loss of stability in the safe return to port framework." *Proc. 11th Int'l. Conf. Stability of Ships and Ocean Vehicles*, Athens, Greece.
- Lee, G. J. (2014) "Moment of Inertia of Liquid in a Tank." *Int'l. J. Naval Architecture and Ocean Engineering*, 6(1):132–150.
- Longuet-Higgins, M. S. (1957) "The statistical analysis of a random moving surface." *Philos. Trans. Royal Soc. London, Series A*, 249:321–387.
- Luke, Y. L. (1976) *Mathematical Functions and their Approximations*. New York, NY, Academic Press, Inc. 584 pp.
- Miller, R., J. Gorski & D. Fry (2002) "Viscous roll predictions of a circular cylinder with bilge keels." *Proc. 24th Symposium on Naval Hydrodynamics*, Fukuoka, Japan.
- Montewka, J., F. Goerlandt, S. Ehlers, T. Hinz & P. Kujala (2013) "A risk framework for maritime transportation systems." *Proc. 13th Int'l. Ship Stability Workshop*, Brest, France, pp. 58–69.
- Naar, H. & S. Vaheer (2010) "Numerical study on the critical pressure heads." FLOOD-  
STAND Report D2.2a
- Naess, A. & T. Moan (2012) *Stochastic Dynamics of Marine Structures*. Cambridge University Press, UK.
- Newman, J. N. (1987) "Evaluation of the wave-resistance Green function: Part 1—The double integral." *J. Ship Research*, 31(2):79–90.
- Ochi, M. K. (1973) "On Prediction of extreme values." *J. Ship Research*, 17(1):29–37.
- Ochi, M. K. (1990) *Applied Probability and Stochastic Processes*. John Wiley and Sons.
- Oliveira, A. C. & A. C. Fernandes (2009) "An alternative approach for roll damping estimation." *Proc. 4th Int'l. Workshop on Applied Offshore Hydrodynamics*, Rio de Janeiro, Brazil.



- Paap, M. (2005) Verification of CFD calculations with experiments on a rolling circular cylinder with bilge keels in a free surface." Masters Thesis, Delft University of Technology & Bluewater Energy Services, Delft, Netherlands.
- Papanikolaou, A., C. Mains, S. Rusaas, R. Szalek, N. Tsakalakis, D. Vassalos & G. Zaraphonitis (2010) "GOALDS – Goal based damage stability." *Proc. 11th Int'l. Ship Stability Workshop*, Wageningen, Netherlands.
- Park, J. C., Y. Uno, H. Matsuo, T. Sato & H. Miyata (2001) "Reproduction of fully-nonlinear multi-directional waves by a 3D viscous numerical wave tank." ISOPE 2001, Stavanger, Norway.
- Pawłowski, M. (2008) "Closure on survival time." *Proc. 10th Int'l. Ship Stability Workshop*, Daejeon, Korea.
- Perrault, D. (2013) "Examination of the probability results for extreme roll of naval vessels." *Proc. 13th Int'l. Ship Stability Workshop*, Brest, France, pp. 178–184.
- Peters, A. J. & P. Harrison (2006) "A potential framework for a performance based damage stability standard for naval vessels." *Proc. 9th Int'l. Conf. Stability of Ships and Ocean Vehicles*, Rio de Janeiro, Brasil.
- Peters, A. J. & D. Wing (2009), "Stability Criteria Evaluation and Performance Based Criteria Development for Damaged Naval Vessels." *Proc. 10th Int'l. Conf. Stability of Ships and Ocean Vehicles*, St. Petersburg, Russia.
- Peters, W. S., V. Belenky & A. M. Reed, (2012) "On regulatory framework of direct stability assessment." *Proc. 11th Int'l. Conf. Stability of Ships and Ocean Vehicles*, Athens, Greece.
- Peters, W., V. Belenky & K. J. Spyrou (2013) "On alignment of the second generation IMO intact stability criteria with the goal based standards: Evaluation of the safety level." *Proc. 13th Int'l. Ship Stability Workshop*, Brest, France, pp. 243–250.
- Pierce, R. D. (1992) "Run length and statistical error estimation for seakeeping tests and trials." *Proc. Twenty-third American Towing Tank Conf.*, pp. 73–82.
- Press, W. H., B. P. Flannery, S. A. Teukolsky & W. T. Vetterling (1986) *Numerical Recipes: The Art of Scientific Computing*. Cambridge University Press, Cambridge, UK.
- Provosto, M. & G. Z. Forristall, (2002) "Statistics of wave crests from models vs. measurements." *Proc. ASME 22th Int'l. Conf. Offshore Mech. & Arctic Engin.*, Oslo, Norway.
- Ran, H., I. Rask & C. E. Janson (2012) "Damaged Ro-Pax vessel time to capsized." *Proc. 11th Int'l. Conf. Stability of Ships and Ocean Vehicles*, Athens, Greece.
- Reed, A. M. (2009). "A naval perspective on ship stability." *Proc. 10th Int'l. Conf. Stability of Ships and Ocean Vehicles*, St. Petersburg, Russia, pp. 21–44.



- Roddier, D. (2000) "Hydrodynamics of rolling cylinders with and without bilge keels." PhD Dissertation, University of California at Berkeley.
- Rosén A., L. Björnsson, M. Palmquist & E. Ovegård (2013) "On the influence of sea state idealizations and wave directionality in dynamic stability assessments." *Proc. 13th Int'l. Ship Stability Workshop*, Brest, France.
- Ruponen, P. (2007) "Progressive flooding of a damaged passenger ship." Doctoral Dissertation, Helsinki University of Technology, Department of Mechanical Engineering, Helsinki, Finland.
- Ruponen, P., M. Larmela, & P. Pennanen (2012) "Flooding prediction onboard a damaged ship." *Proc. 11th Int'l. Conf. Stability of Ships and Ocean Vehicles*, Athens, Greece.
- Sadat-Hosseini, H., F. Stern, A. Olivieri, E. F. Campana, H. Hashimoto, N. Umeda, G. Bulian & A. Francescutto (2010) "Head-wave parametric rolling of a surface combatant." *Ocean Engineering*, 37(10): 859–878.
- Sarkar, T. & D. Vassalos (2000) "A RANS-based technique for simulation of the flow near a rolling cylinder at the free surface." *Mar. Sci. Technol.*, 5:66–77
- Sclavounos, P. D. (1992) "On the quadratic effect of random gravity waves on floating bodies." *J. Fluid Mechanics*, 242:475–489.
- Sheinberg, R., K. Stambaugh, A. Eisele & R. Leadbetter (2006) "Estimating probability of capsizing for operator guidance." *Proc. 9th Int'l. Conf. Stability of Ships and Ocean Vehicles*, Rio de Janeiro, Brasil.
- Shigunov, V., N. Themelis & K. J. Spyrou (2012) "Critical wave groups vs. direct Monte-Carlo simulations for typical stability failure modes of a container ship." *Proc. 11th Int'l. Conf. Stability of Ships and Ocean Vehicles*, Athens, Greece.
- Skjong, R., E. Vanem & S. Rusås (2006) "Holistic and risk based approach to collision damage stability of passenger ships." *Proc. 9th Int'l. Conf. Stability of Ships and Ocean Vehicles*, Rio de Janeiro, Brasil.
- Smith, T. & B. Campbell (2013) "On the validation of statistical extrapolation for stability failure rate." *Proc. 13th Int'l. Ship Stability Workshop*, Brest, France, pp. 79–87.
- Spanos, D. & A. Papanikolaou (2007) "On the time to capsize of a damaged RoRo/Passenger ship in waves." *Proc. 9th Int'l. Ship Stability Workshop*, Hamburg, Germany.
- Spanos, D. & A. Papanikolaou (2010) "On the time dependent survivability of ROPAX ships." *Proc. 11th Int'l. Ship Stability Workshop*, Wageningen, Netherlands, pp. 143–147.



- Spanos, D. & A. Papanikolaou (2012) “Time dependent survivability against flooding of passenger ships in collision damages.” *Proc. 11th Int’l Conf. Stability of Ships and Ocean Vehicles*, Athens, Greece, pp. 401–410.
- Spanos, D. & A. Papanikolaou (2014) “On the time for the abandonment of flooded passenger ships due to collision damages.” *J. Mar. Sci. & Technol.*
- Spyrou, K. J. & I. Roupas (2006) “Damaged-ship survivability: A step beyond Wendel.” *Proc. 9th Int’l. Conf. Stability of Ships and Ocean Vehicles*, Rio de Janeiro, Brasil.
- STAB (2012) *Proceedings of the 11th International Conference on the Stability of Ships and Ocean Vehicles*. K. J. Spyrou, N. Themelis & A. D. Papanikolaou, Eds., Athens, Greece, 927 p.
- Stansberg, C. T., O. T. Gudmestad & S. K. Haver (2006) “Kinematics under extreme waves.” *Proc. ASME 25th Int’l. Conf. Offshore Mech. & Arctic Engin.*, Hamburg, Germany, OMAE2006-92491.
- Stern, F., J. Yang, Z. Wang, H. Sadat-Hosseini, M. Mousaviraad, S. Bhushan & T. Xing (2013) “Computational ship hydrodynamics: Nowadays and way forward.” *Int’l. Shipbuilding Progress*, 60:3–105.
- Tagg, R. & C. Tuzcu, (2002) “A performance-based assessment of the survival of damaged ships—Final outcome of the EU research project HARDER.” *Proc. 6th Int’l. Ship Stability Workshop*, New York, USA.
- Tanaka, N., Y. Himeno, Y. Ikeda & K. Isomura (1981) “Experimental study on bilge-keel effect for shallow-draft ship.” *J. Soc. Naval Arch. Japan*, 180:69–75.
- Tellkamp, J. & H. Cramer, (2002) “A methodology for design evaluation of damage stability.” *Proc. 6th Int’l. Ship Stability Workshop*, New York, USA.
- Themelis, N. & K. J. Spyrou (2006) “Probabilistic assessment of resonant instability.” *Proc. 9th Int’l. Conf. Stability of Ships and Ocean Vehicles*, Rio de Janeiro, Brasil.
- Thompson, A. & B. N. Taylor (2008) “Guide for the use of the International System of Units (SI).” NIST Special Publication 811, National Institute of Standards and Technology, Gaithersburg, MD.
- Tsakalakis, N., J. Cichowicz & D. Vassalos (2010) “The capsize band concept revisited.” *Proc. 11th Int’l. Ship Stability Workshop*, Wageningen, Netherlands.
- Umeda, N. (2013) “Current status of second generation intact stability criteria development and some recent efforts.” *Proc. 13th Int’l. Ship Stability Workshop*, Brest, France, pp. 138–157.



- van't Veer, R., J. de Kat & P. Cojeen (2002) "Large passenger ship safety: Time to sink." *Proc. 6th Int'l Ship Stability Workshop*, New York, USA.
- van't Veer R., W. Peters, A. L. Rimpela & J. de Kat (2004) "Exploring the influence of different arrangements of semi-watertight spaces on survivability of a damaged large passenger ship." *Proc. 7th Int'l. Ship Stability Workshop*, Shanghai, China.
- Vassalos, D. (2012) "Damage stability of passenger ships—notions and truths." *Proc. 11th Int'l. Conf. Stability of Ships and Ocean Vehicles (STAB'12)*, Athens, Greece, pp. 775–790.
- Vassalos D. & A. Jasionowski (2013) "Emergency response in ship flooding casualties." *Proc. 13th Int'l. Ship Stability Workshop*, Brest, France.
- Vassalos, D., A. Jasionowski & L. Guarin (2005) "Passenger ship safety—Science paving the way." *Proc. 8th Int'l. Ship Stability Workshop*, Istanbul, Turkey.
- Vugts, J. H. (1968) "The hydrodynamic coefficients for swaying, heaving and rolling cylinders in a free surface." *International Shipbuilding Progress*, 15(167):251–276.
- Vugts, J. H. (1970) "The hydrodynamic forces and ship motions in waves." Doctoral Thesis, Delft University of Technology, Delft, Netherlands, 115 p.
- Waals, O. J., A. B. Aalbers & J. A. Pinkster (2002) "Maximum likelihood method as a means to estimate the directional wave spectrum and the mean wave drift force on a dynamically positioned vessel." *Proc. ASME 21th Int'l. Conf. Offshore Mech. & Arctic Engin.*, Oslo, Norway.
- Wanderley, J. B. V., A. Ramiro, T. Reis, A. C. Fernandes & C. Levi (2007) "Numerical simulation of roll damping of a FPSO." *Proc. ASME 26th Int'l. Conf. Offshore Mech. & Arctic Engin.*, San Diego, USA, OMAE2007-29017.
- Wang, L. & T. Moan (2004) "Probabilistic analysis of nonlinear wave loads on ships using Weibull, Generalized Gamma, and Pareto Distributions." *J. Ship Research*, 48(3):202–217.
- Webster, W. C. (2009) "Evolution and kinematics of steep, random seas: A comparison with usual engineering estimates." *Proc. 4th Int'l. Workshop on Applied Offshore Hydrodynamics*, Rio de Janeiro, Brazil.
- Wilson, R. V., P. M. Carrica & F. Stern (2006) "Unsteady RANS method for ship motions with application to roll for a surface combatant." *Computers & Fluids*, 3:501–524.
- Yago, K., Y. Ohkawa, T. Chuji & T. Utsunomiya (2008) "Experimental study on viscous damping force of box-shaped body with fin." *J. Soc. Naval Arch. Japan*.
- Yang, B., Z.-C. Wang & M. Wu (2012) "Numerical simulation of naval ships' roll damping based on CFD." *Procedia Engineering*, 37:14–18.



Yeung, R. & P. Ananthkrishnan (1992) “Oscillation of a floating body in a viscous fluid.” *J. Engin. Math.*, 26:211–230

Yeung, R, S.-W. Liao & D. Roddier (1998) “On roll hydrodynamics of rectangular cylinders.” *Proc. 8th Int’l. Offshore & Polar Engin. Conf.*, Montreal, Canada, Vol. 3. pp. 445–53.

Yeung, R, R. K. M. Seah & J. T. Imamura (2013) “Lateral force and yaw moment on a slender body in forward motion at a yaw angle.” *J. Offshore Mech. & Arctic Engin.*, 135(3): 031101–031109.

Ypma, E. & E. Harmsen (2012) “Development of a new methodology to predict the capsizing risk of ships.” *Proc. 11th Int’l. Conf. Stability of Ships and Ocean Vehicles*, Athens, Greece.

Zaraphonitis, G., A. Papanikolaou, C. Roussou & A. Kanelopoulou (2013) “Comparative study of damage stability regulations and their impact on the design and safety of modern ROPAX ships.” *Proc. 13th Int’l. Ship Stability Workshop*, Brest, France, pp. 235–242.

## 11.2. Nomenclature

ASME American Society of Mechanical Engineers  
 BIPM Bureau Internat’l. Poids Mesures  
 CFD Computational Fluid Dynamics  
 CG Centre of Gravity  
 CPU Central Processing Unit

CresT JIP Cooperative Research on Extreme Seas and their impact Joint Industry Project  
 CTO Centrum Techniki Oretowej (Poland)  
 DoF Degree of Freedom  
 DTMB David Taylor Model Basin  
 EMLM Extended Maximum Likelihood Method  
 EPOT Envelope Peaks Over Threshold  
 EU European Union  
 FEM Finite Element Method  
 FLOODSTAND Integrated Flooding Control & Standards for Stability & Crisis Management (EU Project)  
 FP Forward Perpendicular  
 FPSO Floating Production Storage & Offloading  
 GM Metacentric Height  
 GOALDS Goal Based Damage Stability  
 GZ Righting Moment Arm  
 ICS Int’l. Council for Science  
 IAPSO Int’l. Assoc. for Physical Sciences of the Ocean  
 IAPWS Int’l. Assoc. for Properties of Water & Steam  
 IMO Int’l. Maritime Organisation  
 IOC Intergovernmental Oceanographic Commission  
 IS Intact Stability  
 ISEI Insufficient Stability Event Index  
 ISCG Intercessional Correspondence Group  
 ISO/ GUM International Standards Group/Guide to the Expression of Uncertainty in Measurements  
 ISSW Int’l. Ship Stability Workshop  
 ITTC Int’l. Towing Tank Conference  
 JCGM Joint Committee for Guides in Methodology  
 JONSWAP Joint North Sea Wave Observation Project  
 KC Keulegan-Carpenter number ( $KC = UT/2h$ )



KRISO	Korean Research Institute of Ships & Ocean Engineering	URANS	Unsteady Reynolds Averaged Navier-Stokes
LaSse	Loads on Ships at Sea	V&V	Verification & Validation
LCG	Longitudinal Centre of Gravity	VCG	Vertical Centre of Gravity
LOAS	Loss-of-Stability Accident		
MARIN	Maritime Research Institute Netherlands		
MEM	Maximum Entropy Method		
MOI	Moment of Inertia		
MSC	Maritime Safety Committee		
NGS	Nat'l. Geologic Survey		
NIST	Nat'l. Institute of Standards & Technology (USA)		
NOAA	Nat'l. Oceanic & Atmospheric Administration (USA)		
NSWCCD	Carderock Division, Naval Surface Warfare Centre		
OMAE	Int'l. Conf. on Ocean, Offshore and Arctic Engineering		
ONR	Office of Naval Research		
PF	Probability of Capsizing		
PIV	Particle Image Velocimetry		
POT	Peak Over Threshold		
RANS	Reynolds Averaged Navier-Stokes		
RAO	Response Amplitude Operator		
RDLI	Relative Damage Loss Index		
RINA	Royal Institution of Naval Architects		
RO-RO	Roll On-Roll Off		
ROPAX	Roll On Passenger		
SAIC	Science Applications Int'l. Corp.		
SCOR	Scientific Committee on Ocean Research		
SI	Int'l. System of Units		
SiW	Specialist Committee on Stability in Waves		
SLF	Sub-committee on Stability, Load Lines & Fishing Vessels Safety		
SOLAS	Int'l. Convention for the Safety of Life at Sea		
STAB	Int'l Conf. Stability of Ships & Ocean Vehicles		
UNESCO	United Nations Educational, Scientific & Cultural Organization		